



universität
wien

DISSERTATION

Titel der Dissertation

Insights into the mechanism of the
Anaphase Promoting Complex (APC/C)

Verfasser

Marc Jarvis

angestrebter akademischer Grad

Doctor of Philosophy (PhD)

Wien, 2014

Studienkennzahl lt. Studienblatt: A 094-490

Dissertationsgebiet lt. Studienblatt: Molekulare Biologie

Betreuer: Dr. Jan-Michael Peters

a ali di mi unterschuetzt hend, mi
biigschtande sind ond a mi gglaubt hend

Table of Contents

| | | |
|-----------|---|-----------|
| 1. | Abstract | 1 |
| 2. | Zusammenfassung | 3 |
| 3. | Introduction | 5 |
| 3.1. | The ubiquitin system | 5 |
| 3.1.1. | Ubiquitin | 5 |
| 3.1.2. | The ubiquitination cascade | 5 |
| 3.1.3. | The E1-E2 interaction | 7 |
| 3.1.4. | E3 ligases and their interactions with E2 enzymes | 7 |
| 3.1.4.1. | RING E3s | 7 |
| 3.1.4.2. | HECT E3 ligases | 9 |
| 3.1.4.3. | RING-in-between-RING (RBR) | 10 |
| 3.1.4.4. | Bacterial E3 ligases | 11 |
| 3.2. | The Cell Cycle | 12 |
| 3.2.1. | The Ubiquitin Proteasome System | 14 |
| 3.2.2. | Mitosis | 14 |
| 3.2.3. | The Anaphase Promoting Complex (APC/C) | 15 |
| 3.2.4. | APC/C architecture and subunit topology | 15 |
| 3.2.5. | The co-activators CDC20 and CDH1 activate and recruit substrates to the APC/C | 17 |
| 3.2.6. | The APC/C functions with two E2s, UBCH10 and UBE2S | 19 |
| 4. | Aim of this study | 20 |
| 5. | Results | 21 |
| 5.1. | UBE2S recruitment and interaction with the APC/C | 21 |
| 5.1.1. | UBE2S binds APC/C through its extreme C-terminal tail residues | 21 |
| 5.1.2. | The APC/C platform domain is sufficient to bind UBE2S | 22 |
| 5.1.3. | The APC2/APC11 is not sufficient to bind UBE2S | 22 |
| 5.1.4. | Catalytic surface alanine scan of UBE2S reveals multiple surfaces | 24 |
| 5.1.4.1. | E1 binding surface | 24 |
| 5.1.4.2. | Donor ubiquitin binding surface | 24 |
| 5.1.4.3. | Acceptor ubiquitin binding surface | 24 |

| | | |
|------------|--|-----------|
| 5.1.4.4. | The ‘backside’ surface | 25 |
| 5.1.4.5. | The UBC domain C-terminal helix | 25 |
| 5.1.4.6. | The C-terminal tail..... | 25 |
| 5.2. | Structural basis for co-activator – substrate interaction | 28 |
| 5.2.1. | A 3Myc-His6 tag stabilises the APC/C co-activator proteins | 28 |
| 5.2.2. | Purification of full length co-activators is troublesome | 28 |
| 5.2.3. | Identification of a structured domain in CDC20/CDH1 | 29 |
| 5.2.4. | Limited proteolysis of CDC20/CDH1 reveals a globular C-terminus..... | 30 |
| 5.2.5. | CDC20/CDH1 deletion constructs are more stable than full length co-activators..... | 33 |
| 5.2.6. | CDH1/CDC20 deletion constructs bind substrates | 35 |
| 5.2.7. | Hsl1 667-872 is unstructured | 36 |
| 5.2.8. | Binding of a ligand is beneficial for CDH1 stability..... | 38 |
| 5.2.9. | Hsl1 D-box binds tighter to CDH1 full length than Hsl1 KEN-box..... | 39 |
| 5.2.10. | 1MH6 CDH1 162-14 + Hsl1 D-box peptide complex yields multi-lattice crystals..... | 40 |
| 5.2.11. | Sodium cacodylate promotes crystal growth | 41 |
| 5.2.12. | Streak seeding yields small single lattice crystals | 42 |
| 5.2.13. | Reducing the Hsl1 KEN-D-box linker length improves complex behaviour | 43 |
| 6. | Discussion..... | 45 |
| 6.1. | UBE2S – a non-canonical E2 | 45 |
| 6.2. | Insights into substrate recruitment to the APC/C | 48 |
| 6.3. | Precise, ordered substrate degradation by the APC/C is multi-modal..... | 52 |
| 7. | Materials and Methods | 57 |
| 7.1. | Surface alanine scan of UBE2S in the laboratory of Brenda A. Schulman..... | 57 |
| 7.2. | Co-activator structural studies | 62 |
| 8. | References | 69 |
| 9. | Experimental Contributions..... | 77 |
| 10. | Acknowledgments | 79 |
| 11. | Curriculum Vitae | 81 |

1. Abstract

Ubiquitination boasts widespread importance in a multitude of cellular signalling events. It utilises a tri-enzyme cascade consisting of an E1 ubiquitin activating enzyme, an E2 ubiquitin conjugating enzyme and an E3 ligase to covalently attach ubiquitin to target substrate proteins. The cascade can be broken down into three main principles: 1: recruitment of an E2~Ub species to the E3, 2: recruitment of the substrate to the E3 and 3: activation of the donor ubiquitin on the E2. Despite the apparent simplicity of the ubiquitination cascade, the full molecular details of how an E3 facilitates transfer of ubiquitin to a substrate still remain elusive. E3s can be classified according to their mechanism; these include the RING, HECT, RING-IBR-RING and bacterial families of E3 ligases. This thesis will focus on the RING E3 ligase the Anaphase Promoting Complex/Cyclosome (APC/C).

The ubiquitin ligase activity of the APC/C is essential for rapid sister chromatid separation and mitotic exit. The APC/C initiates these events by ubiquitinating securin, an inhibitor of the cohesin cleaving protease separase, and B-type cyclins, the activating subunits of cyclin-dependent kinase 1 (CDK1). These ubiquitination events are initiated by the E2 UBCH10 with subsequent K11 linked ubiquitin chains built by UBE2S.

We set out to understand the first two principles of the APC/C ubiquitination cascade: how UBE2S is recruited to the APC/C and the residues of UBE2S that are important for its function. To address this, we assessed the ability of UBE2S mutants to stably bind the APC/C. The C-terminal tail residues were essential to recruit UBE2S to the APC/C. Furthermore, we performed a surface alanine scan of UBE2S to identify residues and surfaces important for the function of UBE2S. Several residues were identified on an unexpected surface that were essential for APC/C dependant ubiquitin chain formation.

The third principle of the ubiquitination cascade is the recruitment of the substrate to the E3. The APC/C recognises its substrates through one of two cell cycle stage specific co-activator proteins, CDH1 and/or CDC20. The C-terminal WD-40 domain of these co-activators recognise specific degradation motifs within substrates. To understand at a molecular level how this is achieved we initiated structural studies using as a model substrate the yeast protein Hsl1, which is known to bind tightly to CDH1. Crystallography trials were conducted with CDH1 and a synthetic Hsl1 D-box peptide, as well as with CDH1 co-expressed with a Hsl1 fragment containing both a D-box and a KEN-box. Furthermore, we used Isothermal Titration Calorimetry (ITC) to understand the relative contribution of D-boxes and KEN-boxes to co-activator binding. These experiments revealed that the Hsl1 D-box binds to the CDH1 WD40 domain with a 3-fold higher affinity than the KEN-box, indicating that interactions with the D-box are of particular importance for CDH1 to be able to recruit substrates to the APC/C.

2. Zusammenfassung

Die kovalente Anbindung von Ubiquitin an Proteine spielt eine grosse Rolle in vielen biologischen Prozessen. Daher ist die korrekte Abfolge der enzymatischen Ubiquitinierungskaskade besonders wichtig. Zu Beginn wird Ubiquitin durch eine E1 Ligase aktiviert und an ein E2 Ubiquitin-konjugierendes Enzym weiter gegeben (E2~Ub). Der E2~Ub Komplex bindet anschliessend an eine E3 Ligase, die durch die Bindung eines Substrats, den Ubiquitintransfer vom E2~Ub Komplex an das Substrat ermöglicht. Obwohl die einzelnen Prozesse der Ubiquitinierung einfach erscheinen, ist der detaillierte molekulare Prozess relative schlecht charakterisiert. Aufgrund ihrer Aktivität werden die E3 Ligasen in verschiedenen Klassen aufgeteilt: HECT, RING, RING-IBR-RING und die bakteriellen Orthologen.

Der Anaphase Promoting Complex/Cyclosome (APC/C), eine E3 Ligase der RING Familie, spielt eine besonders wichtige Rolle im Zellzyklus, besonders während der Mitose. Sie ist verantwortlich für die Ubiquitinierung von Sekurin und B-typ spezifischen Zyklinen. Sekurin ist ein Inhibitor der Cohesin Protease Separase und B-typ spezifische Zykline aktivieren die Zyklin abhängige Kinase 1 (CDK1). Durch deren Inaktivierung wird der korrekte Ausgang der Mitose sichergestellt und unter anderem auch die schnelle Aufteilung der Schwesterchromatiden auf die zwei Tochterzellen. Der APC/C Komplex wird indirekt durch UBE2S aktiviert. UBE2S führt zur Lysin 11 Ubiquitinkettenbildung auf der E2 Ligase, UBCH10. Diese Kettenbildung wird dann zur Ubiquitinierung von Sekurin und B-typ spezifischen Zyklinen durch den APC/C Komplex weiter verwendet.

Das Ziel meiner Doktorarbeit ist die Aktivierung des APC/C Komplexes besser zu verstehen. Wie wird UBE2S an APC/C gebunden? Welche Aminosäuren sind dabei besonders wichtig? Zu diesem Zweck wurde die Interaktionsfähigkeit von UBE2S Mutanten an APC/C mit Hilfe von "Co-IP" Experimenten analysiert und Mutationen im C-Terminus haben sich dabei als essentiell erwiesen. In anderen Experimenten wurde die Funktionalität der Interaktionsoberfläche von UBE2S mittels Alanin Mutationen getestet. Mehrere, unerwartete Mutationen weisen auf eine wichtige Funktion in der APC/C abhängigen Ubiquitinkettenformation hin.

Ein weiterer wichtiger Punkt in der Ubiquitinierungskaskade ist die Substratbindung. APC/C benötigt dazu die Hilfe von einem der beiden Zellzyklus spezifischen Kofaktoren, CDH1 oder CDC20. APC/C gebundene Kofaktoren erkennen spezielle Abbaumotive in Substratproteinen mit Hilfe ihres C-terminalen β -Propellers. Um diesen Prozess besser verstehen zu können, verwendete ich ein Hefe spezifisches Modellprotein, Hsl1, das besonders gut an CDH1 bindet. Um eine hochauflösende Proteinstrukturen dieser Interaktion zu erhalten, wurden Kristallisierungsexperimente mit CDH1 und synthetischen Hsl1 D-Box

4 | Zusammenfassung

Peptiden angesetzt. In anderen Kristallisierungsversuchen wurden CDH1 und Hsl1 Fragmenten, die sowohl die D- als auch KEN-Box enthalten, in Insektzellen ko-exprimiert. Um herauszufinden wie sehr das D-Box bzw. KEN-Box Motif die Bindung an die Kofaktoren beeinflussen, habe ich zusätzlich Isothermal Titration Calorimetry (ITC) Experimenten durchgeführt. Die Hsl1 D-Box scheint mit einer dreifach höheren Affinität an den CDH1 β -Propeller zu binden als die KEN-Box. Daraus schliesse ich, dass die D-Box besonders wichtig ist für die korrekte CDH1 abhängige Rekrutierung von Proteinsubstraten an den APC/C Komplex.

3. Introduction

3.1. The ubiquitin system

Ubiquitination, the covalent modification of a protein by ubiquitin is a major mechanism for regulating cellular processes, such as the cell cycle, and protein function and fate such as protein half-life, sub-cellular localisation, and interactions with other proteins. Given the diverse nature of outcomes, there would be catastrophic consequences if ubiquitination defects were to occur and as such, this mechanism is highly regulated (Kerscher et al., 2006).

3.1.1. Ubiquitin

Ubiquitin is a small, highly conserved, protein of 8.5 kDa (76 amino acids). A very versatile protein, its many features include seven key lysine residues, (K6, K11, K27, K29, K33, K48, K63), determining the type of ubiquitin chain linkage (Fig.1B), its hydrophobic patch, encompassing I44 which mediates interactions with E2 ubiquitin conjugating enzymes (Fig.1A) (Sloper-Mould et al., 2001) and its C-terminal tail, which is involved in thioester bond formation. The lysine residues play a critical role in determining the meaning of the ubiquitin signal with poly-ubiquitin chains of different lysine linkages, in addition to mono- and di-ubiquitin, mediating different outcomes by means of the structural conformation they adopt (Varadan et al., 2002; Tenno et al., 2004). For example, K63 chains are predominantly involved in signalling, while K11 chains target cell cycle proteins for proteasomal degradation whereas mono and di-ubiquitin signals have been implicated in intra-cellular trafficking (Dikic et al., 2009; Komander and Rape, 2012; Berndsen and Wolberger, 2014).

3.1.2. The ubiquitination cascade

Ubiquitination is mediated by a tri-enzyme cascade consisting of a ubiquitin activating enzyme (E1), a ubiquitin conjugating enzyme (E2) and a ubiquitin ligase (E3) (Fig.1C). The cascade begins with the E1 ubiquitin activating enzyme activating ubiquitin in an ATP-dependent manner, adenylating and so forming a high energy thioester bond with the C-terminal glycine residue of ubiquitin. The active ubiquitin then undergoes a trans-thioesterification in which the E2 catalytic cysteine attacks the E1~Ub thioester bond forming an E2~Ub intermediate. Lastly, the E3 ubiquitin ligase mediates the binding of both the E2~Ub conjugate and the substrate, albeit in spatially distinct locations. This facilitates the transfer of ubiquitin from the E2 to a specific ϵ -NH₂ group on a target substrate lysine or N-terminal methionine, forming an isopeptide bond (or on an α -NH₂ group in the case of linear ubiquitin chain formation) (Pickart and Eddins, 2004; Metzger et al., 2014).

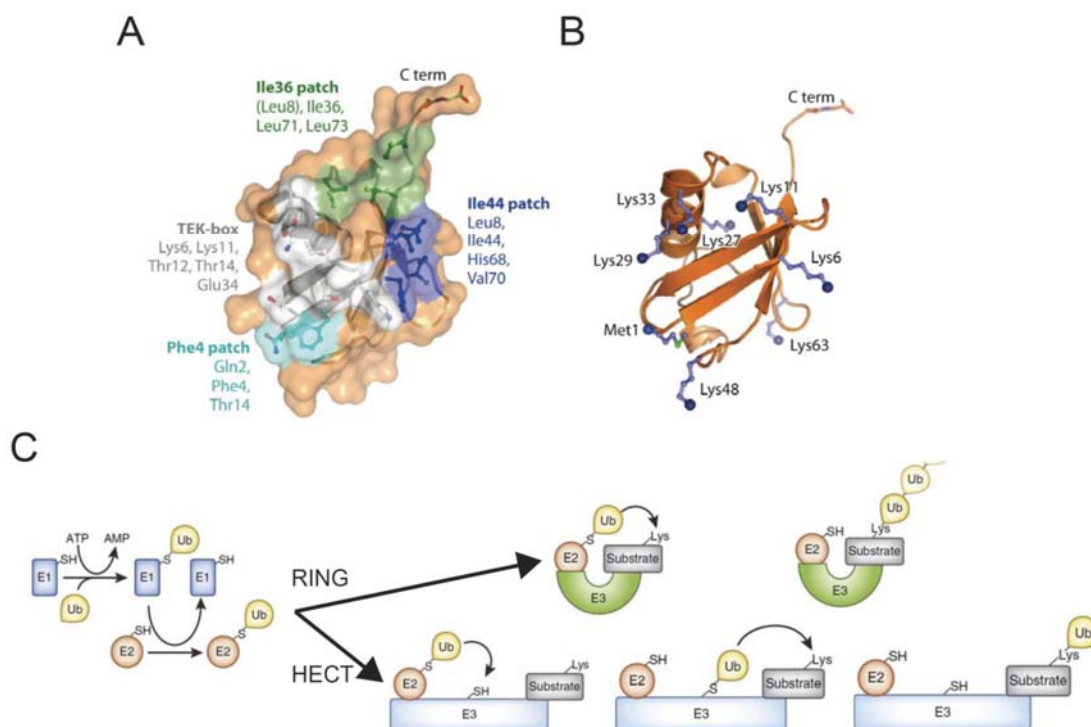


Figure 1: Ubiquitin and mechanisms of conjugation.

(A) Schematic representation of ubiquitin surfaces involved in protein-protein interactions important for its function. (B) The structure of ubiquitin showing the seven key lysine residues. (C) Schematic representation of the ubiquitination cascade illustrating the differences between the canonical RING and HECT mechanisms. (Komander and Rape, 2012; Berndsen and Wolberger, 2014)

Currently, ~40 E2 enzymes and ~600 E3 ligases have been identified. Given the vast excess of E3s over E2s and the ability of E3 enzymes to interact with thousands of substrates, ubiquitination provides a mechanism to regulate many proteins. As mentioned, the lysine linkage of a poly-ubiquitin chain is critical in determining the implication of the 'signal'. General substrate recognition by the E3 infers only a low specificity for a specific lysine (Mattioli and Sixma, 2014). E2 enzymes have been shown to play an important role in determining the chain linkage type. However, it is not fully understood how lysine selection is achieved given that it could be mechanistically or through structural constraints. Some E3 ligases have also been shown to function with multiple E2 enzymes, with the first E2 initiating ubiquitin chain formation and a second E2 building a poly-ubiquitin chain upon the initial ubiquitin, adding a further layer of complexity to ubiquitin signalling. It is therefore of vital importance to understand how E2 and E3 enzymes interact and function together in order to appreciate the mechanistic details of ubiquitination. (Berndsen and Wolberger, 2014; Metzger et al., 2014)

3.1.3. The E1-E2 interaction

Insights into how the E1 recruits and binds the E2 were first put forward by Huang and colleagues who studied the interaction between the hetero-dimeric E1 APPBP1-Uba3 and the E2 Ubc12. They found that Uba3's C-terminal ubiquitin fold domain binds the $\alpha 1$ helix in Ubc12's ubiquitin conjugating (UBC) domain with the interaction driven by hydrophobic contacts similar to interactions observed between ubiquitin and a ubiquitin binding domain (UBD). (Huang et al., 2004, 2005). Furthermore, together with published E1 structures, the authors inferred that a large conformational change would be needed for the E1 and E2 catalytic cysteines to interact since the Ubc12 catalytic cysteine faces away from the E1 active site, separated by 50Å (Huang et al., 2005). This interaction was further characterised through a Uba1-Ubc4-Ub-ATP•Mg crystal structure illustrating the conformational rearrangements in the E1 required for the E1 and E2 active sites to interact (Olsen and Lima, 2013).

3.1.4. E3 ligases and their interactions with E2 enzymes

Central to the ubiquitination cascade is the interaction between the E2 enzymes and E3 ligases. E3s act as a platform to facilitate the transfer of ubiquitin from the E2~Ub species to the substrate thus increasing the rate of ubiquitination. There is great diversity within the known ~600 E3 ligases however, they can be classified into four major families according to the domains they contain and their catalytic mechanism (Fig.1C). Namely, these E3 families are known as RINGs (really interesting new gene) which directly facilitate the transfer of ubiquitin from the E2~Ub to the substrate, HECTs (homologous to E6-AP carboxy terminus) which form an E3~Ub intermediate before transferring the ubiquitin to the substrate, RBRs (RING-in-between-RING) which employ a hybrid RING/HECT mechanism and bacterial E3 ligases (Berndsen and Wolberger, 2014). These will be briefly discussed.

3.1.4.1. RING E3s

The largest class of E3s are the RING E3 ligases. RINGs have no intrinsic catalytic activity, owing to their lack of a catalytic cysteine but provide a platform for the direct transfer of ubiquitin from the active E2~Ub species to the substrate. This emphasises the importance of the interaction between the RING E3 and the E2~Ub species, since the active enzyme ubiquitin complex will define the type of ubiquitin chain linkage formed on the target substrate.

RINGs co-ordinate two Zn^{2+} ions (three in the case of APC11 and Rbx1), through a combination of eight cysteine and histidine residues, in a so called 'cross braced' arrangement. The two loops involved in co-ordinating the Zn^{2+} ions border a groove formed by the central α helix. These structural features provide a platform with which the N-terminus of the E2s can interact. RINGs can be found in many different structural contexts: as a monomer, a homo- or

hetero-dimer, or as part of multi subunit complexes. The latter as illustrated by the cullin RING ligases (CRL). CRLs, such as the Anaphase Promoting Complex and Skp1, Cul1, F-box (SCF), can uniquely recruit many different substrates as they function with multiple substrate recruitment factors (Berndsen and Wolberger, 2014; Metzger et al., 2014).

It has been shown that in the presence of a minimal RING domain the rate of ubiquitination is greatly increased. However, it is unclear: how the RING domain stimulates ubiquitination events given that RINGs display no intrinsic catalytic activity and that the RING domain is too far from the E2 active site cysteine when bound (Tang et al., 2001). Hypotheses have focused on stimulation by the RING through allosteric changes in the E2, by positioning the E2~Ub species with respect to the substrate or by activating the E2~Ub species in some manner.

Structural studies investigating the interactions between the E2~Ub and the RING domain have shed light on this quandary. Studies on the CRL SCF, Cul5-Rbx1, showed dramatic reorientation of the cullin and RING domains towards the E2~Ub, making catalytic interactions possible and demonstrating the importance of structural rearrangements in catalysis (Fig.2A) (Duda et al., 2008).

Furthermore, solution-based studies on Ubc5B-RNF4 have illustrated that the ubiquitin in E2~Ub adopts a large range of conformations with respect to the E2, so called open conformations. However, when in contact with the RING domain, a closed active conformation is preferred (Pruneda et al., 2011; Dou et al., 2013). From RNF4-UBCH5B~Ub and BIRC7-UBCH5B~Ub crystal structures this has been attributed to an arginine linchpin in loop2 of the RING domain wedges itself between the E2 and ubiquitin with hydrogen bonding forming an allosteric link favouring closed E2~Ub conformations. This organised Ile44 in the hydrophobic patch of ubiquitin to nestle against the α 2 helix and active site of the E2 and the RING (Fig.2B) (Dou et al., 2012; Plechanovová et al., 2012). In these cases the RING, as well as non-RING priming elements, must position the active donor ubiquitin in a way to react with the substrate lysine (Dou et al., 2013; Scott et al., 2014). It is however interesting to note that E2s such as UBC1 and UBE2S, which also exhibit E3-independent ubiquitin transfer, seemingly show closed E2~Ub conformations even in the absence of the E3. So in the case of these E2s, it is not clear what the RING/E3 is actually doing.

In addition to canonical RING interactions with an E2, additional factors binding 'backsides' of E2s can also invoke allosteric changes. An example of this the E3 gp78 which contains a C-terminal G2BR domain which interacts with the backside (the side distal to the cysteine active site) of Ube2g2. This induces an allosteric change in the E2, opening up the E2 active site for substrate binding. E2 backsides have also been shown to non-covalently interact with ubiquitin in a low affinity manner through a UBD. In the case of BRCA1-BARD1, this interaction also increases poly-ubiquitination (Das et al., 2009, 2013).

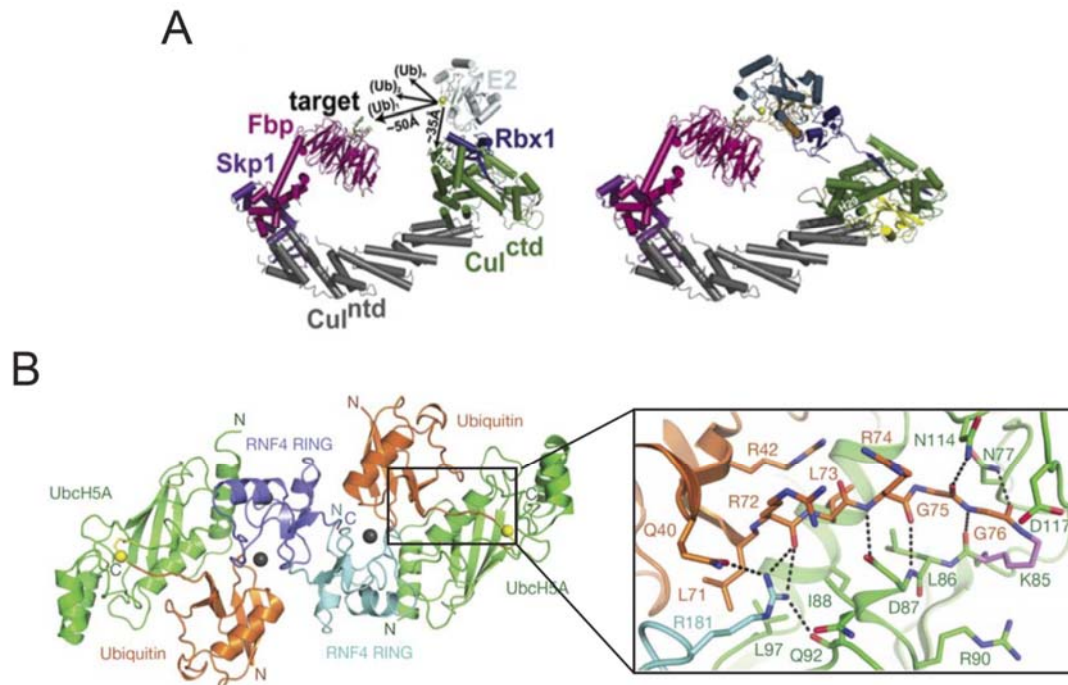


Figure 2: An insight into RING E3 mechanism.

(A) Model of SCF^{βTRCP} illustrating the distance needed to span for ubiquitin transfer from the E2 to the target substrate (left) and ubiquitin transfer following structural rearrangement of Rbx1 (right). F-box-purple, E2-light blue, Rbx1-blue, Cul1-green/grey-. (B) UBCH5A~Ub~RNF4 crystal structure showing the Arg linchpin (R181-light blue) coordinating interactions with the E2 and ubiquitin. UBCH5A-green, Ub-orange, RNF4 -purple. (Duda et al., 2008; Plechanovová et al., 2012)

3.1.4.2. HECT E3 ligases

HECT E3 ligases contain the other major domain associated with E3 ligases, the HECT domain. The HECT domain consists of two flexibly connected lobes, the catalytic cysteine containing C-terminal lobe and the N-terminal lobe, which confers substrate specificity. The HECT domain mediates interaction with E2s, predominantly from the UBCH5 and UBCH7 class. Kamadurai and colleagues set out to visualise the first step of this two-step mechanism and crystallised an UBCH5B~Ub~HECT 'intermediate' complex, namely UBCH5B~Ub~NEDD4L. What they found was that both the N- and C-lobes of the HECT bound the E2 and ubiquitin respectively bringing together the active sites of both enzymes (Kamadurai et al., 2009). This was in contrast to previous E2~HECT structures, such as E6AP, where there was a 41 Å gap between the two active sites. When the authors probed the second stage of the two-step HECT mechanism by crystallising a Rsp5~Ub~Sna3 intermediate they found the C-lobe rotates 130° from facing the E2 to facing the substrate giving priority to the lysines on the substrate to act as acceptors (Fig.3) (Kamadurai et al., 2013).

Despite the increasing understanding of HECT E3 ligase mechanism, there are still many open questions particularly with respect to how poly-ubiquitin chains are formed. This may occur in a sequential manner similar, to RING E3 ligases, or in blocks on the HECT catalytic cysteine with the whole poly-ubiquitin chain being subsequently transferred to the substrate.

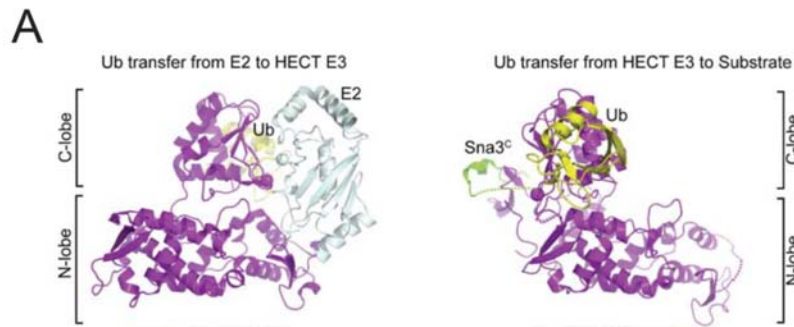


Figure 3: Insights into HECT mechanism.

(A) Structural view of the E2 transferring Ub to E3 (left) and E3 transfer Ub to substrate (right) highlighting structural rearrangement. E2-light blue, E3-purple, ubiquitin-yellow, substrate-green. (Kamadurai et al., 2013)

3.1.4.3. RING-in-between-RING (RBR)

RING-in-between-RING E3s share features with both the RING and HECT classes of E3 ligases. RBRs consist of a RING1 domain, two Cys/His rich Zn^{2+} binding surfaces (in between ring domain), followed by a RING2 domain. RING1 and RING2 are functionally distinct, with RING1 performing the canonical function of interacting with the E2, and RING2 containing the catalytic cysteine (Duda et al., 2013). To confuse matters, some RBR E3s require only RING1 is necessary to interact with the E2, whereas other RBR E3s, require both RING domains for interaction with the E2.

Recent work studying the E2 UBCH7 and its interaction with Parkin and HHARI has shed light on the mechanism of RBRs. UBCH7 is an E2 that lacks intrinsic E3-independent activity towards lysines which but does have activity towards cysteines explains why it functions with HECT but not RING E3s. Interestingly, UBCH7 functions with RBRs, such as Parkin and HHARI. Wenzel et al showed that RBRs function as RING/HECT hybrids with the E2 binding via the RING1 domain and transferring the ubiquitin to a conserved cysteine in the RING2 domain (Wenzel et al., 2011). This was followed up by Duda and colleagues who showed in a crystal structure of HHARI that the E2 binding site of RING1 is exposed to allow binding of UBCH7, whereas the catalytically important RING2 domain active cysteine is masked by a flanking, auto-inhibitory, 'Ariadne' domain giving an insight into how this E3 ligase is regulated (Fig.4) (Duda et al., 2013).

A

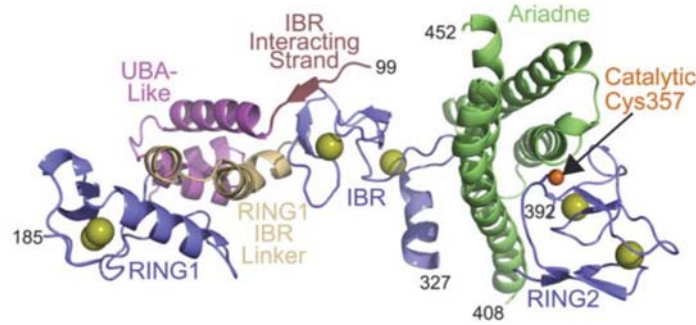


Figure 4: Structure into RBRs.

Representation of the structural features of the RBR HHARI.
RBR-blue, Ariadne domain-green. (Duda et al., 2013)

3.1.4.4. Bacterial E3 ligases

Many pathogenic bacteria have evolved a system where they inject virulence factors into eukaryotic host cells that function as E3 ligases and modulate numerous host cell processes, particularly the ubiquitin pathway. Despite not sharing any sequence homology with their eukaryotic counterparts, these virulence factors mimic RING and HECT E3 ligases and include also a novel E3 ligase (NEL) class, which undergo a dramatic re-orientation upon substrate recognition (Hicks and Galan, 2010; Xin et al., 2012).

An example of a RING mimic includes AvrPtoB from *Pseudomonas syringae*. Structurally, AvrPtoB has a RING domain fold similar to Rbx1 and contains a conserved binding site to interact with E2s similar to eukaryotes (Janjusevic et al., 2006). SopA from *Salmonella enterica* illustrates a nice example of HECT mimicry. It contains a N-terminal substrate binding domain and a C-terminal HECT like domain with the HECT-like domain having an N- and C-lobe connected by a flexible linker, as observed with eukaryotic counterparts (Diao et al., 2008; Hicks and Galan, 2010; Lin et al., 2012).

The importance of the ubiquitin system can be nicely illustrated by its significance in the regulation of the cell cycle.

3.2. The Cell Cycle

The transmission of genetic information from the mother cell to its daughter cells is one of the fundamental building blocks of life. The extremely regulated, uni-directional and systematic process of the cell cycle ensures this happens in a high fidelity manner.

The eukaryotic cell cycle comprises distinct phases, namely: Gap 1 (G₁), Synthesis (S), Gap 2 (G₂) and Mitosis (M) (Fig.5). In G₁, the cell starts its preparations for the ensuing S phase, synthesising enzymes, accumulating cellular components, as well as making sure that favourable environmental conditions allow the successful completion of DNA replication and cell division. Once committed to the cell cycle by passing through the irreversible START checkpoint, the cell enters S phase. In S phase, the cell commences DNA replication, doubling its genome to 4N. Upon completion of DNA replication, the cell advances into G₂, another phase of synthesis of cellular components. At this point the cell also screens itself for DNA damage, with the G₂/M checkpoint preventing entry into mitosis until the genome is considered acceptable to divide to the daughter cells. Upon entry into mitosis, subsequent chromosome segregation occurs leading ultimately to cell division (Morgan, 2007).

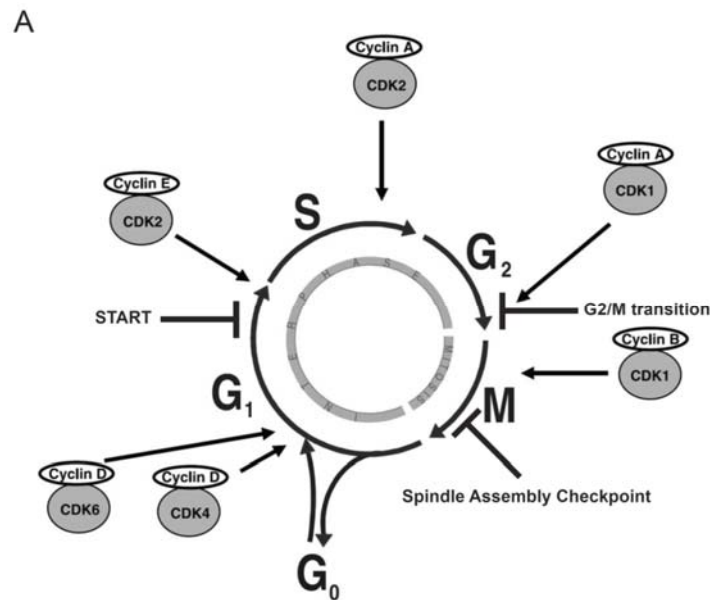


Figure 5: Schematic representation of the cell cycle. Representation of the five cell cycle faces together with the associated Cdk-cyclin complexes and the regulatory checkpoints. Modified from (Vermeulen et al., 2003).

The uni-directional progression through the cell cycle is regulated by a complex network of regulatory proteins. This ensures that the distinct order of events and timings of the cell cycle occur as intended. Progression through the cell cycle is driven by oscillations in the activity of four cyclin dependent kinases (Cdk) which are activated and de-activated by waves of transcription/translation and proteasomal degradation of their respective regulatory cyclins (Fig.6) As the intra-cellular concentration of a cyclin increases, equilibrium dictates that more active cyclin-Cdk complexes will form, thus modulating cell cycle stage specific events. As the cell progresses through the cell cycle, the enzymatic activity of each respective Cdk changes, this results in a change in phosphorylation state of target cell regulatory proteins influencing their cell cycle stage specific function as well as their interaction with other proteins (Nigg, 2001; Murray, 2004; Morgan, 2007). A fine example of this are the cyclins A and B. Both cyclins activate Cdk1 however, Cyclin A accumulates throughout S phase owing to its role in initiating DNA replication and preventing the re-assembly of additional replication complexes (Woo and Poon, 2003). As the cell cycle progresses towards mitosis, Cyclin A begins to be degraded with levels of cyclin B increasing favouring association with Cdk1 promoting entry into mitosis and subsequent mitotic spindle assembly (Morgan, 2007; Hochegger et al., 2008).

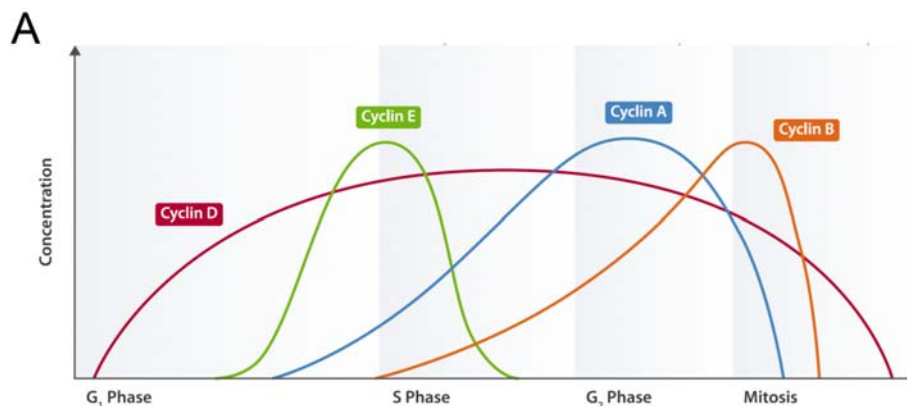


Figure 6: Schematic representation of the oscillating concentrations of cyclins throughout the cell cycle.

Representation of the waves of cyclin concentrations throughout the cell cycle. There is a correlation between the accumulation in cyclin concentrations, Cdk activity and the regulatory checkpoints. Modified from (Morgan, 2007).

3.2.1. The Ubiquitin Proteasome System

It is clear that the degradation of cyclins, as well as other cell regulatory proteins, is crucial in ensuring the high fidelity and uni-directionality of the cell cycle. This key function is mediated by the ubiquitin proteasome system in a two-step mechanism: 1, the tagging of a substrate protein by the covalent attachment of ubiquitin and 2, degradation of the protein by the 26S proteasome. Throughout the cell cycle this is mediated by two CRLs: the APC/C and the SCF. The APC/C is active during mitosis until late G1 whereas the SCF is active throughout late G1, S phase and G2. Both CRLs are characterised by a common catalytic core containing a RING domain (APC11 in the APC/C and Rbx1 in the SCF) and the associated cullin subunit (APC2 in the APC/C and Cul1 in the SCF). As mentioned, CRLs demonstrate huge plasticity in their substrate specificity which is ideal to target the plethora of cell cycle regulatory proteins for proteasomal degradation. The SCF has offered many insights to date on how RING E3 ligases interact with their E2s, substrates and facilitates the transfer of ubiquitin from one to the other. In contrast, not much is understood about how the APC/C functions as an E3 ligase despite it regulating one of the most important events in the cell cycle, chromosome segregation (Morgan, 2007; Duda et al., 2013).

3.2.2. Mitosis

At the heart of the cell cycle lies mitosis, one of the most beautiful and intricate processes in biology. It comprises of six phases: prophase, pro-metaphase, metaphase, anaphase, telophase and cytokinesis.

During the initial stages of mitosis, in prophase, the replicated genome undergoes chromosome condensation together with nucleation of the mitotic spindle. This leads into pro-metaphase, when the nuclear envelope breaks down and initial microtubule kinetochore interactions start to occur. Once all the chromosomes are attached in a bipolar manner to the mitotic spindle and are aligned at the metaphase plate, the cell is said to have satisfied the spindle assembly checkpoint and be at metaphase. At this point the Anaphase Promoting Complex/Cyclosome (APC/C) is activated and rapidly targets securin and cyclin B for proteasomal degradation, allowing separation of sister chromatids, by the proteolytic cleavage of cohesion, and progression to mitotic exit and cytokinesis, by de-activation of Cdk1 (Shirayama et al., 1999; Morgan, 2007).

The Spindle Assembly Checkpoint (SAC) has an important role in ensuring that all sister chromatids are bi-orientated and aligned on the metaphase plate before being segregated. Up until the last kinetochore is attached to the mitotic spindle, a 'wait' signal is generated by the tension-sensing kinase Aurora B, which stimulates the recruitment of Mad2 to the kinetochore (Liu et al., 2009; Rieder et al., 1995). Mad2 in turn promotes the assembly

of the mitotic checkpoint complex (MCC) which inhibits the APC/C and thus progression into anaphase (Musacchio and Salmon, 2007; Herzog et al., 2009; Uzunova et al., 2012; Foley and Kapoor, 2013; Primorac and Musacchio, 2013).

3.2.3. The Anaphase Promoting Complex (APC/C)

The Anaphase Promoting Complex (APC/C) is a CRL RING E3 ligase that has been intensely studied with respect to its important role mitosis. Of particular significance are the APC/C's function in chromosome segregation and mitotic exit where the APC/C builds poly-ubiquitin chains on substrate regulatory proteins, marking them for proteasomal degradation (King et al., 1995; Peters, 2006; Primorac and Musacchio, 2013).

Activation of the APC/C is multi-layered. It is activate-ably phosphorylated by Cdk1, particularly on APC3, from pro-metaphase until the end of G1 at which point it is inactivated during S and G2 phase by de-phosphorylation (King et al., 1995; Kramer et al., 2000; Rudner and Murray, 2000; Kraft et al., 2003). Furthermore, it is also subject to pseudo-substrate inhibition binding of Emi1 and subsequently at the beginning of mitosis by the MCC (Reimann et al., 2001; Sudakin et al., 2001; Miller et al., 2006; Braunstein et al., 2007; Burton and Solomon, 2007; Herzog et al., 2009; Lara-Gonzalez et al., 2011; Frye et al., 2013). Additionally, phosphorylated APC/C activity is controlled by two co-activators, CDC20 and CDH1, which recruit target substrates to the APC/C (Kraft et al., 2005). The co-activators will be discussed in more detail later (Peters, 2006; Primorac and Musacchio, 2013).

The APC/C is a huge 1.5MDa complex comprising of at least 15 subunits (Peters, 2006; Thornton, 2006; Schreiber et al., 2011). Due to its multifaceted nature, its structural organisation as well as catalytic activity and inhibition are only recently starting to be understood through mutational and structural studies. However, it still remains unclear why the APC/C is such a large and complex E3, for example, compared, for example, to the other cell cycle regulating E3, the SCF, which contains three to five subunits (Peters, 2006; Deshaies and Joazeiro, 2009; Primorac and Musacchio, 2013).

3.2.4. APC/C architecture and subunit topology

Electron microscopy, as well as yeast studies assessing APC/C subunit knockout strains, has revealed a very distinctive structure of the APC/C, which can be simplified into three major sub-complexes: the platform, the arc lamp and the catalytic core (Fig.7,8A) (Gieffers et al., 2001; Vodermaier et al., 2003; Dube et al., 2005; Passmore et al., 2005; Thornton, 2006; Herzog et al., 2009; Barford, 2011; Buschhorn et al., 2011; Schreiber et al., 2011; Chang et al., 2014).

The platform contains the subunits APC1, APC4 and APC5 forming the base of the APC. Apart from proposed structural integrity, data also suggests that these subunits play an

important role in the binding of co-factors to the APC/C such as inhibitors (Dube et al., 2005; Passmore et al., 2005; Peters, 2006; Thornton, 2006).

The arc lamp is composed of the dimeric subunits (from bottom to top) APC8, APC6 and APC3. These proteins are known as the tetratricopeptide repeat (TPR) subunits, having a 34 amino acid helix-turn-helix structure, with the subunits APC3 and APC8 having been shown to be involved in binding two co-factors of the APC, the co-activators CDH1 and CDC20 (Herzog et al., 2009; Matyskiela and Morgan, 2009). To stabilise the TPR subunits, APC9, APC13 and Cdc26 localise between them acting as a form of glue. The arc lamp domain has been shown to exhibit flexibility and this has been speculated to relate to the APC/C's catalytic activity by stabilising the substrate-bound form of APC/C. Furthermore, in human APC/C, APC7 sits on top of the TPR subunits, although its function is not clearly understood (Vodermaier et al., 2003; Schwickart et al., 2004; Dube et al., 2005; Kraft et al., 2005; Thornton, 2006).

The catalytic core comprises the C-terminal cullin domain containing subunit APC2, which associates with the RING domain containing subunit APC11 and APC10 (Kurasawa and Todokoro, 1999). The minimal complex of APC2/APC11 is analogous to the Cul1/Rbx1 complex found in the SCF complex and is the minimum domain required to stimulate APC/C-dependent ubiquitination (Tang et al., 2001). The co-activators face into this catalytic core, opposite APC2/APC11, positioning the substrate with help of APC10 (da Fonseca et al., 2010; Buschhorn et al., 2011). The importance of APC10 will be discussed later.

A

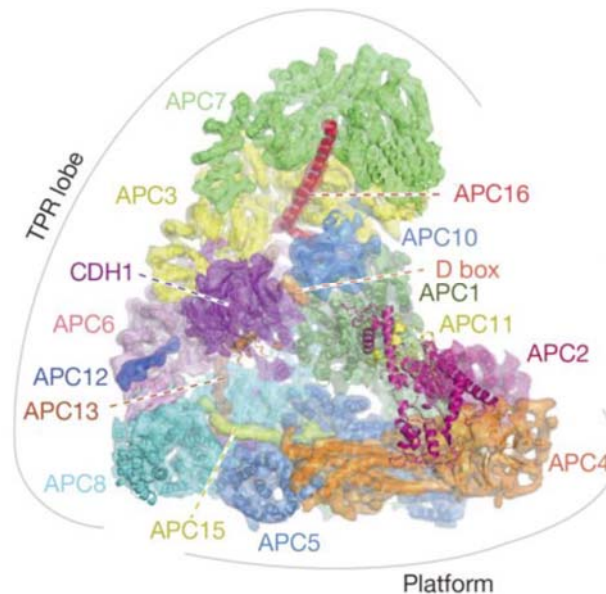


Figure 7: EM structure of the APC/C.

Subunits painted and labelled with respective colours. Resolution 7.4 Å (Chang et al., 2014).

3.2.5. Substrate recruitment by co-activators CDC20 and CDH1

The co-activators, CDC20 and CDH1, are required for the activation, as well as the recruitment of substrates to the APC/C. Association of the co-activators with the APC/C is highly regulated as it determines when the APC/C can wield its destructive force (Visintin et al., 1997; Peters, 2006).

CDC20 binding to the APC/C is promoted by phosphorylation of the APC/C by Cdk1-CylinB. Concurrently, phosphorylation of CDH1 prevents its binding to APC/C. At the metaphase to anaphase transition, as discussed, cyclin B is targeted to the proteasome, inactivating Cdk1. This stimulates the dephosphorylation of APC/C and CDH1, promoting the dissociation of CDC20 from the APC/C and the binding of CDH1 through to mid G1 phase (Kramer et al., 2000; Zachariae et al., 1998; Rudner and Murray, 2000; Kraft et al., 2003).

Structurally the co-activators are much conserved with both containing an unstructured N-terminus, as well as many tertiary structural elements, such as a C-box, WD40 domain and an IR tail. Both the C-box and the IR tail have been implicated in co-activator binding to the APC/C, the IR tail specifically through the TPR containing subunit APC3 (Fig.8B,D) (Passmore et al., 2003; Vodermaier et al., 2003; Dube et al., 2005). It is the C-terminal WD40 domain of the co-activators that is involved in substrate recognition, similar to the WD40 domain containing F-box protein in the SCF (Kraft et al., 2005).

The WD40 domain of both CDC20 and CDH1 interacts with specific degradation motifs or degrons found in APC/C substrates (Burton et al., 2005; Kraft et al., 2005). These short, conserved sequences are known as the D-box (RxxLxxxxN) and the KEN-box (KENxxxN/D/E) and APC/C substrates contain at least one of these elements (King et al., 1996; Pfleger and Kirschner, 2000; Burton and Solomon, 2001). For example, Cyclin B contains a D-box in its N-terminus which is sufficient for it to be ubiquitinated by the APC/C. Deletion of the N-terminal residues of Cyclin B prevents ubiquitination. Both Cyclin B and securin have been shown to bind in a D-box dependent manner to a conserved surface on one side of the co-activators WD40 domain and residues involved in this interaction have been identified (Kraft et al., 2005).

There are, however, many more substrates than just Cyclin B and these are ubiquitinated and targeted for degradation throughout mitosis and G1. For example, Cyclin A and Nek2A are targeted to the proteasome in pro-metaphase, escaping the spindle assembly checkpoint (Fiore and Pines, 2010; Hayes et al., 2006). On the other hand substrates like Cyclin B and securin are degraded at the metaphase to anaphase transition while other substrates like Aurora B and Plk1 are degraded even later, in G1. The ordered degradation of substrates has been attributed to kinetic differences of ubiquitination, with earlier degraded substrates more processively ubiquitinated. The co-activators CDC20 and CDH1 are believed

to play a role in this ordered degradation and the binding affinities of the D-box and KEN-box may influence this (Rape et al., 2006; Pines, 2011).

In addition to CDC20 and CDH1 acting as substrate adaptors for the APC/C, core subunits of the APC/C have also been implicated in substrate binding, particularly APC10. The crystal structure of APC10 revealed a jellyroll fold, which in other proteins has been shown to function as a binding surface, particularly for sugars (Wendt et al., 2001; Au et al., 2002). Indeed electron microscopy studies suggest that APC10 functions as a substrate binding surface (Fig. 8E) (Passmore et al., 2003; Carroll et al., 2005; da Fonseca et al., 2010; Buschhorn et al., 2011). Yeast experiments have shown that strains lacking APC10 (*doc1* in yeast) have difficulty in building higher molecular weight ubiquitin chains on substrates consistent with APC10 being part of the ligand binding interface. APC10 has therefore been labelled a processivity factor (Carroll and Morgan, 2002; Passmore et al., 2003; Carroll et al., 2005).

Recently, crosstalk between substrate-bound co-activators and, the APC/C E2, UBE2S was reported to greatly stimulate the rate of substrate ubiquitination. This nicely illustrates the multifaceted nature of the constituents of the APC/C in that co-activators are not just substrate receptors but are also involved in catalysis (Van Voorhis and Morgan, 2014).

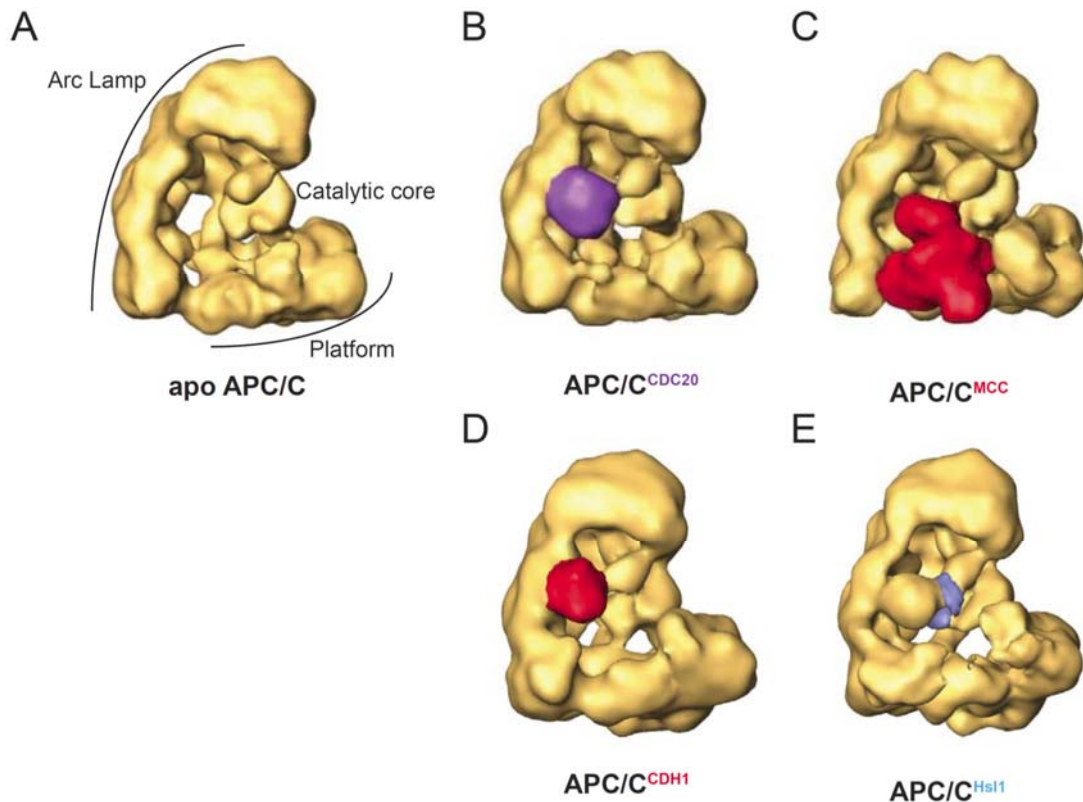


Figure 8: EM structures of different APC/C states.

EM structures of (A) apo-APC/C with domains labelled (B) APC^{CDC20} CDC20-purple (C) APC^{MCC} MCC-red (D) APC^{CDH1} CDH1-red (E) APC^{CDH1+Hsl1} Hsl1-light blue. Modified from (Buschhorn et al., 2011)

3.2.6. The APC/C functions with two E2s, UBCH10 and UBE2S

The APC/C functions in conjunction with two E2s to initiate and assemble K11 linked poly-ubiquitin chains on substrates. This two-step mechanism was first identified in yeast where it was found that Ubc4 and Ubc1 sequentially build poly-ubiquitin chains on substrates. Ubc4 promotes rapid mono-ubiquitination on multiple substrate lysines whereas Ubc1 catalyses K48 linked poly-ubiquitination. In humans, this same principle has also been established in that the APC/C functions together with UBCH10 and UBE2S (Rodrigo-Brenni and Morgan, 2007; Williamson et al., 2009). Depletion of both UBCH10 and UBE2S leads to a dramatic stabilisation of APC/C substrates (Townesley et al., 1997).

UBCH10 has been shown to mono-ubiquitinate substrates, initiating ubiquitin chain formation through recognition of a TEK box, a lysine-rich sequence found downstream of D- and KEN-boxes. Deletion of TEK boxes has been shown to stabilise APC/C substrates (Lin et al., 2002; Jin et al., 2008). When incubated with the minimal APC/C ligase module of APC2/APC11 UBCH10 bound APC2 and was able to catalyse low molecular weight ubiquitin chains (Tang et al., 2001). Surprisingly, however, that depletion of UBCH10 stabilised APC/C substrates to a lesser extent than inhibiting the APC/C suggesting that there could be another E2 functioning with the APC/C (Jin et al., 2008). In vitro, the E2 UBCH5 has also been shown to interact with the APC/C and build ubiquitin chains albeit with reduced efficacy. UBCH5 however, is a very promiscuous E2 since it has been shown to interact with many E3s.

Suitably, a second, and arguably more interesting E2, UBE2S was identified (Garnett et al., 2009; Williamson et al., 2009; Wu et al., 2010). In contrast to UBCH10, UBE2S can function in the absence of APC/C, as it can orient its donor ubiquitin in a closed, active conformation allowing APC/C-independent discharge (Pruneda et al., 2011). Following ubiquitin chain initiation by UBCH10, UBE2S builds ubiquitin chains in a K11 linked manner. K11 linkage specificity seems to be determined by residues in the $\alpha 3$ helix of the UBE2S UBC making contact with the acceptor ubiquitin (Wickliffe et al., 2011; Sheng et al., 2012). Interestingly UBE2S has also been shown to interact with the WD40 domains of CDC20 and CDH1; this has not been observed for UBCH10, and suggests being a mode in which both E2s can occupy the APC/C concurrently (Williamson et al., 2009; Garnett et al., 2009; Wu et al., 2010; Sako et al., 2014). UBE2S catalytic activity is regulated by Emi1, which shares a common C-terminus and so blocks UBE2Ss binding to the APC/C (Frye et al., 2013; Sako et al., 2014).

4. Aim of this study

As introduced, ubiquitination is a key mechanism by which the cell can control important cellular events. The RING E3 ubiquitin ligase, the anaphase promoting complex (APC/C) regulates critical cell cycle events, particularly the metaphase to anaphase transition, by catalysing ubiquitin chain formation on key substrates, targeting them for proteasomal degradation. As an E3 ligase, the APC/C provides a platform which can bind E2~Ub and substrate, and facilitates the transfer of ubiquitin from the E2~Ub to the substrate promoting ubiquitin chain formation. Despite the increased understanding of the APC/C and in general of RING mechanism, critical details still elusive.

We aimed to decipher how the E2 UBE2S interacts with the APC/C and the molecular mechanism by which UBE2S transfers ubiquitin to substrate. We conducted UBE2S immunoprecipitation experiments with APC/C and identified residues in UBE2S important for its stable association with APC/C. Furthermore, a surface alanine scan of UBE2S identified residues critical for its APC/C dependent and independent function.

Having addressed the principle of how an E3 binds E2~Ub, it was logical to also investigate how the APC/C recognises its substrates. At the initiation of this study, it had been identified that the co-activators CDC20 and CDH1 interacted, through their C-terminal WD40 domains with D-box and KEN box degrons found in APC/C substrates. To understand this at a molecular level, we pursued crystallographic studies to determine the crystal structure of a co-activator in complex with a substrate. Firstly, we identified a structurally compact form of the WD40 domain of the co-activators and showed its ability to bind the *Saccharomyces cerevisiae* APC/C substrate Hsl1 as well as peptides containing Hsl1's respective D-box and KEN-box degrons. We then subjected the complexes to crystallographic screening with promising conditions identified and optimised to yield single crystals.

5. Results

5.1. UBE2S recruitment and interaction with the APC/C

Despite the increasing molecular understanding of how RING E3 ligases interact with their E2 partners, it is becoming apparent that while many E2-E3 interactions follow a canonical mechanism, many exceptions exist. The APC/C functions with two E2s, UBCH10, which initiates ubiquitin chain formation and UBE2S, which subsequently builds poly-ubiquitin chains (Rodrigo-Brenni and Morgan, 2007; Williamson et al., 2009). From previous studies, it has become evident that UBCH10 interacts and functions with the APC/C in the canonical way through a well understood RING E3 mechanism. However, there are indications that UBE2S may interact with the APC/C differently.

We therefore set out to understand how UBE2S functions with the APC/C by addressing the first two principles of ubiquitination; 1: How does the APC/C recruit the UBE2S~Ub species and 2: how does the APC/C activate the UBE2S~Ub species.

5.1.1. UBE2S binds APC/C through its extreme C-terminal tail residues

To elucidate what UBE2S residues are necessary for the interaction with the APC/C, we performed co-IP assays in which we observed the ability of a panel of Flag-tagged UBE2S mutants to form stable complexes with recombinant APC/C.

Wild type UBE2S was able to co-IP wild type APC/C, with both CDC20 and CDH1 and in the presence and absence of the substrate Ub-Cylin B1-95, as expected (Fig.9). Mutants in the ubiquitin conjugating (UBC) domain were also able to co-IP APC/C indicating, as the name suggests, that this domain has a different function than to the one that was being assayed. However, from our panel of UBE2S mutants it became apparent that C-terminal residues, L219A, R221A and L222A, of UBE2S were involved in APC/C binding since these mutants did not co-IP APC/C (Fig.9•).

A

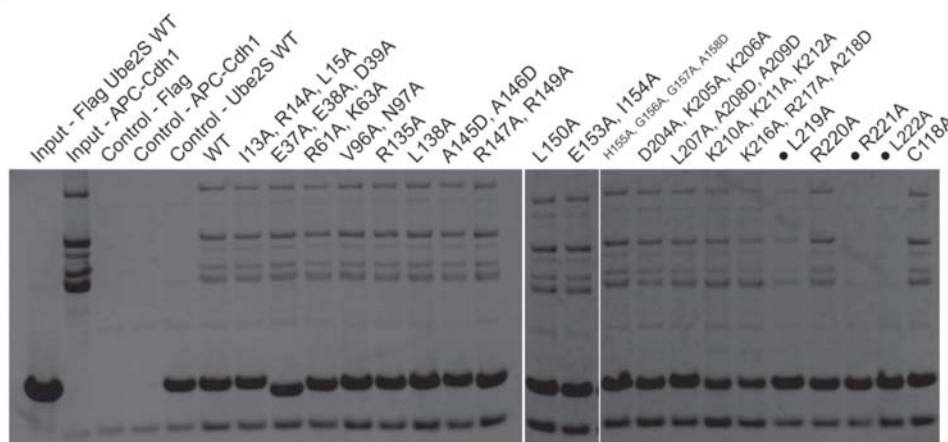


Figure 9: UBE2S stably binds the APC/C through its C-terminal residues.
Flag-UBE2S mutants were incubated with APC^{CDH1} for 3 hours before a Flag IP was performed and samples were analysed by SDS-PAGE and stained with coomassie.

5.1.2. The APC/C platform domain is sufficient to bind UBE2S

Having identified the UBE2S residues important for APC/C binding, we set out to map the subunits of the APC/C that are required for recruitment of this non-canonical E2. It was hypothesised that the platform domain (APC1/APC2/APC4/APC5/APC11) of the APC/C could bind UBE2S. To test this hypothesis, Flag-UBE2S (wild type and mutant L222A) were incubated with variants of the platform domain.

Flag-UBE2S, wild type, was able to co-IP the platform domain and APC/C in similar amounts (Fig.10). In contrast and as expected, the UBE2S C-terminal tail mutant, Flag-UBE2S L222A, was unable to co-IP the platform domain and its variants (Fig.10).

5.1.3. The APC2/APC11 is not sufficient to bind UBE2S

Having identified that UBE2S binds to the APC/C platform domain, we speculated if the catalytic, cullin-RING subunits, APC2/APC11, of the APC/C, were sufficient to recruit UBE2S to the APC. We again performed the co-IP assays, as previously described, however, this time the assay was performed with Flag UBE2S, wild type and L222A, in the presence of either APC/C or only APC2/APC11.

Both wild type and mutant L222A UBE2S were unable to co-IP the APC2/APC11 complex compared to wild type APC/C (Fig.10,•). This suggests that the UBE2S does not bind the catalytically implicated cullin/RING subunits of the APC/C with high affinity but to other proximal platform subunits in the APC/C.

A

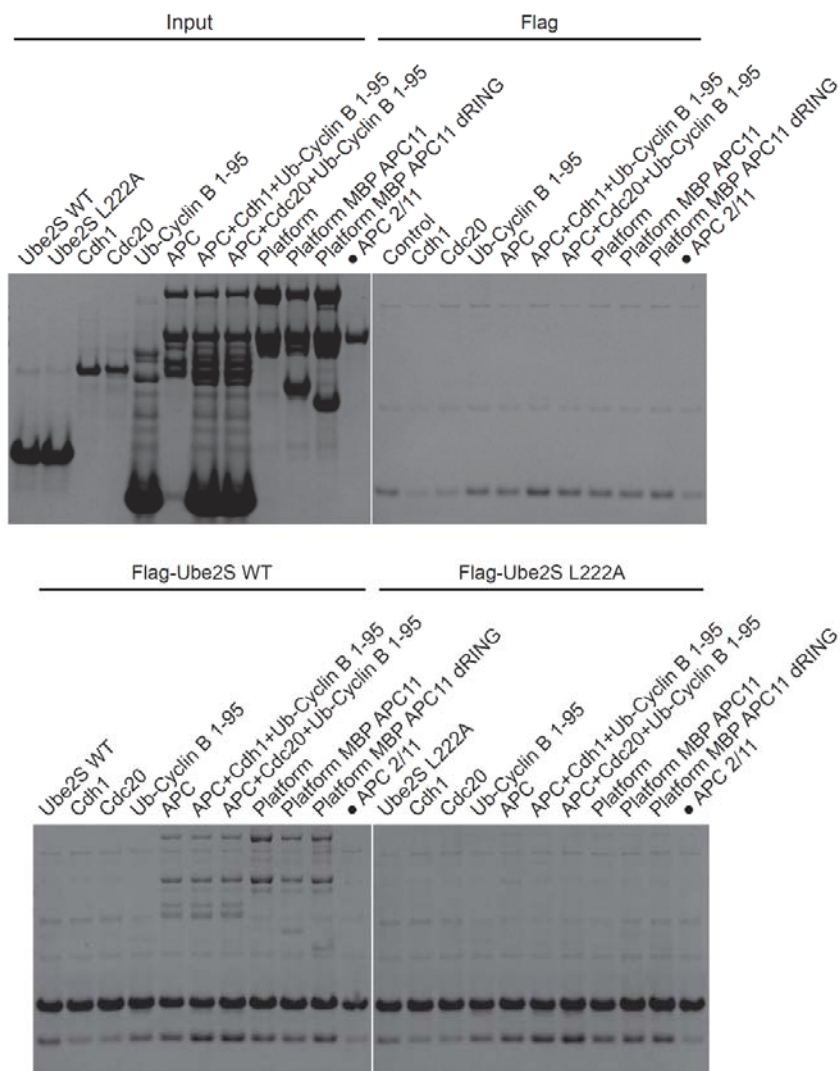


Figure 10: UBE2S binds to the APC/ platform domain.

Flag-UBE2S WT and Flag-UBE2S mutant L222A were incubated with APC^{CDH1}, APC^{CDH1}+CyclinB 1-95, APC^{CDC20}+CyclinB 1-95 or the respective APC/C platform domain variant for 3 hours before a Flag IP was performed and samples were analysed by SDS-PAGE and stained with coomassie.

5.1.4. Catalytic surface alanine scan of UBE2S reveals multiple surfaces

Having identified the APC/C domain to which UBE2S is recruited to and binds, our attention shifted to UBE2S itself and trying to elucidate the mechanism by which UBE2S functions with the APC/C.

We performed a two-step in vitro assay of over 130 UBE2S mutants that were designed, by aid of the published UBE2S core domain crystal structure, to probe the various surfaces of UBE2S. First, UBE2S mutants were evaluated in their ability to catalyse APC-dependent ubiquitination of Ub-Cyclin B1-95 identifying mutants that disrupt the tri-enzyme ubiquitination cascade. Subsequently, defective UBE2S mutants were assessed in their ability to auto-ubiquitinate themselves in an APC-independent manner, following the reasoning that APC-dependent mutants would still be expected to display intrinsic activity.

This two-part screen identified six surfaces of UBE2S: an E1 binding surface, the donor ubiquitin binding surface, the acceptor ubiquitin binding surface, a 'backside' surface and a helix at the C-terminus of the UBC domain as well as the C-terminus of the tail (Fig.12).

5.1.4.1. E1 binding surface

The first, most N-terminal, residues identified corresponded to the $\alpha 1$ helix of UBE2S. These displayed quite a severe defect in APC-dependent ubiquitination of Ub-Cyclin B1-95, particularly mutant I13A,R14A,L15A (Fig.11A,blue). The ability of these UBE2S mutants to auto-ubiquitinate themselves was also markedly reduced (Fig.11B,blue). Published crystal structures have identified this helix as interacting with E1 therefore one could assume that the defects observed are due to a lack of ability to load activated donor ubiquitin (Fig.26).

5.1.4.2. Donor ubiquitin binding surface

The second surface identified was the donor ubiquitin binding patch as identified by Wickliffe and colleagues (Wickliffe et al., 2011). UBE2S mutants, such as K117A,C118A, corresponding to this surface, were deficient in both APC/C dependent and independent ubiquitination (Fig.11A,B,purple). This reflects their inability to load and interact with donor ubiquitin due to disruption of the hydrophobic binding surface of UBE2S.

5.1.4.3. Acceptor ubiquitin binding surface

The next surface identified was the acceptor ubiquitin binding patch also identified by Wickliffe (Wickliffe et al., 2011). Similar to mutants in the donor ubiquitin binding surface, these mutants were also defective in APC/C-dependent and -independent ubiquitination consistent

with the inability to interact with acceptor ubiquitin (Fig.11A,B,pink). Mutant V96A,N97A showed a more pronounced defect in both assays possibly reasoned by this mutant being situated right next to the catalytic cysteine, C95, of UBE2S accentuating the effects already observed by disrupting the acceptor ubiquitin interacting surface.

5.1.4.4. The ‘backside’ surface

On the opposite face to the donor and acceptor ubiquitin binding surfaces we identified our next surface (Fig.12,green). The backside of UBE2S consists of a four bladed beta sheet forming a rather large surface. Previous studies have implicated this surface in protein-protein interactions and allosteric regulation of an E2 (Das et al., 2009). Five UBE2S mutants were mapped to this surface owing to their inability to ubiquitinate Ub-Cyclin B1-95 in an APC-dependent manner (Fig.11A,green). These mutants were also unable to auto-ubiquitinate themselves except for UBE2S mutants R61A,K63A which displayed increased auto-ubiquitination compared to wild type UBE2S (Fig.11B,green). This suggests that R61A,K63A displays some kind of APC/C dependent function since this mutant is only defective in APC/C dependent assays; this will be discussed later.

5.1.4.5. The UBC domain C-terminal helix

The fifth surface identified corresponded to the C-terminal helix of the UBC domain of UBE2S (Fig.12,orange). These mutants all showed defects in their ability to ubiquitinate Ub-Cyclin B1-95 in an APC-dependent manner however, mutant E153A,I154A had the most pronounced effect with very few low molecular weight ubiquitin conjugates being formed (Fig.11A,orange). In contrast, when assessing the ability of this mutants to auto-ubiquitinate themselves, E153A,I154A seemed to behave similarly to wild type UBE2S. Strikingly, UBE2S mutant R147A,R149A show a greatly increased ability to auto-ubiquitinate itself compared to wild type (Fig.11B,orange). This suggests that the C-terminal helix of the UBC domain interacts with the APC/C, as mutation obliterates APC-dependent but not -independent activity.

5.1.4.6. The C-terminal tail

The final surface identified was the C-terminal tail of UBE2S. The last three residues of UBE2S: R220, R221 and L222, showed defects in both their APC/C-dependent and -independent function (Fig.11A,B,red). Identification of this surface in our assays provided a validation for the co-IP experiments already presented. Interestingly L219, which did not co-IP APC/C, showed no catalytic defect. Mass-spectrometry validated the UBE2S mutants used in the experiments.

Figure 17: Catalytic surface ubiquitin load of UBE2S.

(A) UBE2S mutants were incubated with APC/C^{CDH1}, *Ub-CycB 1-95 and ubi mix for 12 minutes before reactions were analysed by SDS-PAGE and visualised by fluorescence detection.

(B) UBE2S mutants were incubated with *Ub and ubi mix for 60 minutes before reactions were analysed by SDS-PAGE and visualised by fluorescence detection.

E1 binding surface-blue, donor ubiquitin surface-purple, acceptor ubiquitin binding surface-pink, UBE2S backside-green, UBC C-terminal helix-orange, tail-red.

A

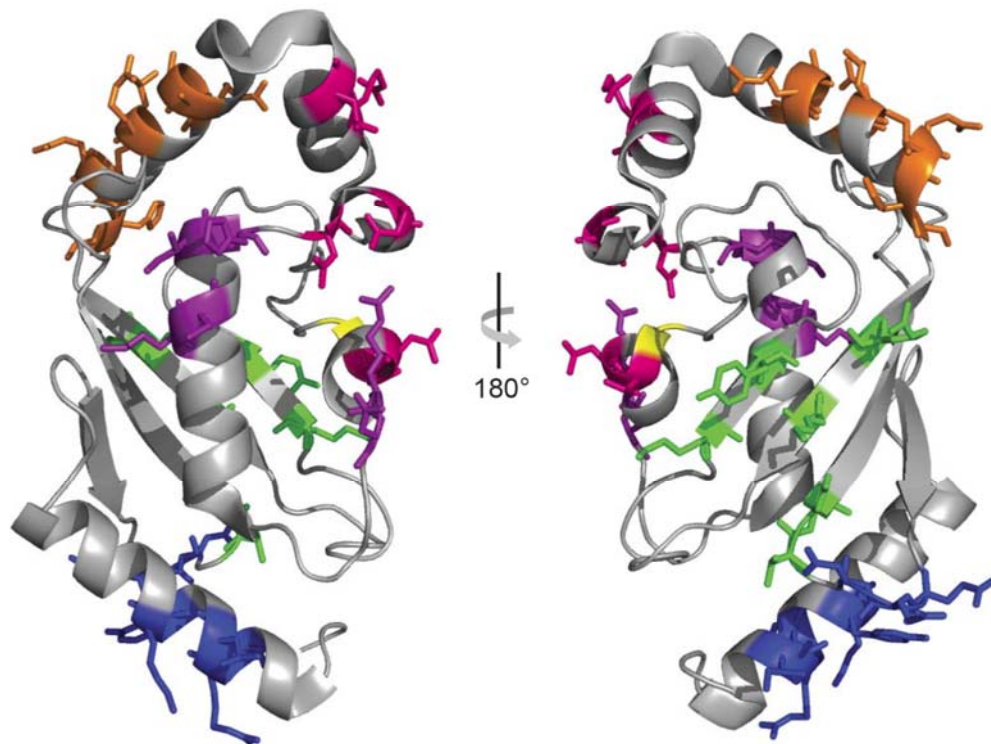


Figure 12: Structural representation of UBE2S mutants found to be defective in APC/C-dependent catalysis.
E1 binding surface-blue, donor ubiquitin surface-purple, acceptor ubiquitin binding surface-pink, UBE2S backside-green, UBC C-terminal helix-orange. PDB:1ZDN

5.2. Structural basis for co-activator – substrate interaction

Activation of the APC/C requires the mitotic stage specific association of one of two co-activator proteins, CDC20 and CDH1. The co-activators contain a C-terminal WD-40 domain which has been shown to mediate the binding of APC/C substrates. The interaction between co-activators and substrates is facilitated by destruction motifs, or degrons, (D-box: RxxLxxxxN/Q/E, KEN-box: KENxxxN/D/E) found within these substrates (Pfleger and Kirschner, 2000; Kraft et al., 2005). Given these sequences are very short and unconserved, they can be found multiple times in the primary amino acid sequence of APC/C substrates. However, only a small fraction of identified degrons have been shown to be important for the degradation of its containing substrate.

This project therefore set out to crystallise a co-activator in the presence of a substrate to determine the structural basis for co-activator – substrate interaction. This project was conducted in part in collaboration with Georg Petzold, a former PhD student of the Peters lab.

5.2.1. A 3Myc-His6 tag stabilises the APC/C co-activator proteins

Previously reported expression levels of both CDH1 and CDC20 indicated that despite using insect cells as an expression system, (co-activators are insoluble from bacteria), purified yields were low, too low to pursue crystallographic studies.

We found however, that when the co-activators were expressed as a fusion protein with an N-terminal 3myc-his6 (3MH6) tag and purified from a similar amount of insect cells, the resulting yield was approximately 15x higher than previously seen. Encouragingly, the 3MH6 tagged co-activators were also able to bind and immuno-precipitate APC/C at similar levels, as well as being functional for APC/C ubiquitination activity (data not shown).

5.2.2. Purification of full length co-activators is troublesome

Despite the encouraging increase in protein yield due to the effects of the N-terminal 3MH6 tag, purification of both co-activators was still not trivial. After initial purification and following subsequent size exclusion chromatography, a large proportion of the co-activators eluted in the void volume, suggesting protein aggregation.

Using the Hofmeister series, we developed a buffer that would stabilise the co-activators during purification. The Hofmeister series ranks ions based on their ability to stabilise proteins, with stabilising ions categorised as kosmotropes and de-stabilising ions as chaotropes (Zhang and Cremer, 2006). According to the series, ammonium sulphate is a strong kosmotrope unlike potassium chloride which had been used in existing protocols thus far. Following size exclusion chromatography, using an ammonium sulphate based buffer, the proportion of the co-activators eluted in the void volume was markedly reduced owing to

ammonium sulphate's stabilising properties. Furthermore, the apparent molecular mass of the co-activators, as judged by the size exclusion chromatography elution volume, did not change, illustrating that the different salt conditions did not have an effect on native protein folding (data not shown).

Given these advances in purifying the full length co-activators, this gave a good foundation to pursue crystallographic trials.

5.2.3. Identification of a structured domain in CDC20/CDH1

An interesting observation following size exclusion chromatography was the exaggerated ~150 kDa apparent mass of the co-activators (actual molecular mass: 55 kDa). This suggested that the co-activators exhibit some unstructured, non-globular regions in their structure, a property not suitable for crystallographic studies.

Assuming that the 3MH6 tag is predicted to be unstructured, a PreScission cleavage site was introduced between the tag and the co-activators. Surprisingly, removal of the 3MH6 tag did not promote aggregation of the co-activators, although the behaviour of the co-activators during purification was markedly compromised compared to the 3MH6 tag fusion forms. Importantly, following size exclusion chromatography, the PreScission cleaved co-activator forms still displayed an exaggerated apparent molecular mass suggesting that it was not just the 3MH6 tag that exhibited an unstructured form but the co-activators themselves.

We therefore used bioinformatics to probe the predicted structure of the co-activators with the aim of designing deletions constructs of the co-activators that would be suitable for crystallographic studies.

Multiple sequence alignments revealed the C-terminus of the co-activators to be highly conserved (Fig.13A). Using DISpro, a server that analyses the protein's primary sequence to predict disordered domains, the N-terminus of the co-activators was assessed to be disordered (Fig.13B) (Cheng et al., 2005). Furthermore, analysis by SMART, revealed that CDC20 was predicted to contain seven WD40 repeats, starting from Pro169, whereas CDH1 was predicted to contain six WD40 repeats, starting from Gln218 (Letunic et al., 2012) (Fig.13C).

The prediction that the co-activators contain a C-terminal WD40 domain is consistent with published literature (Kraft et al., 2005). CDH1 however, is more than likely to contain seven not six WD40 repeats since residues Leu179 and Pro182 were implicated by Kraft et al. in D-box binding (one would expect protein-protein interactions are mediated by a structured protein domain not an unstructured domain as bioinformatically predicted).

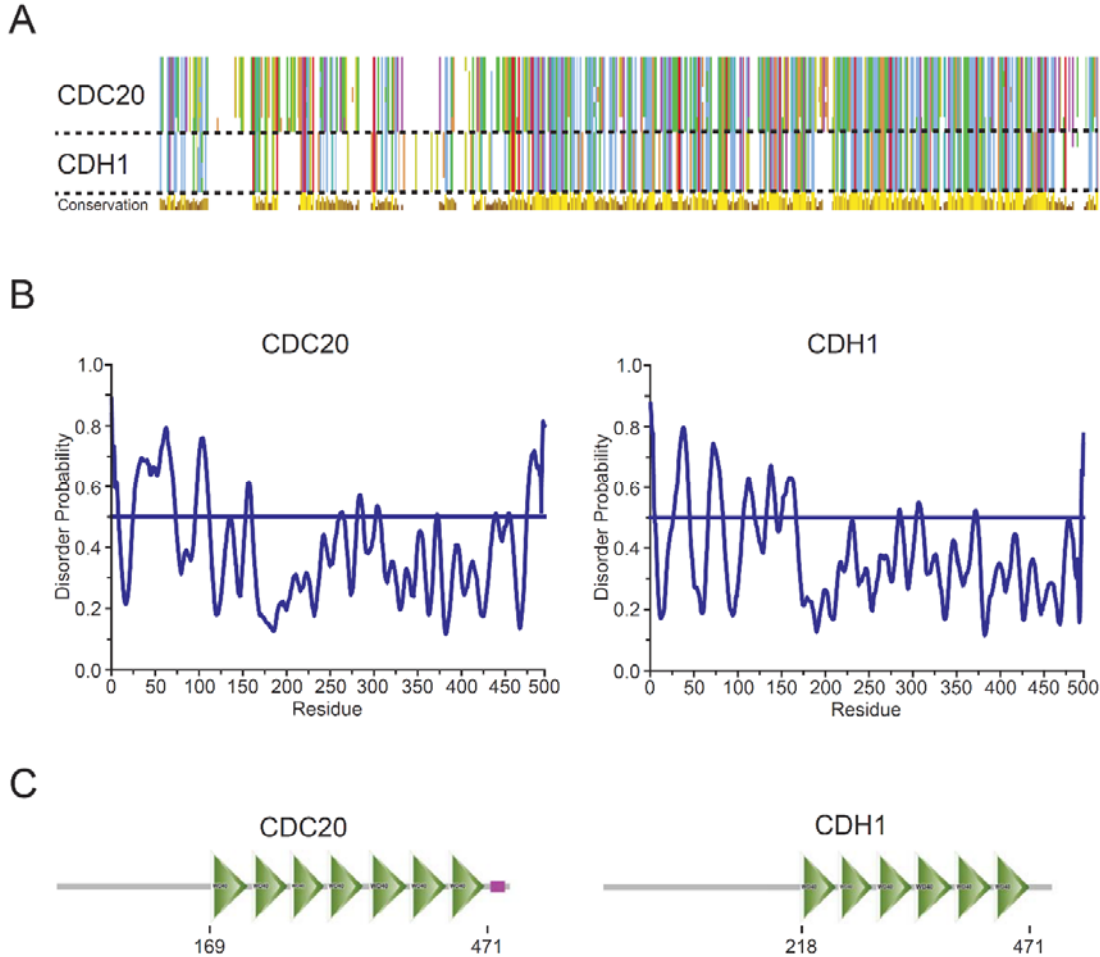


Figure 13: Bioinformatical analysis of CDC20 and CDH1.

(A) Multiple sequence alignment of CDC20 and CDH1 performed using Jalview. ClustalX colouring. (B) Structural disorder prediction of CDC20 and CDH1 performed using DisPro (Cheng et al., 2005). Probability >0.5 denotes disorder. (C) Domain prediction of CDC20 and CDH1 performed using SMART (Letunic et al., 2012) (<http://smart.embl-heidelberg.de/>).

5.2.4. Limited proteolysis of CDC20/CDH1 reveals a globular C-terminus

To confirm our bioinformatical analysis, 3MH6 CDC20 FL and 3MH6 CDH1 FL were subjected to limited proteolysis to identify globular domains within the co-activators. The co-activators were treated with 1 μ g of the protease chymotrypsin over a time course of 3 hours. After chymotrypsin treatment, the samples were separated by SDS-PAGE with observed stable fragments sent for analysis by N-terminal Edman sequencing.

SDS-PAGE analysis of CDC20 revealed three major stable fragments of ~40 kDa in size forming after one hour of chymotrypsin digestion (Fig.14). Analysis by N-terminal Edman sequencing identified these fragments as starting from Leu94, Ala117 and Arg132 (Fig.15A, Δ). Interestingly, when identifying potential chymotrypsin cleavage sites in CDC20,

using the ExPASy PeptideCutter, four sites were identified between the last identified stable fragment start site and the predicted start of the WD40 domain suggesting the WD40 domain extends slightly more to the N-terminus than predicted (Fig.15A,8<).

With CDH1 however, a different type of behaviour was observed. After two hours of chymotrypsin digestion, two prominent bands of ~34 kDa in size appeared (Fig.14). When these two fragments were analysed by N-terminal Edman sequencing they surprisingly started with the same residue, Ser149, suggesting that the difference observed between the two fragments was due to variances in the C-terminus (Fig.15B,Δ). In addition, N-terminal Edman sequencing also identified a fragment starting at Arg162 however, the confidence in the sequencing result was not very high. Like CDC20, the CDH1 fragments identified also contained potential chymotrypsin cleavages sites between their N-terminus and the predicted start of the WD40 domain suggesting that the WD40 domain extends towards the N-terminus of CDH1 beyond Gln218 (Fig.15B,8<). Interestingly within this region, a non-predicted WD40 repeat could exist since the ~70 amino acids in question could easily accommodate a WD40 repeat of ~20 (plus linker to the following WD40 repeat) amino acids in length. Furthermore, WD40 repeats often terminate with a Trp-Asp dipeptide, although this is not always the case, and within this region there are potential WD40 repeat terminating dipeptides involving Trp-Ser.

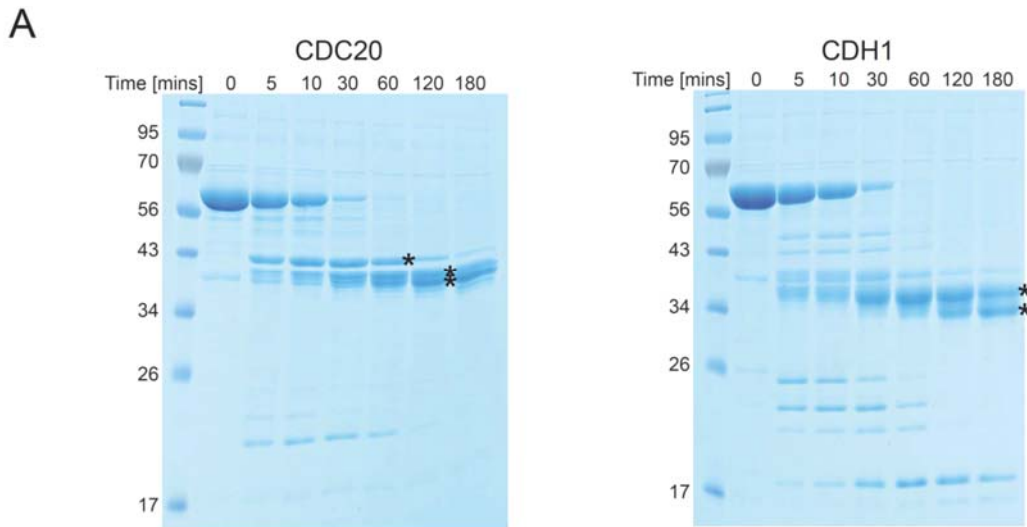
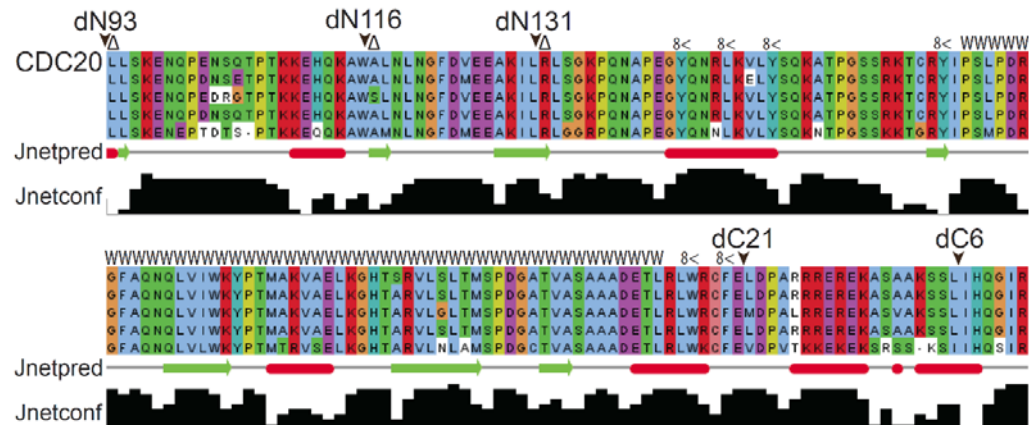


Figure 14: Limited proteolysis of CDC20 and CDH1.

(A) CDC20 and CDH1 were incubated with 1 μ g chymotrypsin over a 3 hour time course at 4°C. Respective time points were taken and analysed by SDS-PAGE.

A



B

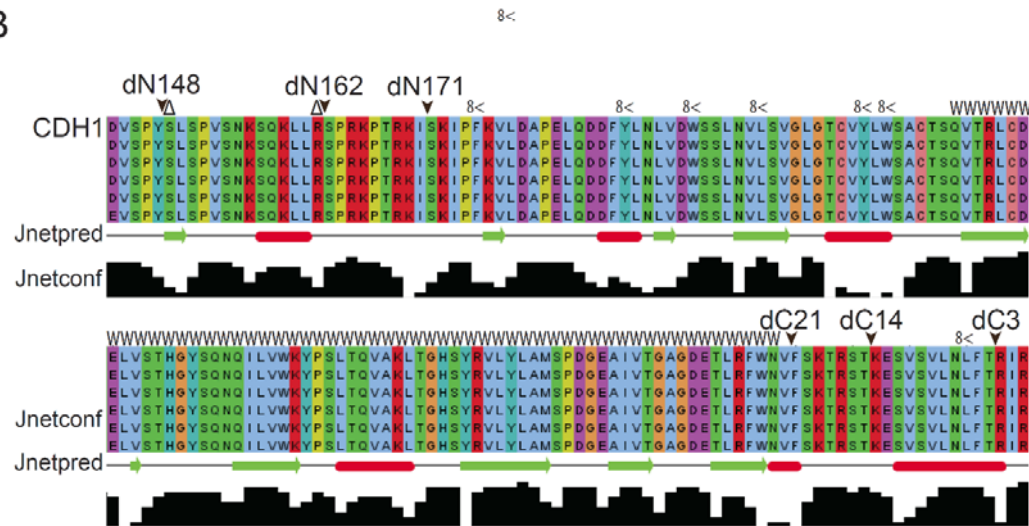


Figure 15: Multiple sequence alignments of CDC20 and CDH1.

(A) Sequence alignment of CDC20 with annotations indicating: Δ -N-terminal Edman sequencing result, \blacktriangledown -engineered N/C-terminus of designed deletion constructs, 8<-predicted chymotrypsin cleavage sites (Expasy-PeptideCutter), W-predicted WD40 domain according to SMART. (A) Sequence alignment of CDH1 with same annotations as in (A).

5.2.5. CDC20/CDH1 deletion constructs are more stable than full length co-activators

Having identified the globular domains of both CDC20 and CDH1, we set out to design and test various deletion constructs with the aim of identifying a construct that was structurally compact and globular and that behaved well during purification. We tested a range, and different combinations, of N- and C- terminal deletions assessing their suitability by size exclusion chromatography.

For CDC20 three N-terminal truncations were tested, (dN96, dN116 and dN131), in combination with two C-terminal truncations, (dC6 and dC21), (Figs.15A▼,16A,). The closer the N-terminal truncation was to the predicted start of the WD40 domain the more unstable the respective deletion construct was. Remarkable was the influence of the C-terminus on the stability of the deletion constructs. Truncating the C-terminus of CDC20 immediately following the predicted end of the WD40 domain, (dC21), dramatically destabilised all the deletion constructs, irrespective of their N-terminal truncation (Fig.16C). In summary we decided that the deletion construct dN96-dC6 looked the most encouraging.

With respect to CDH1, we tested N-terminal truncation, (dN148, dN162 and dN171), in combination with C-terminal truncation, (dC3, dC14 and dC21), (Figs.15B▼,16B). As with CDC20, a similar trend was observed when comparing N- and C- terminal truncation of CDH1. The N-terminal truncation closest to the predicted start of the WD40 domain, dN171, dramatically destabilising CDH1. However, no marked difference was observed between the N-terminal truncations of dN148 and dN162. For the C-terminus, similar results were observed, with the truncation closest to the predicted end of the WD40 domain, dC21, dramatically destabilising the deletion constructs with no major difference observed between the dC14 and dC3 truncations (Fig.16D).

Given these results we settled on using 3MH6 CDC20 dN96-dC6 and 3MH6 CDH1 dN162-dC14 as the deletion constructs to pursue crystallographic studies with CDC20 and CDH1.

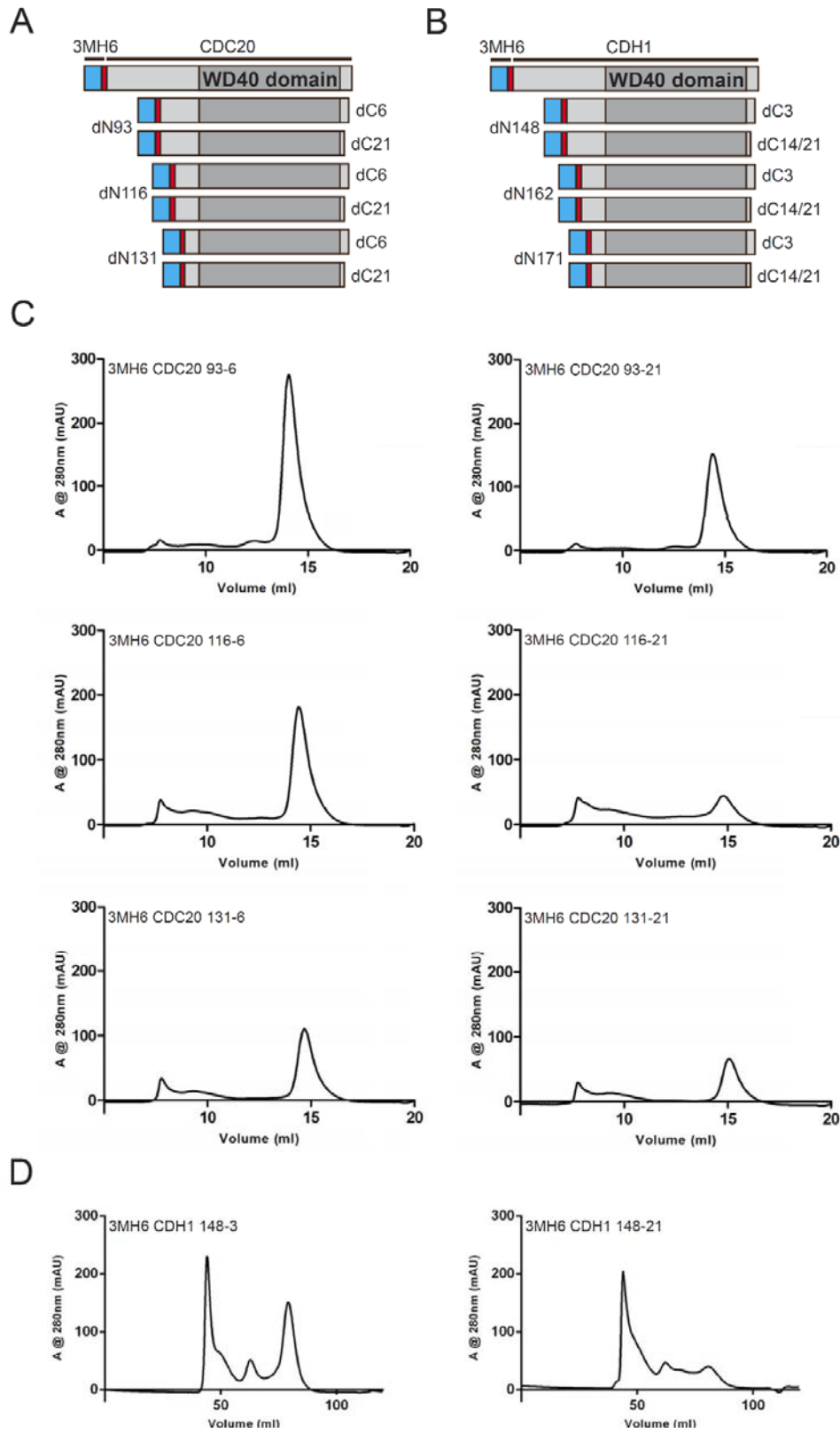


Figure 16: Screening of co-activator deletion constructs to identify optimal candidates for crystallographic studies.

(A) Schematic representation of Cdc20 deletion constructs tested for optimal stability. (B) As (A) but for CDH1. (C) Size exclusion chromatography profiles of CDC20 deletion constructs tested illustrated N- and C- terminal dependence on stability. (D) As (C) but for CDH1

5.2.6. CDH1/CDC20 deletion constructs bind substrates

Having selected CDC20 and CDH1 deletion constructs that we deemed promising for crystallographic studies, it was important to determine if the WD40 domain was still functional and could bind substrates.

For CDC20, we tested this with securin. Insect cells infected with a baculovirus co-expressing 3MH6 CDC20 93-6 and Flag-securin were purified and analysed by size exclusion chromatography as well as by SDS-PAGE. Unfortunately the interaction between the WD40 domain of CDC20 and securin appeared to be very weak as we were unable to co-purify securin with CDC20 (data not shown).

With CDH1, our substrate of choice was a fragment of the yeast protein Hsl1, Hsl1⁶⁶⁷⁻⁸⁷². Following co-expression and analysis by size exclusion chromatography and SDS-PAGE, it was observed that the CDH1 WD40 domain could impressively co-purify Hsl1⁶⁶⁷⁻⁸⁷². Size exclusion chromatography showed a dramatic shift to a higher molecular mass species when analysing the 3MH6 CDH1 162-14 + Hsl1⁶⁶⁷⁻⁸⁷² complex compared to just 3MH6 CDH1 162-14 (Fig.17A). This was further confirmed by SDS-PAGE when analysing the respective size exclusion chromatography fractions. The fractions corresponding to the higher molecular weight species, presumed the 3MH6 CDH1 162-14 + Hsl1⁶⁶⁷⁻⁸⁷² complex, showed two prominent bands of ~40 kDa and ~35 kDa, whereas fractions corresponding to just 3MH6 CDH1 162-14 showed just one band of ~40 kDa (Fig.17B).

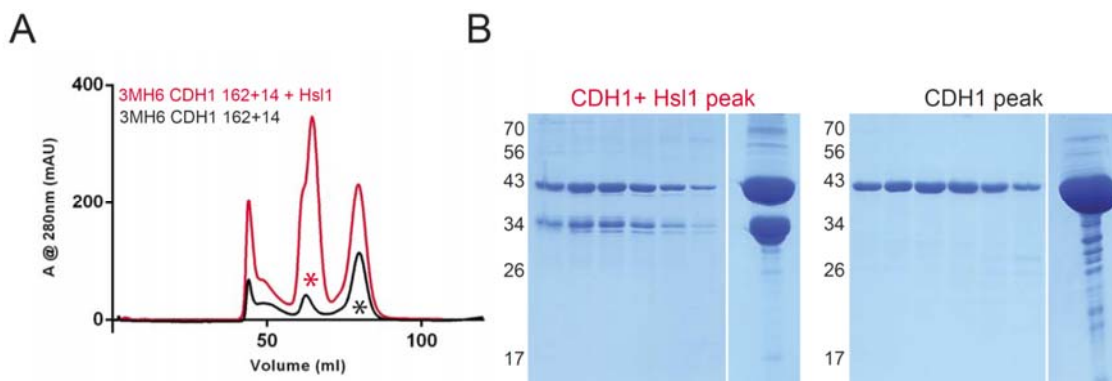


Figure 17: CDH1 WD40 domain binds substrates.

(A) Size exclusion chromatography profile overlays of 3MH6 CDH1 162-14 and 3MH6 CDH1 162-14 + Hsl1⁶⁶⁷⁻⁸⁷². (B) SDS-PAGE analysis of the respective peak fraction (*)

5.2.7. Hsl1 667-872 is unstructured

Comparable to the full length co-activators, we observed a large exaggeration of the apparent molecular mass of the 3MH6 CDH1 162-14 + Hsl1⁶⁶⁷⁻⁸⁷² complex as judged by size exclusion chromatography, ~110 kDa compared to an expected 65 kDa, suggesting that the complex exhibited some unstructured domains.

Limited proteolysis, using 1 µg of the protease chymotrypsin, revealed that the 3MH6 CDH1 162-14 + Hsl1⁶⁶⁷⁻⁸⁷² complex was rapidly proteolytically cleaved compared to the 3MH6 CDH1 162-14 deletion construct suggesting that Hsl1⁶⁶⁷⁻⁸⁷ is unstructured (Figs. 19A,B). This was confirmed by western blotting which showed many degradation products of Hsl1⁶⁶⁷⁻⁸⁷ forming throughout the duration of the limited proteolysis time course (Figs. 19C).

We therefore designed a minimal deletion construct based on Hsl1⁶⁶⁷⁻⁸⁷ that contained both its D-box and KEN-box, referred to as Hsl1^{mini}. We were able to show by size exclusion chromatography and SDS-PAGE that Hsl1^{mini} was still able to bind the CDH1 deletion construct, 3MH6 CDH1 162-14 (Figs 19A,B).

Attempts to crystallise the 3MH6 CDH1 162-14 + Hsl1^{mini} complex were positive and we were able to obtain crystals in a condition containing 100 mM sodium cacodylate pH 6.5, 300 mM ammonium sulphate and 30% (v/v) PEG 8000 however, the resulting crystals diffracted in a weak and streaky manner (Figs.19C,D).

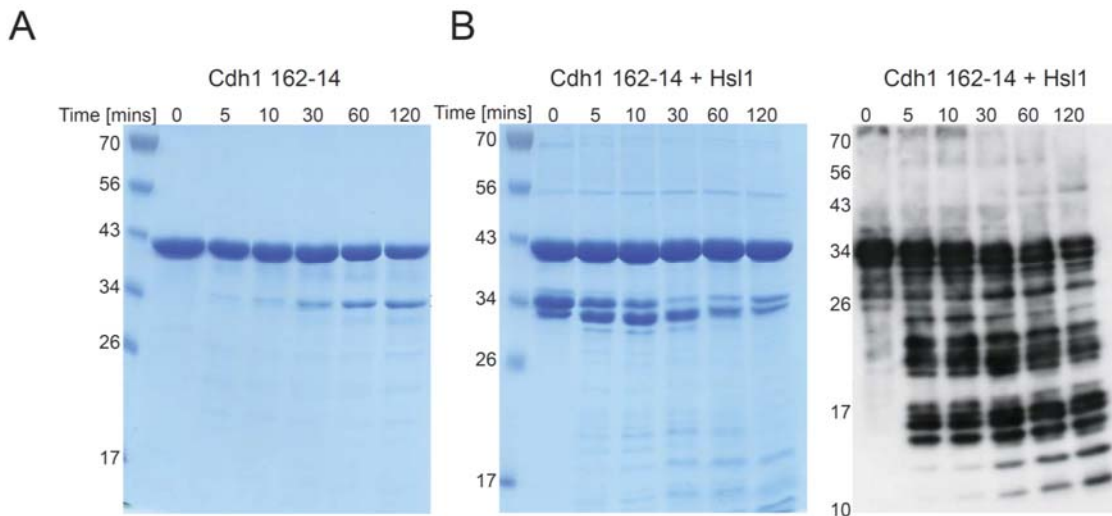


Figure 18: Limited proteolysis of 3MH6 CDH1 162-14 and 3MH6 CDH1 162-14 + Hsl1⁶⁶⁷⁻⁸⁷². (A) 3MH6 CDH1 162-14 was incubated with 1 µg chymotrypsin over a 2 hour time course at 4°C. Respective time points were taken and analysed by SDS-PAGE. (B) As (A) but for 3MH6 CDH1 162-14 + Hsl1⁶⁶⁷⁻⁸⁷² with the associated Western blot against Hsl1, α1739.

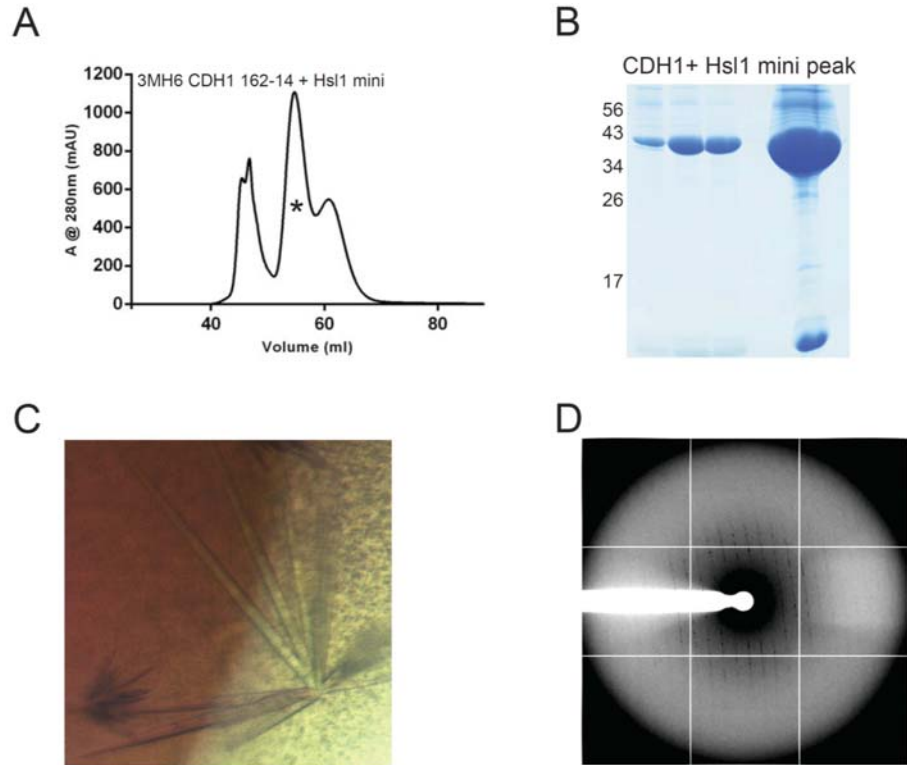


Figure 19: Crystallisation of 3MH6 CDH1 162-14 + Hsl1^{mini}.

(A) 3MH6 CDH1 162-14 + Hsl1^{mini} was purified and analysed by size exclusion chromatography profile. (B) SDS-PAGE analysis of the respective peak fraction (*) (C) Image of crystals grown with 3MH6 CDH1 162-14 + Hsl1^{mini} in 100 mM sodium cacodylate pH 6.5, 300 mM ammonium sulphate and 30% (v/v) PEG 8000 (D) Resulting diffraction pattern from crystals grown.

5.2.8. Binding of a ligand is beneficial for CDH1 stability

Having had not much success in growing well diffracting crystals of our 3MH6 CDH1 162-14 + Hsl1^{mini} complex, our attention focused to the binding properties of Hsl1 towards CDH1. Currently, all purifications and crystallography trials had been conducted in ammonium sulphate based buffers, a high ionic strength buffer. We considered that the high ionic strength of the buffer might interfere with the binding of the two degrons to CDH1 and so create a situation where we have heterogeneous binding of the Hsl1^{mini} degrons to CDH1 adversely affect crystal growth. To investigate this problem, we performed a thermal shift assay (differential scanning fluorimetry – DSF), assessing the thermal stability of CDH1 in different salts. We aimed to identify an optimal buffer condition that encompassed a lower ionic strength salt, such as sodium chloride, while still keeping CDH1 stable. In addition, we also compared the stability of CDH1 in the presence or absence of Hsl1⁶⁶⁷⁻⁸⁷².

As can be seen in figure (Fig. 20A), sodium chloride was more stabilising in the thermal shift assay than ammonium sulphate suggesting that further crystallography trials should be pursued in a sodium chloride buffer. Furthermore, and somewhat expectedly, the binding of Hsl1⁶⁶⁷⁻⁸⁷² to CDH1 greatly stabilised the complex as a whole (Fig. 20B).

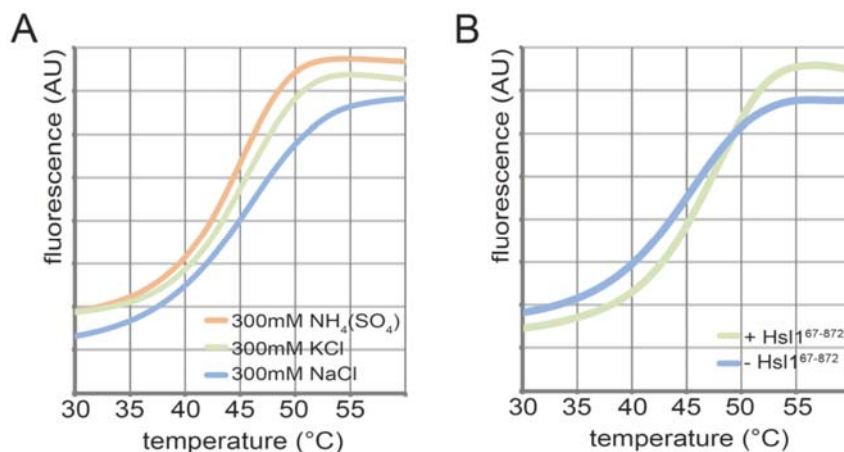


Figure 20: Differential scanning fluorimetry of CDH1 and CDH1 +Hsl1

(A) DSF of 3MH6 CDH1 162-14 in the presence of different salt buffers. (B) As (A) but of 3MH6 CDH1 162-14 and 3MH6 CDH1 162-14 + Hsl1⁶⁶⁷⁻⁸⁷² in 300mM NaCl.

5.2.9. Hsl1 D-box binds tighter to CDH1 full length than Hsl1 KEN-box

Having not had much success in growing well diffracting crystals of our 3MH6 CDH1 162-14 + Hsl1^{mini} complex, our attention turned to the binding properties of the Hsl1 D-box and KEN-box towards CDH1. One hypothesis was that the D- and KEN-boxes had different binding affinities towards the WD40 domain of CDH1 and so may be in various heterogenic orientations during crystallisation, thus allowing sub-optimal crystal growth.

To investigate this, isothermal titration calorimetry (ITC) experiments were performed where a ligand solution containing either an Hsl1 D-box or KEN-box peptide was titrated into a sample solution containing 3MH6 CDH1 full length. ITC measurements revealed that the Hsl1 D-box binds 3MH6 CDH1 ~3 fold tighter than the Hsl1 KEN-box does (450nM compared to 1.5 μ M) (Figs.21A,B).

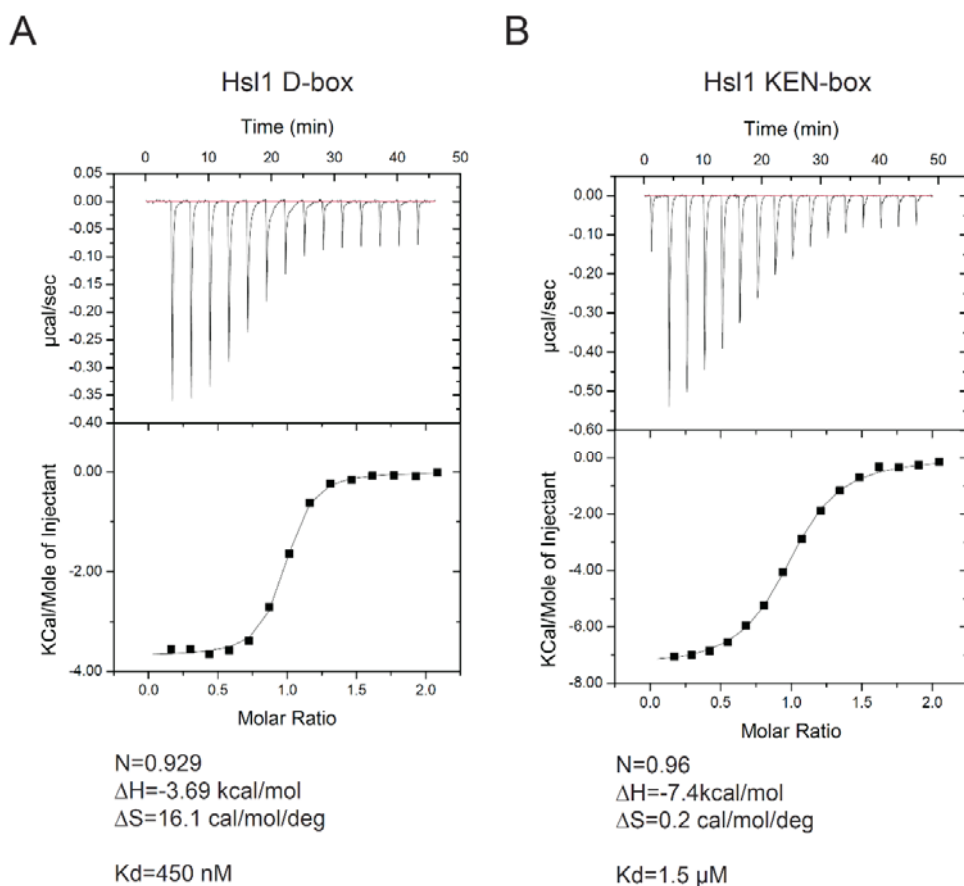


Figure 21: Isothermal titration calorimetry of Hsl1 D- and KEN-box peptides against CDH1. (A) ITC of Hsl1 D-box peptide titrated into CDH1. (B) As (A) but for Hsl1 KEN-box peptide. Peptide at 500 μ M and CDH1 at 50 μ M.

5.2.10. 1MH6 CDH1 162-14 + Hsl1 D-box peptide complex yields multi-lattice crystals

Identifying that the Hsl1 D-box had a ~3 fold smaller K_d towards CDH1 compared to the Hsl1 KEN box correlated with our hypothesis that we could indeed be trying to crystallise a heterogeneous complex population. It was therefore decided to pursue crystallography trials with the CDH1 162-14 deletion construct mixed in equi-molar amounts with an Hsl1 D-box peptide instead of Hsl1^{mini}.

Furthermore, we performed an experiment evaluating the importance of the 3MH6 tag in the stability of the CDH1 162-14 deletion construct. 1MH6, 2MH6 and 3MH6 versions of the tag were assessed in parallel and analysed by size exclusion chromatography. We found that the 1MH6 tag stabilised CDH1 162-14 to an equal degree with purified yields similarly unaffected (data not shown). It was therefore decided to use the deletion construct 1MH6-CDH1 162-14 in future crystallography trials.

Crystallisation attempts with the 1MH6 CDH1 162-14 + Hsl1 D-box complex yielded small multi-lattice crystals that were grown in the presence 100 mM sodium cacodylate pH 6.5 and 1 M sodium citrate (Fig.22C).

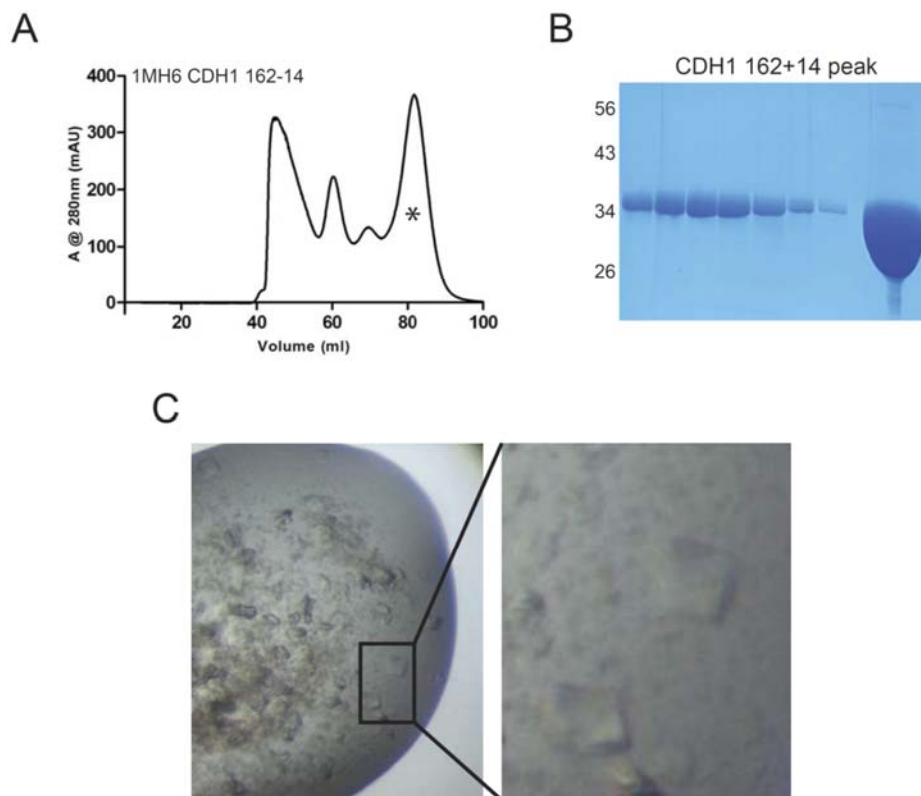


Figure 22: Crystallisation of 1MH6 CDH1 162-14 + Hsl1 D-box peptide.

(A) Purification and analysis by size exclusion chromatography profile 1MH6 CDH1 162-14 (B) SDS-PAGE analysis of the respective peak fraction (*) (C) Image of crystals grown with 1MH6 CDH1 162-14 + Hsl1^{mini} in 100 mM sodium cacodylate pH 6.5 and 1 M sodium citrate.

5.2.11. Sodium cacodylate promotes crystal growth

What became apparent from the crystallography trials tried thus far was that the presence of sodium cacodylate was consistently found in conditions that produced hits. We therefore repeated our initial crystal screening using 10 mM sodium cacodylate as an additive. This spurred reproducible crystal growth in multiple conditions, broadening the possibility of optimising a condition to obtain diffracting crystals (Table.1).

Crystals grown in 50 mM sodium cacodylate, 2 M ammonium sulphate and 10 mM magnesium sulphate were sent to the Schulman Lab at St Judes Childrens Research Hospital who kindly recorded diffraction data. Although the crystals showed an improvement in growth compared to previous crystals, the diffraction was still streaky, consistent with the multiple lattice crystals observed growing.

| | | | |
|---|--------------------------------|---|---------------------------|
| 1 | 100 mM Tris pH 7.0 | 1.0 M Sodium citrate | 200 mM Sodium chloride |
| 2 | 100 mM Sodium citrate pH 5.6 | 30% (w/v) PEG 4000 | 100 mM Ammonium sulphate |
| 3 | 100 mM Hepes pH 7.5 | 12% v/v (+/-)-2-Methyl-2,4-pentanediol | 100 mM Sodium citrate |
| 4 | 50 mM Sodium cacodylate pH 6.5 | 2.0 M Ammonium sulphate | 10 mM Magnesium sulphate |
| 5 | 50 mM Hepes pH 7.0 | 1.6 M Lithium sulphate | 50 mM Magnesium sulphate |
| 6 | 100 mM Imidazole pH 8.0 | 40% (v/v) 2-Methyl-2,4-pentanediol | 200 mM Magnesium chloride |
| 7 | 100 mM acetate pH 4.5 | 800 mM NaH ₂ PO ₄ / 1.2 M K ₂ HPO ₄ | |
| 8 | 100mM CAPS pH 10.5 | 1.2 M NaH ₂ PO ₄ / 800 mM K ₂ HPO ₄ | 200mM Lithium Sulphate |
| 9 | 100mM Tris pH 8.5 | 1.2 M Ammonium sulphate | 15% Glycerol |

Table 1: Conditions that produced crystal growth in the presence of 10 mM Sodium cacodylate

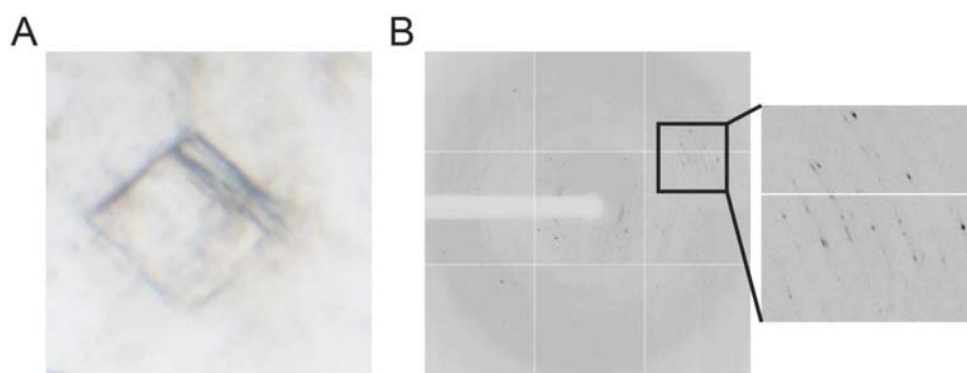


Figure 23: Crystalisation of 'large drop' 1MH6 CDH1 162-14 + Hsl1 D-box peptide.

(A) Multi-lattice crystals grown in 100 mM Tris pH 7, 1 M sodium citrate and 200 mM sodium chloride (B) respective diffraction pattern recorded at Ser-CAT, Argonne National Laboratory, IL, USA.

5.2.12. Streak seeding yields small single lattice crystals

Despite being able to diffract, the crystals grown thus far grew in multiple lattices meaning that any diffraction data collected appeared streaky due to the X-ray beams travelling through multiple lattices.

We therefore invested a lot of effort in trying to grow single lattice crystals. We focused on three conditions, 1, 4 and 7 in table 1, which we found to be the most reproducible. We performed grid screens around these conditions as well as additive screens which gave rise to the fact that the addition of lithium sulphate and sodium chloride had a beneficial effect. A big step forward came when we were able to translate crystal growth from 300 nL drops, using a protein: liquor ratio of 2:1, to 2 μ L drops, using a ratio of 1:1. This made crystal drops more amenable to manipulation. Analysis of a crystal grown in such a large drop in the condition 100 mM Tris pH 7, 1 M sodium citrate and 200 mM sodium chloride yielded higher diffracting data however the diffraction pattern was still very streaky, reminiscent of previous multi-lattice crystals (Figs.23A,B).

Modification of this condition to 100 mM Tris pH 7, 0.8 M sodium citrate and 200 mM sodium chloride coupled with streak seeding gave single lattice crystals albeit really tiny ones of approximately 0.2-0.4 μ m in size (Fig.24A). Sadly however, despite observing single lattice diffraction, these crystals diffracted very weakly, albeit to 3Å (Fig.24B).

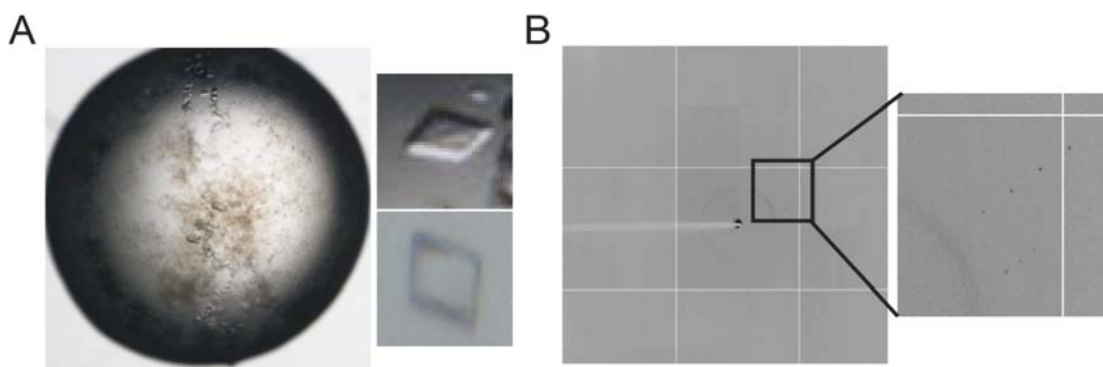


Figure 24: Crystalisation with streak seeding of 1MH6 CDH1 162-14 + Hsl1 D-box peptide.

(A) Multi-lattice crystals grown in 100 mM Tris pH 7, 0.8 M sodium citrate and 200 mM sodium chloride
 (B) respective diffraction pattern recorded at Ne-CAT, Argonne National Laboratory, IL, USA.

5.2.13. Reducing the Hsl1 KEN-D-box linker length improves complex behaviour

Given the lack of success in producing a well diffracting crystal, we reflected on the optimisations that already had been tried and what else there was left to explore. Thus far crystallisation trials were heavily pursued using a Hsl1 D-box peptide as a substrate on the basis that it binds with a higher K_d to CDH1 than the KEN-box. However, what if the binding effect of both the D-box and KEN-box was additive, in that the strongest complex formed was with a substrate that contained both degrons. Although this had been investigated with respect to the Hsl1 mini construct, an important fact, the linker length between the Hsl1 KEN-box and D-box, was overlooked and could now be taken into account due to the publication of the mitotic checkpoint complex (MCC) structure (Fig.25A) (Chao et al., 2012).

The MCC structure revealed that the KEN-box binds on the top of CDC20 with the D-box binding on the side of the WD40 domain (this will be discussed further in the discussion). The distance between these two sites of degron recognition was $\sim 50\text{\AA}$ equating to ~ 30 amino acids of an alpha helical secondary structure, about half the current Hsl1 KEN-D-box linker length (Chao et al., 2012).

Since this avenue of investigation had not yet been tapped we designed GST-TEV-Hsl1 mini constructs containing various linker lengths ranging from 10-30 amino acids between the KEN-box and the D-box (Fig.25B). Crystal trials with a 1MH6 CDH1 162-14 and Hsl1 mini linker-25 complex produced small crystals in many conditions however, these did not look better than the ones already grown using the D-box peptide possibly due to the unstructured nature of the 1MH6 tag (Fig.25C).

We therefore created a 1MH6 PS CDH1 162-14 and GST PS Hsl1 mini linker-25 version (Fig.25D), where we could cleave the tags of both our proteins of interest. This, like the previous complex purified very well, with no marked signs of CDH1 instability due to the lack of a stabilising tag and purified complex yields dramatically increased (Figs.25E,F).

Attempts were also made to crystallise CDH1 from the thermophile *Chaetomium thermophilum*. Hsl1 mini linker 25 bound and dramatically stabilised CDH1 and crystal trials were initiated (Fig.25G). However, due to the publication of the crystal structures of human CDC20 and *S. cerevisiae* CDH1, it was decided to terminate the project.

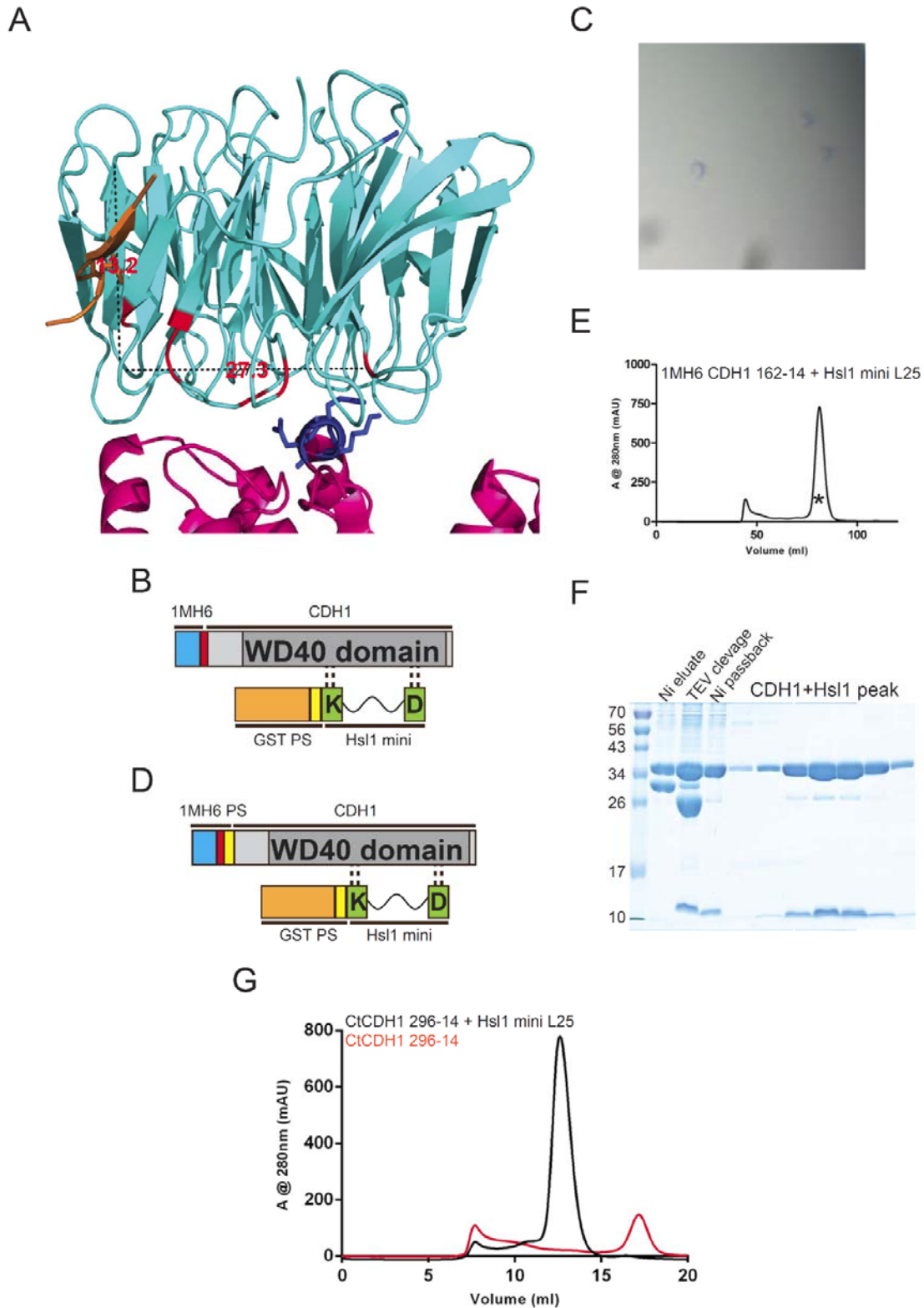


Figure 25: Summary of optimisations to tag and linker of 1MH6 CDH1 162-14 + Hsl1^{mini} complex. (A) Crystal structure of the MCC complex. (B) Schematic representation of the 1MH6 CDH1 162-14 + GST PS Hsl1^{mini} linker 25 complex (C) Crystals of 1MH6 CDH1 162-14 + GST PS Hsl1^{mini} linker 25 complex grown in 100 mM Tris pH 7, 0.8 M sodium citrate and 200 mM sodium chloride (D) Schematic representation of the 1MH6 PS CDH1 162-14 + GST PS Hsl1^{mini} linker 25 complex (E) Size exclusion profile of Prescission cleaved 1MH6 PS CDH1 162-14 + GST PS Hsl1^{mini} linker 25 complex and (F) corresponding SDS-PAGE analysis (G) Size exclusion chromatography profile overlays of CtCDH1 296-14 and CtCDH1 296-14 + Hsl1^{mini} linker 25.

6. Discussion

6.1. UBE2S – a non-canonical E2

The mechanism by which RING E3 ligases interact with their E2 ubiquitin conjugating enzymes and build ubiquitin chains has been well documented but despite this, many exceptions to the established mechanism are still being uncovered. The cullin-RING E3 ligase, the Anaphase Promoting Complex (APC/C), functions together with two E2s, UBCH10, which initiates ubiquitin chain formation and UBE2S, which elongates poly-ubiquitin chains. From previously published studies it has become evident that UBCH10 interacts and functions with the APC/C according to the canonical E3 RING mechanism with the $\alpha 1$ helix interacting with the RING domain and the RING domain biasing 'closed' conformations of the E2~Ub species (Rodrigo-Brenni and Morgan, 2007; Pruneda et al., 2011; Berndsen and Wolberger, 2014). However, UBE2S displays indications that this may not be the case (Williamson et al., 2009; Wickliffe et al., 2011; Sako et al., 2014). Donor ubiquitin is self-orientated into a closed-conformation, defining the UBE2S~Ub species as active. This is in contrast to UBCH10 which needs the RING to form an active E2~Ub species. One could argue that the UBCH10-esque activation switch has been removed from UBE2S. Given that UBE2S can only build chains on pre-conjugated ubiquitin however, there seems little reason to have a kill switch in UBE2S.

We therefore set out to elucidate how UBE2S functions in conjunction with the APC/C by understanding the first two principles of ubiquitination: How does the APC/C recruit the UBE2S~Ub species and how does the APC/C activate the UBE2S~Ub species. To address this we prepared over 135 Ala, Asp and Trp UBE2S mutants of the ubiquitin conjugating domain (UBC) and C-terminal tail and tested these in their ability to stably bind APC and build ubiquitin chains in an APC-dependant and -independent manner.

We identified that UBE2S binds stably to the APC platform domain, through its C-terminal residues L219, R221 and L222. This is different to what is described for UBCH10 which interacts with the APC/C through the canonical RING mechanism, by interacting with the catalytic subunits APC2/APC11.

To which subunit UBE2S binds is open to speculation however, one could assume it is the same location as to where the APC/C inhibitor Emi1 binds, APC4, since they both share the same LRRL tail and it has been shown that Emi1 prevents chain elongation (Frye et al., 2013; Wang and Kirschner, 2013).

In addition to understanding how UBE2S binds the APC/C, we also wanted to understand how UBE2S catalytically interacts with and is activated by the APC/C. We subjected all the UBE2S mutants to a two-part ubiquitination screen, the first part testing APC-dependent function and the second part assessing intrinsic catalytic activity. From this screen,

we identified six functional surfaces, three canonical surfaces which had already been identified (E1 binding, donor ubiquitin binding and acceptor ubiquitin binding) and three novel surfaces, the 'backside', the C-terminal helix of the UBC domain and the C-terminal tail.

The E1 binding surface of an E2 had already been identified by Huang and colleagues and showed the N-terminal extension of the E2 to be implicated in this interaction. We used published crystal structures to model this interaction allowing us to assign UBE2S mutants that we identified to this interaction surface (Huang et al., 2004, 2005; Olsen and Lima, 2013)

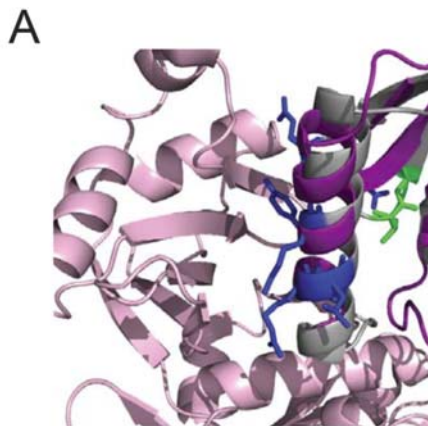


Figure 26: Interaction between E1 and E2.

Crystal structures of Uba1-Ubc4 overlaid with UBE2S to illustrate N-terminal helix of UBE2S interacting with UBD of Uba1. Uba1-pink, Ubc4-purple, UBE2S-grey, UBE2S E1 assigned deficient mutants-blue. UBE2S PDB: 1ZDN (Olsen and Lima, 2013)

Both the donor and acceptor surfaces had been assigned to UBE2S by Wickliffe and colleagues. The donor ubiquitin binds through hydrophobic interactions around Ile44 orienting itself in a closed conformation on UBE2S. Acceptor ubiquitin on the other hand was assigned through HADDOCK modelling since this interaction is too transient to be visualised by NMR (Wickliffe et al., 2011). Given the published data we were able to assign residues to these surfaces. Interestingly UBE2S mutant R135A displayed intrinsic activity suggesting this residue has an APC/C-dependent function (Fig.11B,pink). Given that this residue had been assigned to the acceptor binding site, it may act as a link to APC/C with respect to the acceptor ubiquitin possibly in helping to orient the acceptor in the presence of APC/C.

The backside of E2 has been implicated in protein interactions and as a communication channel to the E2 by inducing allosteric changes (Das et al., 2009). We identified two residues on this surface, in the middle of the beta sheets, R61A,K63A, that showed APC/C-dependent ubiquitination deficiency and intrinsic, APC/C-independent activity stronger than observed with wild type UBE2S (Fig.11A,B,green). Taken the latter finding, it suggests these residues are involved in slowing down the catalytic activity of UBE2S in an APC/C-dependent manner,

possibly through allosteric interactions with the APC/C. Functionally it is open to speculation what this surface might be doing but one possibility could be that it functions as an 'overflow', directing un-needed ubiquitin for auto-ubiquitination. Intrinsically UBE2S is designed to auto-ubiquitinate itself at a high rate whereas the APC/C favours conjugation of ubiquitin to substrates. If there is no substrate acceptor ubiquitin present for UBE2S to discharge to then R61,K63 may act as an allosteric switch invoking rapid auto-ubiquitination.

The second novel surface was the C-terminal helix of the UBC domain, with the most interesting mutants encompassing residues R147A,R149A and E153A,I154A. The latter mutant showed a dramatic deficiency in APC-dependent ubiquitination compared to the former (Fig.11A,orange). The opposite was observed when assessing intrinsic activity with mutants R147A,R149A showing greater activity than wild type UBE2S whereas E153A,I154A showed wild type levels (Fig.11B,orange).

Although these mutants are on the same helix, it appears they do not perform the same function. Given UBE2S mutant E153A,I154A has intrinsic activity similar to wild type, the extreme APC-dependent deficiency observed leans towards the hypothesis that these residues are activating UBE2S in an APC-dependent manner. Further work is needed to understand how this occurs since UBE2S lacks critical RING interacting residues (Markson et al., 2009). The R147A,R149A mutant is 'closer' to the helix that has been noted to orient the acceptor ubiquitin for specific K11 linkages (Sheng et al., 2012). It could therefore be that it is involved in orienting the acceptor ubiquitin in an APC/C-dependent manner. As with the backside mutants, R147A,R149A showed higher intrinsic activity than wild type suggesting that the APC/C is slowing down the intrinsic function of these residues down possibly by invoking catalytic machinery to generate only K11 chains. In an APC/C free system this constraint does not exist, therefore the higher rate of catalysis is observed.

The surface alanine scan has produced remarkable data illustrating how multiple surfaces function together to regulate the transfer of ubiquitin from the E2 to the substrate. UBE2S coordinates many factors simultaneously to be able to catalyse ubiquitin chain building on a substrate, and it has been efficiently designed to accomplish this.

We have identified novel surfaces that stimulate APC/C-dependent function of UBE2S yet UBE2S has been shown not to interact with the RING and inactive UBCH10 has no effect on UBE2S ruling out cooperativity. The questions arise what is the APC/C doing to UBE2S that does not involve the RING domain or what is UBE2S doing to the APC/C? The novel surface residues identified are all on the opposite surface to the catalytic cysteine. Given UBE2S functions together with a huge 1.5 MDa complex, there are many possibilities to interact with surfaces on the APC/C that may invoke an activating allosteric effect either on UBE2S or vice versa. Does this activation rely on the presence of substrate, or is the intrinsic activity of UBE2S sufficient? Much work is still needed to get answers to these questions.

6.2. Insights into substrate recruitment to the APC/C

The third principle of ubiquitination is substrate recruitment. The APC/C has been shown to mediate substrate recruitment by the co-activators CDH1 and CDC20 (Burton et al., 2005; Kraft et al., 2005). The co-activators contain a C-terminal WD40 domain which has been shown to bind substrates analogous to the method employed by the SCF complex (Fig.8E). This interaction is mediated by the D-box and KEN-box degrons which are found in APC/C substrates. To understand the molecular basis for the interaction between APC/C substrate degrons and the co-activators, we set out to crystallise a co-activator-substrate complex, namely a CDH1-Hsl1 complex.

We showed that the WD40 domain of CDH1 is sufficient to bind a fragment of the *S. cerevisiae* substrate Hsl1 as well as Hsl1 D-box and KEN-box peptides, with the D-box peptide having a higher affinity towards CDH1 than the KEN-box peptide (Fig.17,21). Previous attempts to crystallise CDH1 in complex with Hsl1 struggled to gain traction due to difficulties in expressing CDH1 in quantities large enough to make crystallographic studies possible. We developed a stable, well expressing CDH1 deletion construct encompassing the WD40 domain. Together with either a Hsl1 fragment, containing both the D-box and the KEN-box, or a peptide of the Hsl1 D-box we pursued crystallographic studies in which we were able to grow crystals. Sadly however, these crystals were not of the quality from which we could attain our ultimate goal of collecting a full dataset of our complex. Despite intense efforts by both myself and Georg Petzold, we were beaten to publishing a novel crystal structure revealing the structural basis for the interaction between co-activator and substrate.

The first indications of how the D-box and KEN-box degrons interact with the co-activators was provided by the publication of the *S. Pombe* mitotic checkpoint complex structure in which the Cdc20 WD40 domain was crystallised together with Mad2 and Mad3 lacking its C-terminal KEN-box (Fig.27A) (Chao et al., 2012). Resolved to 2.3Å, the crystal structure revealed that the KEN-box of Mad3 interacted with the top side of the WD40 domain whereas a Mad3 D-box mimic slots into a groove between blades 1 and 7 of the WD40 domain. The Mad3 KEN-box formed a helix-loop-helix architecture with the KEN box residues (Lys20, Glu21 and Asn22) presenting themselves in the loop region facing towards the Cdc20 WD40 domain with Glu21 slotting into the depression at the centre of the Cdc20 WD40 domain and forming hydrophobic interaction with Tyr181 (Fig27B). All the other interactions observed between Mad3 and Cdc20 are polar encompassing Cdc20 residues Asp180, Asn326, Thr368, Gln392 and Arg438 and conserved between Cdc20 and Cdh1 suggesting this mechanism of interaction is common, indeed mutation of the equivalent residues in Cdh1 abolished KEN-box mediated binding (Chao et al., 2012).

The authors of the MCC structure were also rather fortunate in that a C-terminal D-box mimic from an adjacent Mad3 molecule contacted Cdc20 through crystal packing (Fig.27C). The mimicking Leu215 side chain buries itself into a pocket between blades 1 and 7 of the WD40 domain created by residues common to both Cdc20 and Cdh1, again suggesting a common mechanism. Although the D-box mimic did not contain the other D-box consensus residues, the authors assigned a potential Arg recognition surface based on a nearby constellation of negatively charged residues located at the top of blade 7. Mutation of the equivalent residues in Cdh1 abolished D-box mediated binding. The authors also speculated that by anchoring the Leu of the D-box consensus sequence in the co-activator, it allowed the Arg, Ile/Leu and Asn side chains of the D-box to hypothetically point towards APC10. This would form a hybrid co-activator-D-box binding surface for APC10 to interact with, consistent with findings that APC10 is a D-box co-receptor (Chao et al., 2012).

The *S. Pombe* Cdc20 interactions with a KEN-box and D-box were further corroborated by the publication of the human CDC20 WD40 domain in complex with a BubR1 KEN-box peptide (Tian et al., 2012). Interestingly, a complementary structure of free CDC20, revealed, as we had described, that the N-terminus is unstructured and that the contained KEN-box did not bind into the KEN-box binding site suggesting that CDC20 does not auto-inhibit itself.

As with the MCC structure, these authors were also lucky in observing a D-box mimic, in this case an 2-Methyl-2,4-pentanediol molecule. This molecule was buried in the same pocket as the Leu in the MCC structure, in the groove between blades 1 and 7 of the WD40 domain postulated to be the D-box binding site (Tian et al., 2012).

The final structure that shed light on the molecular basis for co-activator-substrate interactions was that of *S. Cerevisiae* Cdh1 in complex with the APC/C inhibitor Acm1 (He et al., 2013). The authors further confirmed the mode of KEN-box binding to the top of the co-activator WD40 domain, in this case Cdh1 (Fig.27D). Of more significance however, was the visualisation of a D-box bound in the groove between blades 1 and 7 of the Cdh1 WD40 domain. As previously observed, the Leu of the D-box was buried in the previously identified pocket with the Arg hydrogen bonding with an acidic patch, as previously speculated. The D-box alanine at position 3 faces towards the WD40 domain forming a hydrophobic contact with a conserved Phe explaining why this position generally contains non-bulky residues. Furthermore the aspartate at position 6 forms a hydrogen bond with Arg253 of Cdh1 explaining why Asp and Glu are common residues at this position (Fig.27E) (He et al., 2013). The residues implicated in D-box binding corroborate the residues identified by Kraft et al. (Kraft et al., 2005).

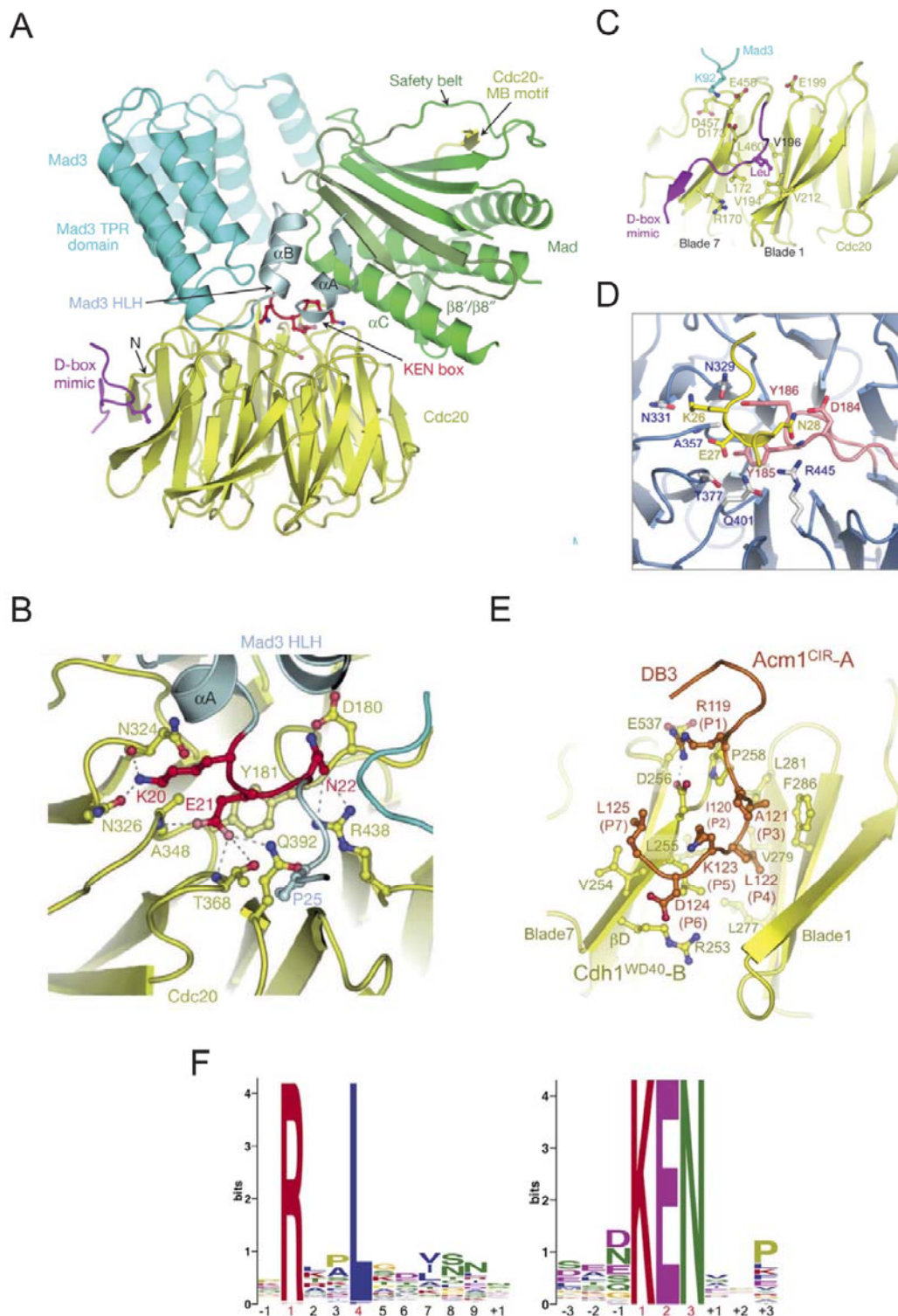


Figure 27: Summary of structures illustrating D-box and KEN-box recognition by the co-activators. (A) MCC structure. Mad2-green, Mad3-blue, Cdc20-yellow (B) Magnification of Cdc20-KEN-box interaction in (A). (C) Magnification of Cdc20-D-box interaction in (A). (D) Cdh1-Acm1 KEN-box interaction. (E) Cdh1-Acm1 D-box interaction. (F) Consensus sequences of D-box and KEN-box. (Tian et al., 2012, He et al., 2013)

Beneficially, the authors compiled an alignment of D-box and KEN-box motifs generating consensus sequences for the regions flanking the D-box and KEN-box (Fig.27F). For the KEN-box, a Pro at position +3 was found to be important in breaking the helix in which the KEN-motif would otherwise find itself in (He et al., 2013).

The structural details the above described crystal structures have provided give valuable insight into how co-activators and substrates interact. Together with the knowledge that the co-activators bind through their C-terminal IR tails to the APC/C via APC3 and APC8, this gives a nice narrative on how substrates are recruited to the APC/C. It is however, important to note that APC/C core subunits have also been implicated in substrates binding, namely APC10.

Electron microscopy studies of the APC/C^{CDH1} and the APC/C^{CDH1}+Hsl1 complex have revealed that a bridge is formed between CDH1 and APC10 by the substrate, with associated structural rearrangements also occurring such as a 7 Å shift of CDH1 towards APC10 (Fig.28). It is important to note however, that the formation of this bridge is D-box dependent as using a KEN-box peptide substrate did not induce such conformational rearrangements (da Fonseca et al., 2010; Buschhorn et al., 2011). This is consistent in that APC10 is involved in D-box dependent substrate recognition however, why such a bi-valent binding mechanism needs to be employed is not fully understood and will be discussed now.

A

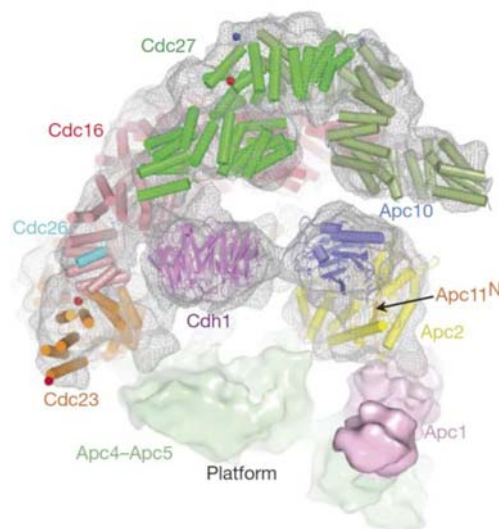


Figure 28: Structural model of human APC/C. Model illustrating the proximity and orientations of Cdh1 and APC10 in relation to one another. (Schreiber et al., 2011)

6.3. Precise, ordered substrate degradation by the APC/C is multi-modal

Although this thesis has focused on the mechanistic features of the APC/C it is important not to forget the biological context in which this E3 ligase functions. Upon the bi-orientation of all the chromosomes on the mitotic spindle, the APC/C initiates the metaphase to anaphase transition, rapidly ubiquitinating cyclin B and securin and targeting these substrates for proteasomal degradation. The job of the APC/C does not stop here though, indeed the APC/C targets many more substrates for degradation over its active phase through late mitosis to late G1 phase ensuring uni-directional progression of the cell cycle (Fig.29) (Sullivan and Morgan, 2007).

What remains a mystery is the regulation that ensures the APC/C knows which substrate to ubiquitinate when. I will discuss three features that play a role in substrate ordering: 1. the affinity of the D-box and KEN-box to the co-activator, 2. substrate interactions with APC10 and 3. ubiquitin chain makeup.

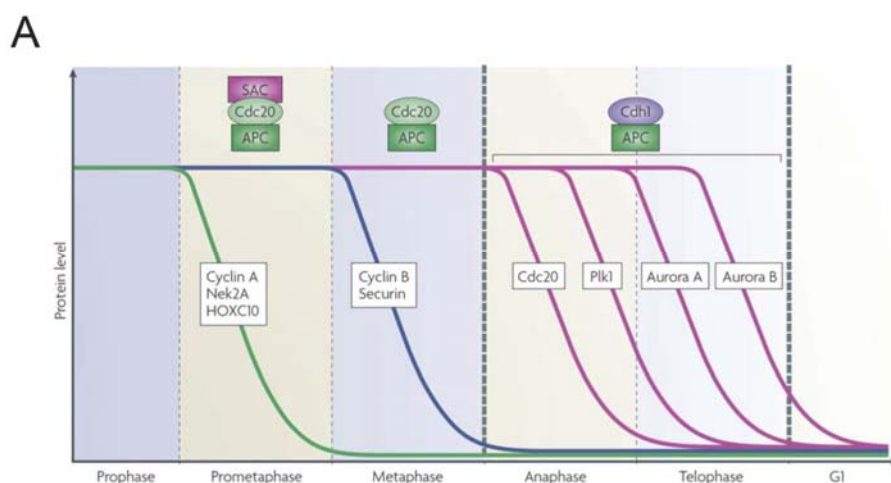


Figure 29: Illustration of the order of protein degradation in mitosis.
(Sullivan and Morgan, 2007)

As discussed, major advances have been made in understanding the molecular basis of how co-activators and substrates interact and we have shown for the substrate Hsl1 that the D-box and KEN box have different binding affinities for CDH1 (Fig.21). Although no systematic studies quantifying the binding affinities of other active mitotic substrate degrons has been conducted, it would be tempting to speculate that early APC/C substrates contain degrons with lower Kds towards their co-activators than late APC/C substrates. This would mean that early degraded substrates would be sufficiently poly-ubiquitinated to be targeted for degradation in one binding event, a so called processive substrate, whereas later degraded substrates need more binding events to be sufficiently poly-ubiquitinated to be targeted for degradation. Indeed

late mitotic substrates have been shown to be less processively ubiquitinated (Rape et al., 2006).

Furthermore, it is interesting to observe the variation in the spacing between the D-box and KEN box in substrates containing both degrons. Chao and colleagues suggested an optimal linker length of between 18 and 24 amino acids is optimal for binding (Chao et al., 2012). Indeed studies we conducted with Hsl1 seem to corroborate this with a Hsl1 substrate with a linker length between the D-box and KEN box of 47 amino acids binding less well to CDH1 than a Hsl1 substrate with a linker length of 25 amino acids.

Additionally, it was also observed that the order of the degrons may influence recognition by the co-activators. A KEN-D peptide was a more potent binder to CDH1 than a D-KEN peptide due to the structural constraints imposed by the binding sites on CDH1. Taken further, the D-KEN peptide inhibited APC/C^{CDH1} to a similar extent as only a D-box peptide suggesting that the D-box and KEN-box bind co-activators in a cooperative manner, therefore having both degrons present in a substrate may make the substrate more processive (Chao et al., 2012).

Together this suggests the presence, order, distance between and affinity of the D-box and KEN-box in a substrate influences how efficiently a substrate is ubiquitinated and how quickly it is degraded. Interestingly, the substrates that are degraded before the APC/C is released from inhibition by the spindle assembly checkpoint do not require the co-activators to bind the APC/C explaining why they are the first APC/C substrates to be degraded. Nek2A contains a MR tail, reminiscent to the IR tail of the co-activators that can bind into the APC/C TPR subunit APC3, suggesting that it itself can bind into the TPR subunits (Hayes et al., 2006). Furthermore, Cyclin A is also degraded at a similar time to Nek2A. Cyclin A is found in complex with Cdk1 which can bind activated, phosphorylated APC/C (Wolthuis et al., 2008).

The APC/C has also been shown to bind substrates in a cooperative bi-valent way. In addition to the co-activators binding substrates, APC10 has also been implicated in binding substrates in a D-box dependent manner. First indications came from Matyskiela and colleagues who showed that despite inducing an increased dissociation of the co-activators by mutagenesis, substrates did not exhibit a similar increased rate of dissociation from the APC/C and were also not less processively ubiquitinated (Matyskiela and Morgan, 2009). This was later confirmed by electron microscopy studies of APC/C^{CDH1} and APC/C^{CDH1}+Hsl1 revealing a substrate bridge forming between CDH1 and APC10 (da Fonseca et al., 2010; Buschhorn et al., 2011). Furthermore, APC10 has been implicated as a processivity factor. Yeast strains containing a Δ doc1 APC/C were less able to build higher molecular weight ubiquitin chains on substrates compared to strains containing wild type APC/C (Carroll and Morgan, 2002; Carroll et al., 2005).

Together this suggests that the binding of substrates to APC10 affects the ability of the APC/C to processively ubiquitinate them. The increased binding affinity to the APC/C caused by APC10 holding substrates on the APC longer thus allowing more time for higher molecular weight ubiquitin chains to be built during one substrate binding event. It is however feasible given the proximity of APC10 to APC2/APC11, the catalytic machinery of the APC/C, that APC10 may manipulate catalysis, either through invoking allosteric changes in APC2/APC11 or possibly through interactions with the chain building E2 UBE2S.

This would suggest that substrates containing only a KEN-box would be less processive in their nature. The securin KEN-box has been shown to be dispensable for CDC20 binding and ubiquitination questioning the purpose of two degrons in a substrate (Tian et al., 2012). Indeed sororin is a late APC/C substrate and only contains a KEN-box.

Until recently, the APC/C was thought to synthesise poly-ubiquitin chains containing only one linkage species, either preferentially K11 or K48. Meyer and colleagues have demonstrated that the APC/C is able to build branched poly-ubiquitin chains of mixed linkage by attaching ubiquitin on two lysines of the same ubiquitin. They showed that these branched ubiquitin chains displayed increased degradation rates as they bind to the proteasome with greater affinity compared to homotypic poly-ubiquitin chains i.e. are stronger proteolytic signals (Meyer and Rape, 2014). The question arises, are early APC/C substrates decorated with branched ubiquitin chains in contrast to late substrates? This would be an elegant way of prioritising which substrates should undergo proteasomal degradation first however, it is somewhat difficult to comprehend a plethora of ubiquitinated APC/C substrates, with varying species of branched ubiquitin chains, in the cytosol queueing to be degraded by the proteasome. It would be interesting to see if there is a difference in the species of ubiquitin chain between early and late APC/C substrates.

In conclusion, the APC/C is manipulated by a whole wrath of mechanisms to ensure it degrades the right substrate at the right time. Given the intra-cellular localisation of the APC/C relative to its target substrates, the switch from CDC20 to CDH1 acts as an abrupt switch in the substrates that are recruited to the APC/C. The associated properties of D-box and KEN-box degrons add a finer touch of regulation manipulating binding affinities towards the co-activators influencing how long a substrate can be bound to the APC/C and thus how efficiently a substrate is ubiquitinated and how quickly it is degraded. In addition to this, the bi-valent recognition of the D-box by APC10 biases D-box containing substrates to be processively ubiquitinated and so degraded faster. The final layer of determining substrate ordering is suitably determined by the APC/C itself in the makeup of the ubiquitin chains it builds on substrates. The three points discussed above are certainly not the only regulatory mechanisms in ensuring cell cycle substrate ordered degradation (Min et al., 2013). It does seem however though to be predominantly controlled by the properties of the D-box and KEN-box. It will be

interesting to see if the properties of these degrons can be modelled against the timing of substrate degradation.

7. Materials and Methods

7.1. Surface alanine scan of UBE2S in the laboratory of Brenda A. Schulman

7.1.1. cDNA constructs used for protein expression in *E. coli*.

UBE2S mutants were all cloned with an N-terminus of His6-TEV-FLAG-Prescission.

| | | | |
|------------------------|----------------------------------|----------------------------------|---------------------------|
| UBE2S WT | UBE2S K63W | UBE2S G156A, G157A, A158D | UBE2S G201A, E202A, R203A |
| UBE2S M1A, N2A, S3A | UBE2S K68W | UBE2S G159A, G160A, P161A | UBE2S G201W |
| UBE2S N4A, V5A, E6A | UBE2S K68A, D69A | UBE2S G159A, G160A, P161A, S162A | UBE2S E202W |
| UBE2S N4A | UBE2S K76W | UBE2S S162A, G163A, R164A | UBE2S R203W |
| UBE2S P9A, P10A | UBE2S K76A, Y78A | UBE2S G163A, R164A, A165D, E166A | UBE2S D204A, K205A, K206A |
| UBE2S H11A | UBE2S Y78W | UBE2S A165D, E166A, A167D | UBE2S D204W |
| UBE2S H11W | UBE2S L80A | UBE2S A167D, G168A, R169A, A170D | UBE2S K205W |
| UBE2S I13A, R14A, L15A | UBE2S K82W | UBE2S G168A, R169A | UBE2S K206W |
| UBE2S L15W | UBE2S N91A | UBE2S A170D, L171A, A172D | UBE2S L207A, A208D, A209D |
| UBE2S Y17A, K18A | UBE2S V96A, N97A | UBE2S L171A, A172D, S173A, G174A | UBE2S L207W |
| UBE2S T21A, T22A | UBE2S R101A, D102A | UBE2S S173A, G174A, T175A | UBE2S A208W |
| UBE2S T24A, A25D, D26A | UBE2S T104A, A105D, E106A | UBE2S T175A, E176A, A177D, S178A | UBE2S A209W |
| UBE2S P27A, P28A | UBE2S T104W | UBE2S E176A, A177D | UBE2S K210A, K211A, K212A |
| UBE2S D29A, G30A, K32A | UBE2S A105W | UBE2S S178A, S179A, T180A | UBE2S K210W |
| UBE2S K32D | UBE2S E106W | UBE2S S179A, T180A, D181A, P182A | UBE2S K211W |
| UBE2S K32W | UBE2S K117A, C118A | UBE2S D181A, P182A, G183A | UBE2S K212W |
| UBE2S F34D | UBE2S C118A | UBE2S G183A, A184D, P185A | UBE2S T213A, D214A, K215A |
| UBE2S F34W | UBE2S I121A, H122A | UBE2S A184D, P185A, G186A | UBE2S T213W |
| UBE2S F34A, P35A, N36A | UBE2S N124A, E126A | UBE2S G186A, G187A, PA88A | UBE2S D214W |
| UBE2S E37A, E38A, D39A | UBE2S E131A, E132A | UBE2S G187A, P188A, G189A, G190A | UBE2S K215W |
| UBE2S L40A | UBE2S R135A | UBE2S G189A, G190A, A191D | UBE2S K216A, R217A, A218D |
| UBE2S D42A | UBE2S L138A | UBE2S A191D, E192A | UBE2S K216W |
| UBE2S Q44D | UBE2S E139A, N140A | UBE2S E192A, G193A, P193A | UBE2S R217W |
| UBE2S T41A, D42A | UBE2S E142A, E143A | UBE2S G193W | UBE2S A218W |
| UBE2S Q44A, T46A | UBE2S A145D, A146D | UBE2S P194W | UBE2S L219A |
| UBE2S E48A | UBE2S R147A | UBE2S M195A, A196D, K1978A | UBE2S L219W |
| UBE2S E51A | UBE2S R147A, R149A | UBE2S M195W | UBE2S R220A |
| UBE2S E51A, G52A | UBE2S R149A | UBE2S A196W | UBE2S R220W |
| UBE2S L59A | UBE2S L150A | UBE2S K197W | UBE2S R221A |
| UBE2S R61A | UBE2S E153A | UBE2S K198A, H199A, A200D | UBE2S R221W |
| UBE2S R61W | UBE2S E153A, I154A | UBE2S K198W | UBE2S L222A |
| UBE2S R61A, K63A | UBE2S I154A | UBE2S H199W | UBE2S L222W |
| UBE2S K63A | UBE2S H155A, G156A, G157A, A158D | UBE2S A200W | UBE2S *223W |

7.1.2. Expression of UBE2S mutants in *E.coli*

All UBE2S mutant listed in table 2 were expressed in BL21 (DE3). Transformed *E. coli* were grown overnight on LB-agar plates containing 50 µg/mL kanamycin and 30 µg/mL chloramphenicol. A single colony was selected and grown up as a liquid pre-culture overnight at 37 °C. 5 mL of pre-culture was used to inoculate 1 L LB media containing 50 µg/mL kanamycin and 30 µg/mL chloramphenicol and incubated at 37 °C until an OD of ~0.8 was reached. Protein expression was induced by the addition of 0.8 mM IPTG with *E. coli* incubated a further 18 hours at 18 °C.

7.1.3. Purification and cleavage of His6-TEV-FLAG-Prescission UBE2S mutants

Following expression *E. coli* were pelleted by centrifugation at 4000 r.p.m. at 4 °C for 15 minutes and re-suspended in 20 mM Tris pH7.6, 200 mM NaCl, 10 mM Imidazole, 0.5 mM TCEP, 2.5 mM PMSF and sonicated on ice for 3x 15 seconds. Bacterial lysates were then cleared by centrifugation at 15,000 r.p.m. at 4 °C for 30 minutes. The supernatant was subsequently incubated with 1 mL His-Select resin (Sigma Aldrich) on a rocking shaker at 4 °C for 1 hour. The suspension was then added to a disposable column with the resin subsequently washed 3x with 5 column volumes of 20 mM Tris pH7.6, 200 mM NaCl, 10 mM Imidazole, 0.5 mM TCEP. His-Select resin was then incubated overnight at 4 °C with 1 column volume of 20 mM Tris pH7.6, 200 mM NaCl, 10 mM Imidazole, 0.5 mM TCEP containing 50 µg/mL Prescission protease. Post incubation, the UBE2S containing flow through was collected together with a further 2 mLs of 20 mM Tris pH7.6, 200 mM NaCl, 10 mM Imidazole, 0.5 mM TCEP buffer that had been subsequently been used to wash the resin. The flow through was then diluted to a volume equating to a NaCl concentration of 100 mM with 20 mM Tris pH7.6, 1 mM DTT and incubated with 2 mL SP IEX resin (Sigma Aldrich) for 10 minutes. The suspension was then added to a disposable column with the resin washed 3x with 5 column volumes of 20 mM Tris pH7.6, 100 mM NaCl, 1 mM DTT. UBE2S was finally eluted with 3x 1mL pulses of 20 mM Tris pH7.6, 400 mM NaCl, 1 mM DTT. Protein concentrations were immediately tuned with protein aliquots subsequently pipetted, snap frozen and stored at -80 °C.

7.1.4. Purification of His6-TEV-FLAG-Prescission UBE2S mutants

Following expression *E. coli* were pelleted by centrifugation at 4000 r.p.m. at 4 °C for 15 minutes and re-suspended in 20 mM Tris pH7.6, 200 mM NaCl, 10 mM Imidazole, 0.5 mM TCEP, 2.5 mM PMSF and sonicated on ice for 3x 15 seconds. Bacterial lysates were then

cleared by centrifugation at 15,000 r.p.m. at 4 °C for 30 minutes. The supernatant was subsequently incubated with 1 mL His-Select resin (Sigma Aldrich) on a rocking shaker at 4 °C for 1 hour. The suspension was then added to a disposable column with the resin subsequently washed 3x with 5 column volumes of 20 mM Tris pH7.6, 200 mM NaCl, 10 mM Imidazole, 0.5 mM TCEP. UBE2S was eluted with 5x 1 column pulses of 20 mM Tris pH7.6, 200 mM NaCl, 250 mM Imidazole, 0.5 mM TCEP. NaCl, 10 mM Imidazole, 0.5 mM TCEP. The eluate was then diluted to a volume equating to a NaCl concentration of 100 mM with 20 mM Tris pH7.6, 1 mM DTT and incubated with 2 mL SP IEX resin (Sigma Aldrich) for 10 minutes. The suspension was then added to a disposable column with the resin washed 3x with 5 column volumes of 20 mM Tris pH7.6, 100 mM NaCl, 1 mM DTT. UBE2S was finally eluted with 3x 1mL pulses of 20 mM Tris pH7.6, 400 mM NaCl, 1 mM DTT. Protein concentrations were immediately tuned with protein aliquots subsequently pipetted, snap frozen and stored at -80 °C.

7.1.5. Culturing of SF9 and Hi5 cells.

Sf9 and Hi5 cells were cultured in suspension in Hyclone media (Thermo Scientific) at 27 °C, rotated at 150 r.p.m. Cell densities were kept in the range of 0.5^6 - 4^6 cells per mL.

7.1.6. Baculovirus Amplification

Sf9 cells were adherently grown to a density of 1^6 cells/mL at which point 1 mL of the respective 2nd amplification baculovirus was added to cells. Cells were left to incubate for 4 days before the supernatant was used to infect protein expression cultures.

7.1.7. Expression of APC/C and APC/C platform variants

Hi5 cells were re-suspended to a density of 10^6 cells/mL with 5 mL of the respective 3rd amplification baculovirus added to cells. Cells were left to incubate for 2 hours at 27 °C shaking at 100 r.p.m before being diluted to 2^6 cells per mL. Cells were then incubated a further 24 hours at 27 °C and then 48 hours at 16 °C before being harvested.

7.1.8. Purification of APC/C and APC/C platform variants

Following expression Hi5 cells were pelleted by centrifugation at 1500 r.p.m. at 4 °C for 15 minutes and re-suspended in 20 mL of 50 mM Hepes pH8.0, 250 mM NaCl, 5% glycerol, 2 mM DTT, 2 mM benzamidine, 0.1 mM PMSF, 5 units/mL bezonase, 10 µg/mL aprotinin, 10 µg/mL leupeptin and 1 protease inhibitor cocktail tablet EDTA free buffer (per litre of cell

culture). Cells were sonicated on ice for 3x 15 seconds and the lysates cleared by centrifugation 2x at 15,000 r.p.m. at 4 °C for 30 minutes. The supernatant was subsequently incubated with 2 mL Strep Tactin Sepharose resin (IBA Lifesciences) on a rocking shaker at 4°C for 1 hour. The suspension was then centrifuged at 1200 r.p.m. at 4 °C for 15 minutes and with the resin re-suspended in 5 mL of 50 mM Hepes pH8.0, 250 mM NaCl, 5% glycerol, 2 mM DTT, 2 mM benzamidine before being transferred to a disposable column where the resin was washed a further 5x 5 column volumes of the previous buffer. APC/C was subsequently eluted by 5x 1 column volume pulses of 50 mM Hepes pH8.0, 250 mM NaCl, 5% glycerol, 2 mM DTT, 2 mM benzamidine, 2.5 mM desthiobiotin. Elution fractions were then analysed by SDS-PAGE and visualised by coomassie staining with the favoured samples pooled and diluted to a volume equating to a NaCl concentration of 100 mM with 20 mM Hepes pH8.0, 5% glycerol, 2 mM DTT and loaded onto an 8 mL Poros HQ IEX FPLC column (Life Technologies). The column was washed with 2 column volumes of 20 mM Hepes pH8.0, 100 mM NaCl, 5% glycerol, 2 mM DTT with the protein eluted over a gradient of 100 mM – 700 mM NaCl. Elution fractions were then analysed by SDS-PAGE and visualised by coomassie staining with the favoured samples pooled and concentrated to a concentration of ~2 mg/mL. APC/C was then loaded onto a 10/300 Superose 6 FPLC column and resolved using a 20 mM Hepes pH8.0, 200 mM NaCl, 1 mM DTT buffer. Elution fractions were then analysed by SDS-PAGE and visualised by coomassie staining with the favoured samples pooled and concentrated to a concentration of 1 mg/mL with protein aliquots subsequently pipetted, snap frozen and stored at -80 °C.

7.1.9. APC/C dependent UBE2S ubiquitination assays

Assays assessing the effect of UBE2S mutants on APC/C dependent ubiquitination activity were conducted, albeit with modifications, according to a previously described protocol (Frye et al., 2013). A ubiquitination mix (APC/C, CDC20/CDH1, *Ub-CycB¹⁻⁹⁵, Uba1, BSA, ATP, MgCl₂, 20 mM Hepes pH 8.0, 200 mM NaCl) was prepared on ice, equilibrated to room temperature and 14 µL was added to a 6 µL mixture containing the respective UBE2S variant and ubiquitin. This gave the following final concentrations: 14 nM APC/C, 250 nM UBE2S variant, 1 µM CDC20/CDH1, 500 nM *Ub-CycB¹⁻⁹⁵, 100 nM Uba1, 200 µM ubiquitin, 250 µg/mL BSA, 2.5 mM ATP, 2.5 mM MgCl₂ buffer. Reactions were incubated at room temperature for 12 minutes before being quenched by the addition of 4x Laemmli buffer containing no DTT. Reactions were separated by SDS-PAGE with *Ub-CycB¹⁻⁹⁵ fluorescein fluorescence detected using a Typhoon FLA 9500 imager (GE Healthcare). All reagents were kind gifts from Nicholas Brown

7.1.10. APC/C independent UBE2S ubiquitination assays

A ubiquitination mix (Uba1, ubiquitin, BSA, ATP, MgCl₂, 20 mM Tris pH 7.6, 200 mM NaCl) was prepared on ice, equilibrated to room temperature 16 μ L was added to a 4 μ L solution containing the respective UBE2S variant. This gave the following final concentrations: 250 nM UBE2S variant, 100 nM Uba1, 4 μ M *ubiquitin, 250 μ g/mL BSA, 2.5 mM ATP, 2.5 mM MgCl₂. Reactions were incubated at room temperature for 60 minutes before being quenched by the addition of 4x Laemmli buffer containing no DTT. Reactions were separated by SDS-PAGE with *Ub-CycB¹⁻⁹⁵ fluorescein fluorescence detected using a Typhoon FLA 9500 imager. All reagents were kind gifts from Nicholas Brown.

7.1.11. FLAG UBE2S co-IP assays

5 μ M Flag UBE2S was incubated with 70 nM APC/C variant and 150 nM CDH1 in 20 mM Hepes pH8, 200 mM NaCl and incubated with 40 μ L equilibrated anti-Flag M2 agarose affinity gel (Sigma) at 4 °C for 3 hours. The Flag resin was subsequently centrifuged at 8000 r.c.f. for 1 minute with the resin re-suspended in 1 mL 20 mM Hepes pH8, 200 mM NaCl. This was repeated a further 2 times. The resin was then re-suspended in 11 μ L of 4x Laemmli buffer with the samples boiled for 3 minutes before being centrifuged at 8000 r.c.f. for 1 minute and analysed by SDS-PAGE.

7.2. Co-activator structural studies

7.2.1. cDNA constructs used for protein expression in insect cells.

The following clones were presented in this thesis. Many, many more were cloned in reality...

| Tag-Gene-Modification | Vector |
|--|--------------|
| 3Myc-His6 CDC20 full length | pFastBac1 |
| 3Myc-His6 CDH1 full length | pFastBac1 |
| 3Myc-His6 CDC20 dN96-dC6 | pFastBac1 |
| 3Myc-His6 CDC20 dN96-dC21 | pFastBac1 |
| 3Myc-His6 CDC20 dN116-dC6 | pFastBac1 |
| 3Myc-His6 CDC20 dN116-dC21 | pFastBac1 |
| 3Myc-His6 CDC20 dN131-dC6 | pFastBac1 |
| 3Myc-His6 CDC20 dN131-dC21 | pFastBac1 |
| 3Myc-His6 CDC20 dN96-dC6 + Flag Securin | pFastBacDual |
| 3Myc-His6 CDH1 dN148-dC3 | pFastBac1 |
| 3Myc-His6 CDH1 dN148-dC14 | pFastBac1 |
| 3Myc-His6 CDH1 dN148-dC21 | pFastBac1 |
| 1Myc-His6 CDH1 dN162-dC14 | pFastBac1 |
| 1Myc-His6 CDH1 dN162-dC14 + GST Hsl1 ^{Linker 25} | pFastBacDual |
| 1Myc-His6-PreScission CDH1 dN162-dC14 + GST PreScissionHsl1 ^{Linker 25} | pFastBacDual |
| 3Myc-His6 CDH1 dN162-dC14 | pFastBac1 |
| 3Myc-His6 CDH1 dN162-dC21 | pFastBac1 |
| 3Myc-His6 CDH1 dN171-dC3 | pFastBac1 |
| 3Myc-His6 CDH1 dN171-dC14 | pFastBac1 |
| 3Myc-His6 CDH1 dN171dC21 | pFastBac1 |
| 3Myc-His6 CDH1 dN162-dC14 + Hsl1 ⁶⁶⁷⁻⁸⁷² | pFastBacDual |
| 3Myc-His6 CDH1 dN162-dC14 + Hsl1 ^{mini} | pFastBacDual |
| 1Myc-His6-PreScission CtCDH1 dN296-dC14 + GST PreScissionHsl1 ^{Linker 25} | pFastBacDual |

7.2.2. Culturing of Sf9 cells

Sf9 cells were cultured in suspension at 27 °C, rotated at 100 r.p.m. in Grace's insect cell media (Sigma Aldrich) supplemented with 10 % heat inactivated FBS (Gibco), 1 % penicillin-streptomycin (Sigma), 0.2 mM L-glutamine (Sigma) and 0.1 % pluronic F-68 (Sigma). Cell densities were kept in the range of 0.5^6 - 4^6 cells per ml.

7.2.3. Generation and isolation of recombinant bacmid DNA

cDNAs of interest were cloned into pFB1 or pFBDual vectors using either the appropriate restriction enzymes or with Gibson assembly. The ligation reaction was subsequently transformed into the *E.coli* strain DH5 α , streaked onto an LB-agar plate containing 32 μ g/ml ampicillin and grown overnight. A single colony was then selected and grown up as a liquid culture overnight at 37 °C with the DNA isolated according to the Qiagen miniprep protocol. Sequence verified plasmids were then transformed into DH10EMBacY, allowed to recover for 4 hours before being streaked onto an LB-agar plate containing 7 μ g/ml gentamycin, 50 μ g/ml kanamycin, 10 μ g/ml tetracyclin, 40 μ g/ml IPTG and 100 μ g/ml x-gal and incubated for 48 hours. White colonies containing the bacmid containing transposed gene of interest, as observed by means of blue-white selection, were picked and liquid cultures containing 1.2 μ g/ml gentamycin, 50 μ g/ml kanamycin and 10 μ g/ml tetracyclin grown overnight at 37 °C (Fitzgerald et al., 2006; Bieniossek et al., 2008; Trowitzsch et al., 2010). Recombinant bacmid DNA was purified according to a modified version of the Qiagen miniprep protocol. Briefly; DH10EMBacY were re-suspended in 300 μ L P1 and mixed with P2 and subsequently P3 and incubated on ice for 10 minutes. Lysates were cleared by centrifugation at 14,200 r.p.m. for 10 minutes. The cleared lysate was added to 800 μ L ice cold iso-propanol and incubated for 20 minutes at -20°C. Following centrifugation at 14.200 r.p.m. for 10 minutes at 4°C, the recombinant bacmid DNA was washed with 70% ethanol. Finally, in a sterile laminar flow hood the bacmid DNA was re-suspended in 30 μ L sterile H₂O.

7.2.4. Generation of recombinant baculoviruses

Sf9 cells were adherently grown to a density of $\sim 1^6$ cells/mL in 6 well plates and washed 3x with 2 mL Sf-900 serum free media (Gibco). Con-currently, a transfection mix comprising 5 μ L of bacmid DNA, 5 μ L Cellfectin II reagent (Life Technologies) and 190 μ L Sf-900 serum free media was incubated for 30 minutes. The transfection mix was then diluted into 800 μ L Sf-900 serum free media and added to 1 respective well of the 6 well plate and incubated for 4 hours

at 27°C. Cells were then washed 2x with Sf-900 serum free media and subsequently incubated for 96-120 hours in 3mL Sf-900 serum free media.

The baculoviruses containing supernatant (known as P0) was then added to a T-175 flask containing Sf9 cells, at a density of $\sim 0.5^6$ cells/mL, in supplemented Grace's medium (as described above). Cells were incubated for 120 hours before being harvested by centrifugation at 2000 r.p.m. for 10 minutes at 4°C followed by subsequent 22 μ m sterile filtering (Millipore). This viral amplification is known as V1. Further viral amplifications involved the addition of 5 mL V1 to 50 mL Sf9 cells at a density of $\sim 0.5^6$ cells/mL in suspension. Cells were incubated at 100 r.p.m for 120 hours at 27°C before being harvested, as described, to yield V2. This protocol was repeated a further time to yield V3 which was generally used for protein expression.

7.2.5. Protein expression in insect cells

Sf9 cells at a density of $\sim 1^6$ cells/mL were infected with 5 mL (per 650ml culture) of the respective V3 baculovirus amplification and generally incubated at 100 r.p.m for 72 hours at 27°C. Given that the transfected bacmid contains a YFP reporter gene as an indicator for expression, YFP intensity was also taken into consideration before harvesting (Bieniossek et al., 2008). Cells were subsequently centrifuged at 1500rpm for 15 minutes at 4°C, washed once with PBS, centrifuged again with the resulting cell pellet flash frozen in liquid nitrogen and stored at -80°C.

7.2.6. Purification of the co-activators +/- substrates

Insect cell pellets containing frozen Sf9 cells having expressed the respective 1/3MH6 co-activator +/- substrate were thawed and suspended in 2x the pellet volume CDH1 lysis buffer (20mM Hepes pH7.0, 300 mM NaCl/(NH₄)SO₄, 20 mM Imidazole, 1 mM DTT and 5% w/v Glycerol) and lysed by douncing on ice. Insect cells lysates were then cleared by ultra-centrifugation at 35,000rpm for 35 minutes at 4°C. Cleared lysates were subsequently incubated with Ni-ATA resin (1.25mL per 10g cell pellet) (Qiagen) on a rotary shaker for 1 hour at 4°C. The resin was then washed 2x with 2 column volumes CDH1 wash buffer (20 mM Hepes pH7.0, 300 mM NaCl/(NH₄)SO₄, 20 mM Imidazole, 1 mM DTT and 2.5% w/v Glycerol) before being transferred to a gravity flow column. The resin was washed a further 3x with 2 column volumes CDH1 wash buffer. The protein of interest was then eluted with 3x 2 column volume pulses of CDH1 elution buffer (20 mM Hepes pH7.0, 300 mM NaCl/(NH₄)SO₄, 250 mM Imidazole, 1 mM DTT and 2.55% w/v Glycerol), with protein elution efficiency monitored by Bradford analysis. The elution fractions were then pooled and transferred to an equilibrated Amicon centrifugal filter with a molecular weight cut off of 50 kDa (MWCO) (Millipore). The

concentrated eluate was then further purified in CDH1 buffer (20 mM Hepes pH7.0, 300 mM NaCl/(NH₄)SO₄, 20 mM Imidazol, 1 mM DTT and 2.5% w/v Glycerol) by size exclusion chromatography using either a Superdex 200 16/60, 26/60 or 10/300 FPLC column (GE Healthcare). The peak fraction was analysed by SDS-PAGE and visualised by coomassie staining with the favoured fractions pooled and concentrated using an equilibrated Amicon 30kDa MWCO centrifugal filter. The co-activators were concentrated to 1mg/ml for biochemistry studies or 5+ mg/ml for crystallographic studies. The purified protein was either aliquoted, snap frozen and stored at -80°C or used immediately for crystallographic studies.

7.2.7. Purification of Prescission cleavable co-activators +/- substrates

Insect cell pellets containing frozen Sf9 cells having expressed the respective prescission cleavable 1/3MH6 co-activator +/- substrate were thawed and suspended in 2x the pellet volume CDH1 lysis buffer (20mM Hepes pH7.0, 300 mM NaCl/(NH₄)SO₄, 20 mM Imidazole, 1 mM DTT and 5% w/v Glycerol) and lysed by douncing on ice. Insect cells lysates were then cleared by ultra-centrifugation at 35,000rpm for 35 minutes at 4°C. Cleared lysates were subsequently incubated with Ni-ATA resin (1.25mL per 10g cell pellet) on a rotary shaker for 1 hour at 4°C. The resin was then washed 2x with 2 column volumes CDH1 wash buffer (20 mM Hepes pH7.0, 300 mM NaCl/(NH₄)SO₄, 20 mM Imidazole, 1 mM DTT and 2.5% w/v Glycerol) before being transferred to a gravity flow column. The resin was washed a further 3x with 2 column volumes CDH1 wash buffer. The protein of interest was then eluted with 3x 2 column volume pulses of CDH1 elution buffer (20 mM Hepes pH7.0, 300 mM NaCl/(NH₄)SO₄, 250 mM Imidazole, 1 mM DTT and 2.55% w/v Glycerol), with protein elution efficiency monitored by Bradford analysis. The elution fractions were then pooled and transferred to an equilibrated 50 kDa MWCO Amicon centrifugal filter. The concentrated eluate was then incubated for 3 hours at 4°C with 0.5 mg/mL Prescission protease in CDH1 wash buffer. Post incubation, the eluate was passed back 5x over fresh Ni-ATA resin, to capture the cleaved Myc-His tag. The eluate was then re-concentrated using an equilibrated 30 kDa MWCO Amicon centrifugal filter. *In the case of purifying the co-activators in complex with a GST prescission tagged substrates, a further passback step was incorporated using GST4B resin (GE Healthcare). The eluate was passed back 5x over GST4B resin, to capture the cleaved GST tag.* The eluate was then re-concentrated using an equilibrated 30 kDa MWCO Amicon centrifugal filter and further purified in CDH1 buffer (20 mM Hepes pH7.0, 300 mM NaCl/(NH₄)SO₄, 20 mM Imidazol, 1 mM DTT and 2.5% w/v Glycerol) by size exclusion chromatography using either a Superdex 200 16/60 or 26/60 FPLC column. The peak fraction was analysed by SDS-PAGE and visualised by coomassie staining with the favoured fractions pooled and concentrated using an equilibrated Amicon 30kDa MWCO centrifugal filter. The

co-activators were concentrated to 1mg/ml for biochemistry studies or 5+ mg/ml for crystallographic studies. The purified protein was either aliquoted, snap frozen and stored at -80°C or used immediately for crystallographic studies.

7.2.8. Limited Proteolysis

A master mix of 250 µL 3MH6 CDH1 full length, 3MH6 CDC20 full length, 3MH6 CDH1 162-14 or 3MH6 CDH1 162-14 + Hsl1⁶⁶⁷⁻⁸⁷² was incubated with 1 µg chymotrypsin on ice over a time course of 3 hours. At the respective time points, 30 µL samples were taken, analysed by SDS-PAGE and visualised by coomassie staining. For N-terminal Edman sequencing, SDS-PAGE resolved samples were transferred to PVDF membrane (Millipore), stained with Ponceau and sent to Alphalyse for sequencing.

7.2.9. Immunoblotting

SDS-PAGE resolved samples were transferred to 0.45 µm immobilon-P PVDF membrane for 2 hours using a semi-dry transfer method. The membrane was subsequently blocked in a 5 % w/v milk solution for 1 hour before being incubated with primary antibody overnight on a rocking shaker at 4°C. The membrane was then washed 2x with TBS-T and incubated for 1 hour with the respective HRP-coupled secondary antibody before being washed a further 2x with TBS-T. ECL detection was then performed (GE Healthcare)

7.2.10. Differential scanning fluorimetry

The proteins 3MH6 CDH1 162-14 and 3MH6 CDH1 162-14 + Hsl1⁶⁶⁷⁻⁸⁷² were diluted to 0.1 mg/mL in 20 mM Hepes pH7.0 to which a 5x stock of sypro orange was added (Life Technologies). A range of 4x buffers was prepared. The protein and buffer stocks were added to a white 96-well plate (BioRad) and mixed on ice resulting in a final protein concentration of 75 µg/mL in a volume of 20 µL. The plate was sealed and briefly centrifuged before being placed in a CFX connect real-time PCR machine (BioRad). After an initial 5 minute equilibration at 20°C, a temperature gradient was conducted over a 75°C range ending 95°C (1°C per 30 seconds), with the resulting fluorescence signal measured using the FRET channel. Data was analysed as published (Niesen et al., 2007).

7.2.11. Isothermal titration calorimetry

All ITC experiments were performed using an ITC200 (GE Healthcare) and was equilibrated to 6°C before being loaded with the respective proteins. The titrate, 3MH6 CDH1 full length,

was diluted to a concentration of 50 μ M in CDH1 buffer (20 mM Hepes pH7.0, 300 mM NaCl, 1 mM DTT and 2.5% w/v Glycerol buffer) and injected into the reference cell. In addition, the titrants, the Hsl1 D-box peptide (EQKPKRAALSDITNSFNKM) and the Hsl1 KEN-box peptide (GVSTNKENEGPEYPTKI) were dissolved in CDH1 buffer at a concentration of 500 μ M and loaded into the injection syringe. An experiment consisted of 20 injections, with an initial delay of 60 seconds after finding a stable baseline, the initial injection being 0.5 μ L with the remaining injections of 1 μ L occurring at 180 second intervals. As standard, the reference power was 11 and the stirrer was set to spin at 1000 r.p.m.

7.2.12. Commercial Crystallisation Screening

The following commercial crystallisation screens were used to screen for conditions that promoted crystal growth: Crystal 1+2 (Hampton Research), Index 1+2 (Hampton Research), Cryo (Emerald Biosystems), Wizard (Emerald Biosystems), JBS 1-4 (Jena Bioscience), JBS 5-8 (Jena Bioscience), JBS 9-10 (Jena Bioscience), Natrix (Hampton Research), Salt Rx 1+2, MembFac (Hampton Research), PEG/Ion (Hampton Research), JCSG+ (Qiagen). These screens were pipetted using a Mosquito crystal robot (ttp:labtech) into MRC2 96-well crystallisation plates (Swissci). Purified protein at a concentration between 5-10 mg/mL was pipetted and mixed with the respective reservoir liquor at a ratio of 1:1 (100 nL protein:100 nL liquor) or 2:1 (200 nL protein:100 nL liquor) with sitting drop vapour diffusion occurring against a 80 μ L reservoir. The pipetting with additives occurred in the following ratios: 1:0.8:0.2 (100 nL protein:80 nL liquor:20 nL additive) or 2:0.7:0.3 (200 nL protein:70 nL liquor:30nL additive). Plates were left to incubate at 19°C for 10 days, with crystals usually growing to their maximum size after 4 days.

7.2.13. Manual Crystallisation Screening

Manual crystallisation screens were pipetted manually directly into 24 well trays (Hampton Research). Purified protein at a concentration of 10 mg/mL was pipetted and mixed with the respective reservoir liquor at a ratio of 1:1 (1 μ L protein:1 μ L liquor) with hanging/sitting drop vapour diffusion occurring against a 2 mL reservoir. To perform grid screens, 5 mL stocks of all conditions were prepared.

To seed crystallisation trays, a column of crystal producing conditions in an MRC2 96-well plate was opened, with the crystal containing drops pooled and transferred to a 10 μ L volume of CDH1 buffer. The crystals were then crushed with 200 nL of the seed stock pipetted into the drops of a freshly pipetted screen (< 1 hour old).

To streak seed crystallisation trays, a column of crystal producing conditions in an MRC2 96-well plate was opened, with the crystal containing drops pooled and transferred to a 10 μ L volume of CDH1 buffer with crystals were then crushed. A cat whisker was then immersed in the seed stock and then streaked through the hanging drop of a freshly pipetted screen (< 1 hour old).

8. References

- Au, S.W.N., Leng, X., Harper, J.W., and Barford, D. (2002). Implications for the Ubiquitination Reaction of the Anaphase-promoting Complex from the Crystal Structure of the Doc1/Apc10 Subunit. *J. Mol. Biol.* **316**, 955–968.
- Barford, D. (2011). Structure, function and mechanism of the anaphase promoting complex (APC/C). *Q. Rev. Biophys.* **44**, 153–190.
- Berndsen, C.E., and Wolberger, C. (2014). New insights into ubiquitin E3 ligase mechanism. *Nat. Struct. Mol. Biol.* **21**, 301–307.
- Bieniossek, C., Richmond, T.J., and Berger, I. (2008). MultiBac: multigene baculovirus-based eukaryotic protein complex production. *Curr. Protoc. Protein Sci.* Editor. Board John E Coligan *AI Chapter 5*, Unit 5.20.
- Braunstein, I., Miniowitz, S., Moshe, Y., and Hershko, A. (2007). Inhibitory factors associated with anaphase-promoting complex/cylosome in mitotic checkpoint. *Proc. Natl. Acad. Sci.* **104**, 4870–4875.
- Burton, J.L., and Solomon, M.J. (2001). D box and KEN box motifs in budding yeast Hsl1p are required for APC-mediated degradation and direct binding to Cdc20p and Cdh1p. *Genes Dev.* **15**, 2381–2395.
- Burton, J.L., and Solomon, M.J. (2007). Mad3p, a pseudosubstrate inhibitor of APCCdc20 in the spindle assembly checkpoint. *Genes Dev.* **21**, 655–667.
- Burton, J.L., Tsakraklides, V., and Solomon, M.J. (2005). Assembly of an APC-Cdh1-substrate complex is stimulated by engagement of a destruction box. *Mol. Cell* **18**, 533–542.
- Buschhorn, B.A., Petzold, G., Galova, M., Dube, P., Kraft, C., Herzog, F., Stark, H., and Peters, J.-M. (2011). Substrate binding on the APC/C occurs between the coactivator Cdh1 and the processivity factor Doc1. *Nat. Struct. Mol. Biol.* **18**, 6–13.
- Carroll, C.W., and Morgan, D.O. (2002). The Doc1 subunit is a processivity factor for the anaphase-promoting complex. *Nat. Cell Biol.* **4**, 880–887.
- Carroll, C.W., Enquist-Newman, M., and Morgan, D.O. (2005). The APC Subunit Doc1 Promotes Recognition of the Substrate Destruction Box. *Curr. Biol.* **15**, 11–18.
- Chang, L., Zhang, Z., Yang, J., McLaughlin, S.H., and Barford, D. (2014). Molecular architecture and mechanism of the anaphase-promoting complex. *Nature advance online publication*.
- Chao, W.C.H., Kulkarni, K., Zhang, Z., Kong, E.H., and Barford, D. (2012). Structure of the mitotic checkpoint complex. *Nature* **484**, 208–213.
- Cheng, J., Sweredoski, M.J., and Baldi, P. (2005). Accurate Prediction of Protein Disordered Regions by Mining Protein Structure Data. *Data Min. Knowl. Discov.* **11**, 213–222.
- Das, R., Mariano, J., Tsai, Y.C., Kalathur, R.C., Kostova, Z., Li, J., Tarasov, S.G., McFeeters, R.L., Altieri, A.S., Ji, X., et al. (2009). Allosteric activation of E2-RING finger-mediated ubiquitylation by a structurally defined specific E2-binding region of gp78. *Mol. Cell* **34**, 674–685.

Das, R., Liang, Y.-H., Mariano, J., Li, J., Huang, T., King, A., Tarasov, S.G., Weissman, A.M., Ji, X., and Byrd, R.A. (2013). Allosteric regulation of E2:E3 interactions promote a processive ubiquitination machine. *EMBO J.* 32, 2504–2516.

Deshai, R.J., and Joazeiro, C.A.P. (2009). RING Domain E3 Ubiquitin Ligases. *Annu. Rev. Biochem.* 78, 399–434.

Diao, J., Zhang, Y., Huibregtse, J.M., Zhou, D., and Chen, J. (2008). Crystal structure of SopA, a Salmonella effector protein mimicking a eukaryotic ubiquitin ligase. *Nat. Struct. Mol. Biol.* 15, 65–70.

Dikic, I., Wakatsuki, S., and Walters, K.J. (2009). Ubiquitin-binding domains — from structures to functions. *Nat. Rev. Mol. Cell Biol.* 10, 659–671.

Dou, H., Buetow, L., Sibbet, G.J., Cameron, K., and Huang, D.T. (2012). BIRC7-E2 ubiquitin conjugate structure reveals the mechanism of ubiquitin transfer by a RING dimer. *Nat. Struct. Mol. Biol.* 19, 876–883.

Dou, H., Buetow, L., Sibbet, G.J., Cameron, K., and Huang, D.T. (2013). Essentiality of a non-RING element in priming donor ubiquitin for catalysis by a monomeric E3. *Nat. Struct. Mol. Biol.* 20, 982–986.

Dube, P., Herzog, F., Gieffers, C., Sander, B., Riedel, D., Müller, S.A., Engel, A., Peters, J.M., and Stark, H. (2005). Localization of the coactivator Cdh1 and the cullin subunit Apc2 in a cryo-electron microscopy model of vertebrate APC/C. *Mol. Cell* 20, 867–879.

Duda, D.M., Borg, L.A., Scott, D.C., Hunt, H.W., Hammel, M., and Schulman, B.A. (2008). Structural insights into NEDD8 activation of cullin-RING ligases: conformational control of conjugation. *Cell* 134, 995–1006.

Duda, D.M., Olszewski, J.L., Schuermann, J.P., Kurinov, I., Miller, D.J., Nourse, A., Alpi, A.F., and Schulman, B.A. (2013). Structure of HHARI, a RING-IBR-RING Ubiquitin Ligase: Autoinhibition of an Ariadne-Family E3 and Insights into Ligation Mechanism. *Structure* 21, 1030–1041.

Fiore, B.D., and Pines, J. (2010). How cyclin A destruction escapes the spindle assembly checkpoint. *J. Cell Biol.* 190, 501–509.

Fitzgerald, D.J., Berger, P., Schaffitzel, C., Yamada, K., Richmond, T.J., and Berger, I. (2006). Protein complex expression by using multigene baculoviral vectors. *Nat. Methods* 3, 1021–1032.

Foley, E.A., and Kapoor, T.M. (2013). Microtubule attachment and spindle assembly checkpoint signalling at the kinetochore. *Nat. Rev. Mol. Cell Biol.* 14, 25–37.

Da Fonseca, P.C.A., Kong, E.H., Zhang, Z., Schreiber, A., Williams, M.A., Morris, E.P., and Barford, D. (2010). Structures of APC/CCdh1 with substrates identify Cdh1 and Apc10 as the D-box co-receptor. *Nature* 470, 274–278.

Frye, J.J., Brown, N.G., Petzold, G., Watson, E.R., Grace, C.R.R., Nourse, A., Jarvis, M.A., Kriwacki, R.W., Peters, J.-M., Stark, H., et al. (2013). Electron microscopy structure of human APC/CCDH1-EMI1 reveals multimodal mechanism of E3 ligase shutdown. *Nat. Struct. Mol. Biol.* *advance online publication*.

- Garnett, M.J., Mansfeld, J., Godwin, C., Matsusaka, T., Wu, J., Russell, P., Pines, J., and Venkitaraman, A.R. (2009). UBE2S elongates ubiquitin chains on APC/C substrates to promote mitotic exit. *Nat. Cell Biol.* 11, 1363–1369.
- Gieffers, C., Dube, P., Harris, J.R., Stark, H., and Peters, J.-M. (2001). Three-Dimensional Structure of the Anaphase-Promoting Complex. *Mol. Cell* 7, 907–913.
- Hayes, M.J., Kimata, Y., Wattam, S.L., Lindon, C., Mao, G., Yamano, H., and Fry, A.M. (2006). Early mitotic degradation of Nek2A depends on Cdc20-independent interaction with the APC/C. *Nat. Cell Biol.* 8, 607–614.
- He, J., Chao, W.C.H., Zhang, Z., Yang, J., Cronin, N., and Barford, D. (2013). Insights into Degron Recognition by APC/C Coactivators from the Structure of an Acm1-Cdh1 Complex. *Mol. Cell* 50, 649–660.
- Herzog, F., Primorac, I., Dube, P., Lenart, P., Sander, B., Mechtler, K., Stark, H., and Peters, J.M. (2009). Structure of the anaphase-promoting complex/cyclosome interacting with a mitotic checkpoint complex. *Sci. Signal.* 323, 1477.
- Hicks, S.W., and Galan, J.E. (2010). Hijacking the Host Ubiquitin Pathway: Structural Strategies of Bacterial E3 Ubiquitin Ligases. *Curr. Opin. Microbiol.* 13, 41.
- Hochegger, H., Takeda, S., and Hunt, T. (2008). Cyclin-dependent kinases and cell-cycle transitions: does one fit all? *Nat. Rev. Mol. Cell Biol.* 9, 910–916.
- Huang, D.T., Miller, D.W., Mathew, R., Cassell, R., Holton, J.M., Roussel, M.F., and Schulman, B.A. (2004). A unique E1-E2 interaction required for optimal conjugation of the ubiquitin-like protein NEDD8. *Nat. Struct. Mol. Biol.* 11, 927–935.
- Huang, D.T., Paydar, A., Zhuang, M., Waddell, M.B., Holton, J.M., and Schulman, B.A. (2005). Structural Basis for Recruitment of Ubc12 by an E2 Binding Domain in NEDD8's E1. *Mol. Cell* 17, 341–350.
- Janjusevic, R., Abramovitch, R.B., Martin, G.B., and Stebbins, C.E. (2006). A bacterial inhibitor of host programmed cell death defenses is an E3 ubiquitin ligase. *Science* 311, 222–226.
- Jin, L., Williamson, A., Banerjee, S., Philipp, I., and Rape, M. (2008). Mechanism of Ubiquitin-Chain Formation by the Human Anaphase-Promoting Complex. *Cell* 133, 653–665.
- Kamadurai, H.B., Souphron, J., Scott, D.C., Duda, D.M., Miller, D.J., Stringer, D., Piper, R.C., and Schulman, B.A. (2009). Insights into ubiquitin transfer cascades from a structure of a UBCH5B~Ubiquitin-HECTNEDD4L complex. *Mol. Cell* 36, 1095–1102.
- Kamadurai, H.B., Qiu, Y., Deng, A., Harrison, J.S., MacDonald, C., Actis, M., Rodrigues, P., Miller, D.J., Souphron, J., Lewis, S.M., et al. (2013). Mechanism of ubiquitin ligation and lysine prioritization by a HECT E3. *eLife* 2.
- Kerscher, O., Felberbaum, R., and Hochstrasser, M. (2006). Modification of proteins by ubiquitin and ubiquitin-like proteins. *Annu. Rev. Cell Dev. Biol.* 22, 159–180.
- King, R.W., Peters, J.-M., Tugendreich, S., Rolfe, M., Hieter, P., and Kirschner, M.W. (1995). A 20S complex containing CDC27 and CDC16 catalyzes the mitosis-specific conjugation of ubiquitin to cyclin B. *Cell* 81, 279–288.

- King, R.W., Glotzer, M., and Kirschner, M.W. (1996). Mutagenic analysis of the destruction signal of mitotic cyclins and structural characterization of ubiquitinated intermediates. *Mol. Biol. Cell* 7, 1343–1357.
- Komander, D., and Rape, M. (2012). The ubiquitin code. *Annu. Rev. Biochem.* 81, 203–229.
- Kraft, C., Herzog, F., Gieffers, C., Mechtler, K., Hagting, A., Pines, J., and Peters, J.-M. (2003). Mitotic regulation of the human anaphase-promoting complex by phosphorylation. *EMBO J.* 22, 6598–6609.
- Kraft, C., Vodermaier, H.C., Maurer-Stroh, S., Eisenhaber, F., and Peters, J.M. (2005). The WD40 propeller domain of Cdh1 functions as a destruction box receptor for APC/C substrates. *Mol. Cell* 18, 543–553.
- Kramer, E.R., Scheuringer, N., Podtelejnikov, A.V., Mann, M., and Peters, J.M. (2000). Mitotic regulation of the APC activator proteins CDC20 and CDH1. *Mol. Biol. Cell* 11, 1555–1569.
- Kurasawa, Y., and Todokoro, K. (1999). Identification of human APC10/Doc1 as a subunit of anaphase promoting complex. *Oncogene* 18, 5131–5137.
- Lara-Gonzalez, P., Scott, M.I.F., Diez, M., Sen, O., and Taylor, S.S. (2011). BubR1 blocks substrate recruitment to the APC/C in a KEN-box-dependent manner. *J. Cell Sci.* 124, 4332–4345.
- Letunic, I., Doerks, T., and Bork, P. (2012). SMART 7: recent updates to the protein domain annotation resource. *Nucleic Acids Res.* 40, D302–D305.
- Lin, D.Y., Diao, J., and Chen, J. (2012). Crystal structures of two bacterial HECT-like E3 ligases in complex with a human E2 reveal atomic details of pathogen-host interactions. *Proc. Natl. Acad. Sci.* 109, 1925–1930.
- Lin, Y., Hwang, W.C., and Basavappa, R. (2002). Structural and functional analysis of the human mitotic-specific ubiquitin-conjugating enzyme, UBC10. *J. Biol. Chem.* 277, 21913–21921.
- Liu, D., Vader, G., Vromans, M.J.M., Lampson, M.A., and Lens, S.M.A. (2009). Sensing Chromosome Bi-Oriented by Spatial Separation of Aurora B Kinase from Kinetochore Substrates. *Science* 323, 1350–1353.
- Markson, G., Kiel, C., Hyde, R., Brown, S., Charalabous, P., Bremm, A., Semple, J., Woodsmith, J., Duley, S., Salehi-Ashtiani, K., et al. (2009). Analysis of the human E2 ubiquitin conjugating enzyme protein interaction network. *Genome Res.* 19, 1905–1911.
- Mattioli, F., and Sixma, T.K. (2014). Lysine-targeting specificity in ubiquitin and ubiquitin-like modification pathways. *Nat. Struct. Mol. Biol.* 21, 308–316.
- Matyskiela, M.E., and Morgan, D.O. (2009). Analysis of activator-binding sites on the APC/C supports a cooperative substrate-binding mechanism. *Mol. Cell* 34, 68–80.
- Metzger, M.B., Pruneda, J.N., Klevit, R.E., and Weissman, A.M. (2014). RING-type E3 ligases: Master manipulators of E2 ubiquitin-conjugating enzymes and ubiquitination. *Biochim. Biophys. Acta BBA - Mol. Cell Res.* 1843, 47–60.

- Meyer, H.-J., and Rape, M. (2014). Enhanced Protein Degradation by Branched Ubiquitin Chains. *Cell* 157, 910–921.
- Miller, J.J., Summers, M.K., Hansen, D.V., Nachury, M.V., Lehman, N.L., Loktev, A., and Jackson, P.K. (2006). Emi1 stably binds and inhibits the anaphase-promoting complex/cyclosome as a pseudosubstrate inhibitor. *Genes Dev.* 20, 2410–2420.
- Min, M., Mayor, U., and Lindon, C. (2013). Ubiquitination site preferences in anaphase promoting complex/cyclosome (APC/C) substrates. *Open Biol.* 3, 130097.
- Morgan, D.O. (2007). *The Cell Cycle: Principles of Control* (New Science Press).
- Murray, A.W. (2004). Recycling the cell cycle: cyclins revisited. *Cell* 116, 221–234.
- Musacchio, A., and Salmon, E.D. (2007). The spindle-assembly checkpoint in space and time. *Nat. Rev. Mol. Cell Biol.* 8, 379–393.
- Niesen, F.H., Berglund, H., and Vedadi, M. (2007). The use of differential scanning fluorimetry to detect ligand interactions that promote protein stability. *Nat. Protoc.* 2, 2212–2221.
- Nigg, E.A. (2001). Mitotic kinases as regulators of cell division and its checkpoints. *Nat. Rev. Mol. Cell Biol.* 2, 21–32.
- Olsen, S.K., and Lima, C.D. (2013). Structure of a Ubiquitin E1-E2 Complex: Insights to E1-E2 Thioester Transfer. *Mol. Cell* 49, 884–896.
- Passmore, L.A., McCormack, E.A., Au, S.W.N., Paul, A., Willison, K.R., Harper, J.W., and Barford, D. (2003). Doc1 mediates the activity of the anaphase-promoting complex by contributing to substrate recognition. *EMBO J.* 22, 786–796.
- Passmore, L.A., Booth, C.R., Vénien-Bryan, C., Ludtke, S.J., Fioretto, C., Johnson, L.N., Chiu, W., and Barford, D. (2005). Structural analysis of the anaphase-promoting complex reveals multiple active sites and insights into polyubiquitylation. *Mol. Cell* 20, 855–866.
- Peters, J.-M. (2006). The anaphase promoting complex/cyclosome: a machine designed to destroy. *Nat. Rev. Mol. Cell Biol.* 7, 644–656.
- Pfleger, C.M., and Kirschner, M.W. (2000). The KEN box: an APC recognition signal distinct from the D box targeted by Cdh1. *Genes Dev.* 14, 655–665.
- Pickart, C.M., and Eddins, M.J. (2004). Ubiquitin: structures, functions, mechanisms. *Biochim. Biophys. Acta BBA - Mol. Cell Res.* 1695, 55–72.
- Pines, J. (2011). Cubism and the cell cycle: the many faces of the APC/C. *Nat. Rev. Mol. Cell Biol.* 12, 427–438.
- Plechanovová, A., Jaffray, E.G., Tatham, M.H., Naismith, J.H., and Hay, R.T. (2012). Structure of a RING E3 ligase and ubiquitin-loaded E2 primed for catalysis. *Nature* 489, 115–120.
- Primorac, I., and Musacchio, A. (2013). Panta rhei: The APC/C at steady state. *J. Cell Biol.* 201, 177–189.

- Pruneda, J.N., Stoll, K.E., Bolton, L.J., Brzovic, P.S., and Klevit, R.E. (2011). Ubiquitin in motion: structural studies of the ubiquitin-conjugating enzyme~ubiquitin conjugate. *Biochemistry (Mosc.)* 50, 1624–1633.
- Rape, M., Reddy, S.K., and Kirschner, M.W. (2006). The Processivity of Multiubiquitination by the APC Determines the Order of Substrate Degradation. *Cell* 124, 89–103.
- Reimann, J.D.R., Freed, E., Hsu, J.Y., Kramer, E.R., Peters, J.-M., and Jackson, P.K. (2001). Emi1 Is a Mitotic Regulator that Interacts with Cdc20 and Inhibits the Anaphase Promoting Complex. *Cell* 105, 645–655.
- Rieder, C.L., Cole, R.W., Khodjakov, A., and Sluder, G. (1995). The checkpoint delaying anaphase in response to chromosome monoorientation is mediated by an inhibitory signal produced by unattached kinetochores. *J. Cell Biol.* 130, 941–948.
- Rodrigo-Brenni, M.C., and Morgan, D.O. (2007). Sequential E2s Drive Polyubiquitin Chain Assembly on APC Targets. *Cell* 130, 127–139.
- Rudner, A.D., and Murray, A.W. (2000). Phosphorylation by Cdc28 Activates the Cdc20-Dependent Activity of the Anaphase-Promoting Complex. *J. Cell Biol.* 149, 1377–1390.
- Sako, K., Suzuki, K., Isoda, M., Yoshikai, S., Senoo, C., Nakajo, N., Ohe, M., and Sagata, N. (2014). Emi2 mediates meiotic MII arrest by competitively inhibiting the binding of Ube2S to the APC/C. *Nat. Commun.* 5.
- Schreiber, A., Stengel, F., Zhang, Z., Enchev, R.I., Kong, E.H., Morris, E.P., Robinson, C.V., da Fonseca, P.C.A., and Barford, D. (2011). Structural basis for the subunit assembly of the anaphase-promoting complex. *Nature* 470, 227–232.
- Schwickart, M., Havlis, J., Habermann, B., Bogdanova, A., Camasses, A., Oelschlaegel, T., Shevchenko, A., and Zachariae, W. (2004). Swm1/Apc13 Is an Evolutionarily Conserved Subunit of the Anaphase-Promoting Complex Stabilizing the Association of Cdc16 and Cdc27. *Mol. Cell. Biol.* 24, 3562–3576.
- Scott, D.C., Sviderskiy, V.O., Monda, J.K., Lydeard, J.R., Cho, S.E., Harper, J.W., and Schulman, B.A. (2014). Structure of a RING E3 Trapped in Action Reveals Ligation Mechanism for the Ubiquitin-like Protein NEDD8. *Cell* 157, 1671–1684.
- Sheng, Y., Hong, J.H., Doherty, R., Srikumar, T., Shloush, J., Avvakumov, G.V., Walker, J.R., Xue, S., Neculai, D., Wan, J.W., et al. (2012). A Human Ubiquitin Conjugating Enzyme (E2)-HECT E3 Ligase Structure-function Screen. *Mol. Cell. Proteomics* 11, 329–341.
- Shirayama, M., Tóth, A., Gálová, M., and Nasmyth, K. (1999). APC(Cdc20) promotes exit from mitosis by destroying the anaphase inhibitor Pds1 and cyclin Clb5. *Nature* 402, 203–207.
- Sloper-Mould, K.E., Jemc, J.C., Pickart, C.M., and Hicke, L. (2001). Distinct Functional Surface Regions on Ubiquitin. *J. Biol. Chem.* 276, 30483–30489.
- Sudakin, V., Chan, G.K., and Yen, T.J. (2001). Checkpoint inhibition of the APC/C in HeLa cells is mediated by a complex of BUBR1, BUB3, CDC20, and MAD2. *J. Cell Biol.* 154, 925–936.
- Sullivan, M., and Morgan, D.O. (2007). Finishing mitosis, one step at a time. *Nat. Rev. Mol. Cell Biol.* 8, 894–903.

- Tang, Z., Li, B., Bharadwaj, R., Zhu, H., Özkan, E., Hakala, K., Deisenhofer, J., and Yu, H. (2001). APC2 Cullin Protein and APC11 RING Protein Comprise the Minimal Ubiquitin Ligase Module of the Anaphase-promoting Complex. *Mol. Biol. Cell* 12, 3839–3851.
- Tenno, T., Fujiwara, K., Tochio, H., Iwai, K., Morita, E.H., Hayashi, H., Murata, S., Hiroaki, H., Sato, M., Tanaka, K., et al. (2004). Structural basis for distinct roles of Lys63- and Lys48-linked polyubiquitin chains. *Genes Cells* 9, 865–875.
- Thornton, B.R. (2006). An architectural map of the anaphase-promoting complex. *Genes Dev.* 20, 449–460.
- Tian, W., Li, B., Warrington, R., Tomchick, D.R., Yu, H., and Luo, X. (2012). Structural analysis of human Cdc20 supports multisite degron recognition by APC/C. *Proc. Natl. Acad. Sci.* 109, 18419–18424.
- Townsley, F.M., Aristarkhov, A., Beck, S., Hershko, A., and Ruderman, J.V. (1997). Dominant-negative cyclin-selective ubiquitin carrier protein E2-C/UBCH10 blocks cells in metaphase. *Proc. Natl. Acad. Sci.* 94, 2362–2367.
- Trowitzsch, S., Bieniossek, C., Nie, Y., Garzoni, F., and Berger, I. (2010). New baculovirus expression tools for recombinant protein complex production. *J. Struct. Biol.* 172, 45–54.
- Uzunova, K., Dye, B.T., Schutz, H., Ladurner, R., Petzold, G., Toyoda, Y., Jarvis, M.A., Brown, N.G., Poser, I., Novatchkova, M., et al. (2012). APC15 mediates CDC20 autoubiquitylation by APC/CMCC and disassembly of the mitotic checkpoint complex. *Nat. Struct. Mol. Biol.* 19, 1116–1123.
- Varadan, R., Walker, O., Pickart, C., and Fushman, D. (2002). Structural Properties of Polyubiquitin Chains in Solution. *J. Mol. Biol.* 324, 637–647.
- Visintin, R., Prinz, S., and Amon, A. (1997). CDC20 and CDH1: a family of substrate-specific activators of APC-dependent proteolysis. *Science* 278, 460–463.
- Vodermaier, H.C., Gieffers, C., Maurer-Stroh, S., Eisenhaber, F., and Peters, J.M. (2003). TPR subunits of the anaphase-promoting complex mediate binding to the activator protein CDH1. *Curr. Biol. CB* 13, 1459.
- Van Voorhis, V.A., and Morgan, D.O. (2014). Activation of the APC/C Ubiquitin Ligase by Enhanced E2 Efficiency. *Curr. Biol. CB*.
- Wang, W., and Kirschner, M.W. (2013). Emi1 preferentially inhibits ubiquitin chain elongation by the anaphase-promoting complex. *Nat. Cell Biol.* 15, 797–806.
- Wendt, K.S., Vodermaier, H.C., Jacob, U., Gieffers, C., Gmachl, M., Peters, J.M., Huber, R., and Sondermann, P. (2001). Crystal structure of the APC10/DOC1 subunit of the human anaphase-promoting complex. *Nat. Struct. Mol. Biol.* 8, 784–788.
- Wenzel, D.M., Lissounov, A., Brzovic, P.S., and Klevit, R.E. (2011). UBCH7 reactivity profile reveals parkin and HHARI to be RING/HECT hybrids. *Nature* 474, 105–108.
- Wickliffe, K.E., Lorenz, S., Wemmer, D.E., Kuriyan, J., and Rape, M. (2011). The mechanism of linkage-specific ubiquitin chain elongation by a single-subunit E2. *Cell* 144, 769–781.
- Williamson, A., Wickliffe, K.E., Mellone, B.G., Song, L., Karpen, G.H., and Rape, M. (2009). Identification of a physiological E2 module for the human anaphase-promoting complex. *Proc. Natl. Acad. Sci.* 106, 18213–18218.

Woo, R.A., and Poon, R.Y.C. (2003). Cyclin-Dependent Kinases and S Phase Control in Mammalian Cells. *Cell Cycle* 2, 315–323.

Wu, T., Merbl, Y., Huo, Y., Gallop, J.L., Tzur, A., and Kirschner, M.W. (2010). UBE2S drives elongation of K11-linked ubiquitin chains by the Anaphase-Promoting Complex. *Proc. Natl. Acad. Sci.* 107, 1355–1360.

Xin, D.-W., Liao, S., Xie, Z.-P., Hann, D.R., Steinle, L., Boller, T., and Staehelin, C. (2012). Functional Analysis of NopM, a Novel E3 Ubiquitin Ligase (NEL) Domain Effector of *Rhizobium* sp. Strain NGR234. *PLoS Pathog* 8, e1002707.

Zachariae, W., Shevchenko, A., Andrews, P.D., Ciosk, R., Galova, M., Stark, M.J., Mann, M., and Nasmyth, K. (1998). Mass spectrometric analysis of the anaphase-promoting complex from yeast: identification of a subunit related to cullins. *Science* 279, 1216–1219.

Zhang, Y., and Cremer, P. (2006). Interactions between macromolecules and ions: the Hofmeister series. *Curr. Opin. Chem. Biol.* 10, 658–663.

9. Experimental Contributions

Many people contributed to the work that I have presented in this thesis.

The UBE2S mutants were conceived and designed by Brenda Schulman, Nicholas Brown and Randy Watson.

I performed all the experiments shown in figures 9-11.

Work on crystallising CDH1, in figures 13-19, was done jointly in collaboration with Georg Petzold.

I performed all the experiments on Cdc20, as well as experiments in figures 20-25.

Work in figures 21, 23-24 was conducted in and with great help from the Schulman lab.

10. Acknowledgments

Firstly, I would like to thank Jan-Michael Peters for giving me the opportunity to undertake my PhD studies in his laboratory. I feel very privileged to have worked with such a well-respected scientist at such an institute like the IMP.

I want to express my sincere gratitude to Brenda Schulman for 'adopting' me as her student. I spent intense but very valuable times in your lab and am very grateful for the opportunities you gave me as well as being mentored, challenged and most importantly made to feel at home by you.

Nick Brown for taking me under your wing and mentoring me in such a wonderful way, scientifically (and not scientifically...). The skills, way of thinking and vision that you instilled in me I will put to great use. Thank you for involving me in the 'back room' banter, 'the infamous' drink in Chicago, my initial welcome 'test' on my visit to Memphis and for being a friend.

Georg Petzold for the initial immersion into the world of the APC/C and structural biology. He taught me a wealth of knowledge to see me on my way.

My PhD committee, Tim Clausen, Claudine Kraft, Alwin Koehler and Jan-Michael Peters for their valuable scientific input and advice throughout my PhD studies.

Andrea Musacchio for agreeing and taking the time to examine my PhD thesis and making the journey to Vienna.

The Peters lab for the scientific discussions and exposing me to such a high quality standard of research. The resources at our disposal really allow us to focus on great science.

The Schulman lab for welcoming me and integrating me so warmly into the lab and the APC/C team for such intellectually stimulating discussions. Miller for procuring anything I needed and solving any issues I had.

The Clausen lab, particularly Marcin and Ricardo for all the help, support and scientific discussions throughout my time at the IMP.

Georg and Mariana, you have been wonderful friends, always there for me and digging me out of numerous holes.

Miro, thank you for being the only and best bench neighbour ever!

Kristina, you were a great support to me in the lab offering me great advice and ideas as well as great reagents!

Ines and Mareike, thank you for all the friendship and support you have given me. Maybe one day I might just come climbing with you!

Martin and Julian for the all the banter. It's always nice to talk with you guys and clear my mind.

Matt and Sophia, having met six years ago, I didn't imagine that we would become such good friends and share so many warm experiences together. Thank you for the support, the photography advice and film trips. I wish you both and Cora all the best.

Venu and Harini, you are two of the nicest people I have met. You have both supported me a lot, showed lots of patience and perfected your sledging technique so much!

Tiago, release those bees!

Randy and Vlad, we shared some epic times together! I am glad we became friends. Maybe one day we really will go to Arkansas...

Ania, thank you for all the support you have given me. You provided me with great strength and happiness over the past years. I have shared some wonderful experiences with you that I will never forget.

Last but not least, and most importantly, my family for the infinite encouragement and support offered to me over the past 26 years. Be it academically, or in sport, you always encouraged me to work towards my dreams.

11. Curriculum Vitae

Personal Data:

Name: Marc A. Jarvis
 Date of Birth: 7th April 1988, London, United Kingdom
 Nationality: British/Swiss

Education:

2010 – Present **Research Institute of Molecular Pathology**, Vienna, Austria
 Ph.D. in Molecular Life Sciences. Laboratory of Dr. Jan-Michael Peters.
 2006 – 2010 **The University of Manchester**, United Kingdom
 B.Sc. Cell Biology with Industrial Experience.
 2002 – 2006 **Chesham High School**, Buckinghamshire, United Kingdom
 1999 – 2002 **Ramsey Grammar School**, Isle of Man, United Kingdom
 1992 – 1999 **Andreas Primary School**, Isle of Man, United Kingdom

Work Experience:

2008 – 2009 **Boehringer Ingelheim RCV GmbH & Co KG**, Vienna, Austria

Conferences:

May 2013 The Ubiquitin Family. Cold Spring Harbor Laboratories, NY, USA
 Poster presentation

Publications:

Electron microscopy structure of human APC/CCDH1–EMI1 reveals multimodal mechanism of E3 ligase shutdown.

Frye, J.J., Brown, N.G., Petzold, G., Watson, E.R., Grace, C.R.R., Nourse, A., **Jarvis, M.A.**, Kriwacki, R.W., Peters, J-M., Stark, H., Schulman, B.A. **Nature Structural & Molecular Biology**, 2013. 20. 827–835

APC15 mediates CDC20 autoubiquitylation by APC/CMCC and disassembly of the mitotic checkpoint complex. Uzunova, K., Dye, B.T., Schutz, H., Ladurner, R., Petzold, G., Toyoda, Y., **Jarvis, M.A.**, Brown, N.G., Poser, I., Novatchkova, M., Mechtler, K., Hyman, A.A., Stark, H., Schulman, B.A., Peters, J-M. **Nature Structural & Molecular Biology**, 2012. 19. 1116–1123

Molecular and cellular pharmacology of BI 811283, a potent inhibitor of Aurora B kinase. Tontsch-Grunt, U., Gürtler, U., Zahn, S.K., Boehmelt, G., **Jarvis, M.**, Adolf, G.R., Solca, F. **Proceedings of the 101st Annual Meeting of the American Association for Cancer Research**, 17-21 April 2010, Washington DC, USA. AACR 2010 abstract number: 1080.

Effect of BI 811283, a novel inhibitor of Aurora B kinase, on tumor senescence and apoptosis. Gürtler, U., Tontsch-Grunt, U., Jarvis, M., **Zahn, S.K.**, Boehmelt, G., Quant, J., Adolf, G.R., Solca, F. *Journal of Clinical Oncology*, **2010. 28. Abstract number: e1363**

